# MOLECULAR MECHANISMS OF COPPER DELIVERY TO THE MITOCHONDRIAL CYTOCHROME *C* OXIDASE

A Dissertation

by

SHIVA THEJA REDDY SOMA

Submitted to the Office of Graduate and Professional Studies of
Texas A&M University
in partial fulfillment of the requirements for the degree of

DOCTOR OF PHILOSOPHY

| | |
|---|---|
| Chair of Committee, | Vishal M. Gohil |
| Committee Members, | Mary Bryk |
| | Paul A. Lindahl |
| | Michael Polymenis |
| Head of Department, | Dorothy E. Shippen |

August 2019

Major Subject: Biochemistry

Copyright 2019 Shiva Theja Reddy Soma

ABSTRACT

Copper is required for the activity of cytochrome *c* oxidase (CcO), the mitochondrial enzyme that catalyzes cellular respiration. Copper delivery to CcO is a complex process requiring a number of proteins, and loss-of-function mutations in these proteins diminish CcO activity, causing rare mitochondrial disorders, for which no effective therapy currently exists. A lack of understanding of the basic mechanisms for copper transport to the mitochondria and ultimately to CcO has been the main bottleneck in developing therapeutic strategies for these disorders. To address this gap in our knowledge, I utilized a multi-disciplinary approach involving chemical biology, structural biology, and yeast genetics to identify small molecules and genes that facilitate copper transport to the mitochondrial CcO.

First, using a chemical biology approach, I determined that elesclomol (ES), an investigational anticancer drug, is a potent copper delivery agent to mitochondria. I showed that ES supplementation rescues respiratory growth of several yeast copper metabolism mutants, including cells lacking Coa6, a CcO assembly factor. ES also restored CcO levels in a series of copper-deficient mammalian cells and in a zebrafish model of copper deficiency. These findings demonstrate the applicability of ES to more complex eukaryotic cells and intact multicellular organisms.

Second, I utilized nuclear magnetic resonance (NMR) spectroscopy to uncover the structure and function of COA6, a new member of the CcO copper delivery pathway that was discovered in our laboratory. I collaborated with structural biologists to solve the solution structure of human COA6, which revealed a CHCH domain typically found in

the redox-active proteins in the mitochondrial intermembrane space. Consistent with its redox role, I showed that COA6 function can be bypassed in the reducing environment. Interaction mapping and redox potential determination of COA6 and its client proteins showed that COA6 facilitates copper delivery to CcO by acting as a thiol-disulfide reductase.

Finally, I utilized yeast genetics to uncover overlapping functions of COA6 and SCO2, a well-known member of the copper delivery pathway to CcO. Taken together, this dissertation describes molecular mechanisms of copper delivery to the mitochondrial CcO by both the interplay of CcO assembly factors and through pharmacological means.

# DEDICATION

I would like to dedicate my dissertation work to my family and to all the scientists who spend their life in the pursuit of knowledge.

# ACKNOWLEDGEMENTS

I would like to thank my advisor, Dr. Gohil, for his constant guidance, care, and support throughout the course of this research. Also, I would like to thank my committee members, Dr. Lindahl, Dr. Polymenis, and Dr. Bryk, for their advice and direction regarding my project. I would also like to thank Dr. Alok Ghosh for his experimental guidance. Thanks also go to Dr. Prachi Trivedi for her constant support in and out of the lab. In addition, thanks to all the members of the Gohil lab for their helpful discussions and suggestions. I would specially like to thank Alison Vicary, who spend hundreds of hours working in the laboratory with me. Finally, I want to thank my wife, Malini, and my dad-Narsi reddy, mom- Vimala, brother- Ravi and sister-in-law Priyanka for their unwavering understanding, encouragement, love, and support throughout this process.

CONTRIBUTORS AND FUNDING SOURCES

## Contributors

This work was supervised by a dissertation committee consisting of my advisor Dr. Vishal M. Gohil of the Department of Biochemistry and Biophysics, Dr. Mary Bryk of the Department of Biochemistry and Biophysics, Dr. Paul A. Lindahl of the Department of Biochemistry and Biophysics as well as the Department of Chemistry, and Dr. Michael Polymenis of the Department of Biochemistry and Biophysics. The head of the Biochemistry and Biophysics department, Dr. Gregory D. Reinhart, and current interim head Dr. Dorothy E. Shippen also supported this work.

Chapter II is a reprint of a *PNAS* paper of which I am the first author. I performed all the experimental work described in this chapter except for the following figures. Haarin Chun at the Department of Animal and Avian Sciences, University of Maryland, College Park performed experiments described in Figure 2.8 A-C. Dr. Andrew J. Latimer, Eugene Bell Center for Regenerative Biology and Tissue Engineering, Marine Biological Laboratory, Woods Hole, performed experiments described in Figure 2.10 and 2.11. Jennifer J. Rahn, Department of Drug Discovery and Biomedical Sciences, Medical University of South Carolina, performed experiments described in the Figure 2.12. I also greatly appreciate the help of Shrishiv Timbalia and Alison Vicary, of the Department of Biochemistry and Biophysics at Texas A&M University, in performing yeast growth assays described in Figure 2.3 and Figure 2.1 and 2.2, respectively.

The manuscript describing the work in Chapter III is in preparation for the submission to a journal, for which I am the first author. I performed all the experimental

work described in this chapter except for the following figures. Dr. Alok Ghosh, of the Department of Biochemistry and Biophysics at Texas A&M University performed experiments described in Fig. 3.8B. Aren Boulet, of the Department of Biochemistry, University of Saskatchewan, Saskatoon, performed experiments described in Fig. 3.4D&E, 3.10F and 3.11. Marcos Morgada, of the Instituto de Biología Molecular y Celular de Rosario, Universidad Nacional de Rosario, performed experiments described in Fig. 3.5, 3.10B-E. Dr. James Ames and his student Qinhong Yu, of the Department of Chemistry, University of California, Davis, provided guidance for the experiments described in Fig. 3.6E. Nathaniel Dziuba of the Department of Biochemistry and Biophysics at Texas A&M University performed experiments described in Fig. 3.8D&F and 3.9. I also greatly appreciate the help of Dr. Mandar Naik, of the Department of Biochemistry and Biophysics at Texas A&M University, in performing NMR experiments described in Fig.3.1D-F, 3.2A-D, 3.3 and 3.6A-D.

The work described in Chapter IV comprises a reprint of a *Human Molecular Genetics* paper to which I contributed as a third author. The authors include Alok Ghosh, Anthony T. Pratt, Shivatheja Soma, Sarah G. Theriault, Aaron T. Griffin, Prachi P. Trivedi and Vishal M. Gohil of the Department of Biochemistry and Biophysics at Texas A&M University. I contributed to the following figures in this publication: Fig. 4.7 and Fig. 4.8.

**Funding Sources**

The research described in this dissertation thesis was supported by the National Institutes of Health award [R01GM111672] to Vishal M. Gohil. The content is solely the

responsibility of myself and fellow authors and does not necessarily the official views of the National Institutes of Health.

# NOMENCLATURE

| | |
|---|---|
| ATP | Adenosine Triphosphate |
| BCS | Bathocuproinedisulfonic acid |
| CcO | Cyctochrome *c* Oxidase |
| ES | Elesclomol |
| ICP-MS | Inductively coupled plasma-mass spectrometry |
| IMS | Mitochondrial intermembrane space |
| IM | Inner mitochondrial membrane |
| OM | Outer mitochondrial membrane |
| MRC | Mitochondrial respiratory chain |
| PCR | Polymerase chain reaction |
| PAGE | Polyacrylamide gel electrophoresis |
| SDS | Sodium dodecyl sulphate |
| mtDNA | mitochondrial DNA |
| TCEP | Tris(2-carboxyethyl)phosphine hydrochloride |

TABLE OF CONTENTS

Page

LIST OF FIGURES

Page

LIST OF TABLES

Page

# CHAPTER I

# INTRODUCTION AND LITERATURE REVIEW

More than a billion years ago, a symbiotic relationship developed between primordial eukaryotic cells and bacteria, which then evolved to become mitochondria. Today, mitochondria are considered the powerhouse of the cell. They have a double membrane, consisting of a permeable outer membrane (OM) and impermeable inner membrane (IM), with the space encompassed between the OM and IM called the intermembrane space (IMS). Mitochondria are involved in many vital cellular processes, especially respiration-driven energy production. Generation of mitochondrial energy in the form of adenosine triphosphate (ATP) relies on the mitochondrial respiratory chain (MRC), which consists of four complexes embedded in the mitochondrial inner membrane. The main function of the MRC is to transfer electrons from the reduced forms of nicotinamide adenine dinucleotide (NADH) and flavin adenine dinucleotide ($FADH_2$) to molecular oxygen. The energy released during the sequential transfer of electrons from molecules with low reduction potential to high reduction potential, is utilized in pumping protons from the mitochondrial matrix into the IMS, creating a proton gradient, which drives mitochondrial ATP synthesis.

## Mitochondrial respiratory chain

In mammalian mitochondria, the MRC and ATP synthase together consists of about 90 core subunits organized into five multimeric protein complexes. These five complexes include: complex I (NADH dehydrogenase–ubiquinone oxidoreductase, composed of 46 subunits), complex II (succinate dehydrogenase–ubiquinone oxidoreductase, 4 subunits),

complex III (ubiquinone–cytochrome *c* oxidoreductase, 11 subunits), complex IV (cytochrome *c* oxidase, 14 subunits), and complex V (ATP synthase, 16 subunits) (Calvo and Mootha, 2010). Only 13 of the 90 core subunits are encoded by mitochondrial DNA (mtDNA), while the rest of the subunits are encoded within the nuclear genome, as are all of the other ~1,000 protein components of the mitochondrion (Calvo and Mootha, 2010). Expression, maturation, and assembly of these subunits into mature complexes is an intricate process requiring many assembly factors (Calvo and Mootha 2010; Ghezzi and Zeviani 2012; Timón-Gómez et al., 2018). My work specifically focused on the biogenesis of MRC complex IV, also referred to as cytochrome *c* oxidase, the only copper-containing enzyme of the MRC.

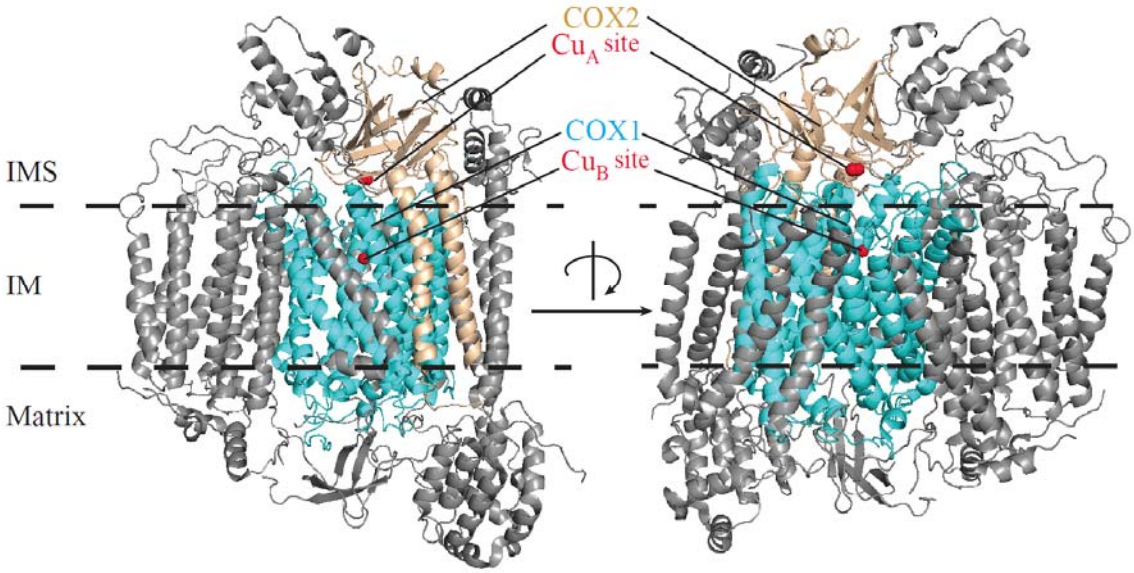


**Figure 1.1. Crystal structure of human cytochrome *c* oxidase.**
A ribbon diagram depicting crystal structure of human mitochondrial cytochrome *c* oxidase (PDB 5Z62). The two copper sites, $Cu_A$ and $Cu_B$, present on subunits COX2 (gold) and COX1 (cyan) are indicated in red.

**Cytochrome *c* oxidase**

Cytochrome *c* oxidase (CcO), also commonly referred to as the MRC complex IV, catalyzes electron transfer from reduced cytochrome *c* to molecular oxygen, while simultaneously pumping protons from the matrix to the IMS to contribute to the proton gradient. Mammalian CcO is a multimeric protein complex consisting of 14 subunits and several cofactors, including two copper (Cu) centers, two heme groups, with single magnesium and zinc ions (Fig. 1.1) (Tsukihara et al., 1995). Of these subunits, three – COX1, COX2 and COX3 – are encoded by the mtDNA and together form the catalytic core of the enzyme. The other 11 subunits, encoded by the nuclear DNA, are required for the assembly and regulation of CcO. Two of these core subunits, COX1 and COX2, require metallation with copper at their $Cu_B$ and $Cu_A$ centers, respectively, for their maturation and stability. $Cu_A$ is a binuclear copper center, accepting electrons from reduced cytochrome *c* and transferring them to the heme *a* center in COX1. Electrons from heme *a* are then transferred to the heme *a3*-$Cu_B$ binuclear center in COX1 and then to molecular oxygen in order to reduce it to water (Ferguson-Miller and Babcock, 1996).

Assembly of CcO is a complex process that requires more than 35 assembly factors for the expression, stability, membrane insertion, and delivery of the metal cofactors (Soto et al., 2012). According to the most popular model, assembly of CcO takes place in a modular fashion (McStay et al., 2013). Pulse-chase analysis of CcO intermediates has shown that the assembly of CcO takes place simultaneously in three different modules: COX1, COX2, and COX3- containing modules (McStay et al., 2013). Each of these modules associates with other nuclear-encoded CcO subunits, as well as the assembly

factors which stabilize complex intermediates and promote maturation, before formation of the CcO holoenzyme (McStay et al., 2013, Franco et al., 2018). To date, the molecular function of many of these assembly factors has remained mysterious. This is particularly true for assembly factors involved in copper delivery to CcO (Soto et al., 2012). The copper delivery to the two copper-sites $Cu_A$ and $Cu_B$ present on the COX2 and COX1 subunits, respectively, occurs on the IMS side of the IM (Baker et al., 2017) (Fig. 1.2). The maturation of $Cu_A$ and $Cu_B$ occurs independently and is facilitated by a sequential transfer of copper from one metallochaperone to the other, in a bucket brigade manner, although the reason for this is unclear at present (Fig. 1.2). Specifically, Cox17, Sco1, Sco2, and Coa6 proteins are involved in copper delivery to the $Cu_A$ site, whereas Cox17, Cox19, and Cox11 are required for the metallation of $Cu_B$ site (Fig. 1.2)

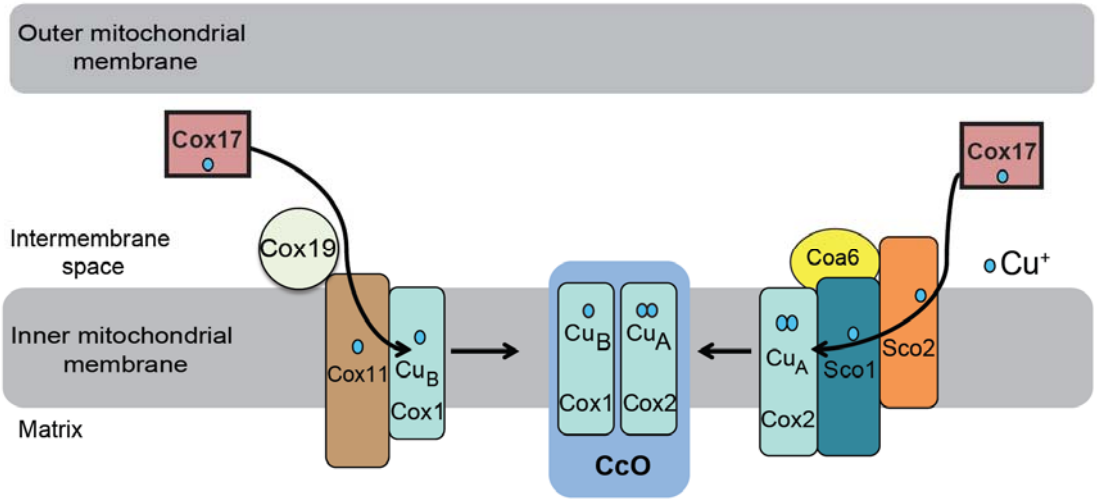


**Figure 1.2. Mitochondrial copper delivery pathway to CcO.**
CcO biogenesis occurs in a modular fashion centered around two catalytic subunits, Cox1 and Cox2, which contain the $Cu_B$ and $Cu_A$ sites, respectively. Concerted actions metallochaperones and thiol-disulfide reductases, including Cox11, Sco1, Sco2, Cox17, Cox19 and Coa6 is required for building $Cu_A$ and $Cu_B$ sites.

**Molecular details of $Cu_A$ site metallation**

The two copper ions in the $Cu_A$ site of COX2 are coordinated by two cysteines, two histidines, and a methionine residue (Tsukihara, et al., 1996). SCO1, the key metallochaperone that is involved in $Cu_A$ site formation, was initially reported as an essential assembly factor involved in a post-translational assembly step for CcO in yeast (Schulze et al., 1988, Krummeck et al., 1990). Later, SCO1 was identified as a multicopy suppressor of *cox17Δ* yeast cells, suggesting its role in mitochondrial copper transport to CcO (Glerum et al., 1996). SCO1 and SCO2, a paralog of SCO1, are inner membrane proteins with soluble IMS domains that bind copper through their $CX_3C$ motif. NMR structural and functional characterization of SCO proteins revealed their copper (I) binding and redox properties (Banci et al., 2007a, Banci et al., 2007b). A follow-up study on SCO1 showed that COX17 loaded with Cu(I) can simultaneously transfer two electrons and a Cu(I) ion to oxidized SCO1 (Banci et al., 2008a). Recently, COA6 (Cytochrome *c* Oxidase Assembly factor 6) was identified as an evolutionarily conserved CcO assembly factor (Vogtle et al., 2012; Ghosh et al., 2014). Initial studies on COA6 by Ghosh *et al.* showed that COA6 plays a critical role in CcO biogenesis and that exogenous copper supplementation can bypass COA6 function, suggesting a role in the copper delivery pathway to CcO (Ghosh et al., 2014). Later studies have revealed that COA6 can genetically and physically interact with COX2 and SCO proteins, thereby placing COA6 in the copper delivery pathway to COX2 subunit of CcO (Ghosh et al., 2016, Stroud et al., 2015, Pacheu-Grau et al., 2015). The exact molecular function of COA6 in COX2 maturation has not yet been identified, although the structure function relationships of

some of the proteins involved in copper delivery that have been thoroughly investigated are summarized in Table 1.1.

**Molecular details of $Cu_B$ site metallation**

The $Cu_B$ site is composed of one copper ion coordinated with three histidine ligands on COX1 (Yoshikawa et al., 2012). The $Cu_B$ site is located in close proximity to the heme *a* moiety in COX1, which together forms a binuclear center responsible for the final step in the delivery of electrons to molecular oxygen. The copper metallochaperone COX11 that carries out the final step in copper delivery to the CuB site is an IM localized transmembrane protein with a single N-terminal transmembrane helix and a soluble C-terminal IMS domain (Hiser et al., 2000). Yeast COX11 forms a homodimer, which can bind two copper ions through the cysteines in its metal binding CFCF motif (Carr et al., 2002). Recently, Cox19, a soluble twin $Cx_9C$-motif containing protein localized to the IMS, was also identified to be involved in $Cu_B$ site maturation (Bode et al., 2015). Cox19 interacts with Cox11 in a dynamic manner and its accumulation in the mitochondria depends on its interaction with Cox11 (Bode et al., 2015). Cox19 binds to Cox11 that has its cysteine residues in an oxidized state, resulting in redox-regulated interplay of Cox19 and Cox11 in $Cu_B$ site maturation (Bode et al., 2015).

**Uptake and subcellular distribution of copper**

In eukaryotes, copper enters the cell through copper transporter CTR1, which is localized in the plasma membrane (Dancis et al., 1994). CTR1 assembles into a homotrimer, creating an ion pore, which selectively transports copper across the plasma membrane into the cytoplasm (De Feo et al., 2009). Copper that has been delivered into

**Table 1.1 Proteins involved in the copper delivery pathway to CcO.**

| Protein | Organism | Method | Copper binding motif | Metal binding | Structure (PDB) | Reference |
|---|---|---|---|---|---|---|
| SCO1 | Human | Solution NMR | $Cx_3C$ | Apo | 1WP0 | Williams et al. 2005 |
| Sco1 | Yeast | X-Ray Diffraction | $Cx_3C$ | Apo | 2B7K | Abajian et al., 2006 |
| Sco1 | Yeast | X-Ray Diffraction | $Cx_3C$ | Copper bound | 2B7J | Abajian et al., 2006 |
| SCO1 | Human | Solution NMR | $Cx_3C$ | Apo | 2GVP | Banci et al., 2006 |
| SCO1 | Human | X-Ray Diffraction | $Cx_3C$ | Nickel bound | 2GGT | Banci et al., 2006 |
| SCO1 | Human | Solution NMR | $Cx_3C$ | Copper bound | 2GT6 | Banci et al., 2006 |
| SCO1 | Human | Solution NMR | $Cx_3C$ | Nickel bound | 2GQL | Banci et al., 2006 |
| SCO1 | Bacillus subtilis | Solution NMR | $Cx_3C$ | Apo | 1ON4 | Balatri et al., 2003 |
| SCO1 | Thermus Thermophilus | Solution NMR | $Cx_3C$ | Apo | 2K6V | Abriata et al., 2008 |
| SCO2 | Human | Solution NMR | $Cx_3C$ | Copper bound | 2RLI | Banci et al., 2007a |
| COX17 | Yeast | Solution NMR | $Cx_3C$ | Apo | 1U97 | Abajian et al., 2004 |
| COX17 | Human | Solution NMR | $Cx_3C$ | Copper bound | 1U96 | Abajian et al., 2004 |
| Cox17 | Yeast | Solution NMR | $Cx_3C$ | Apo | 1Z2G | Arnesano et al., 2005 |
| COX17 | Human | Solution NMR | $Cx_3C$ | Apo | 2RN9 | Banci et al., 2008b |
| COX17 | Human | Solution NMR | $Cx_3C$ | Copper bound | 2RNB | Banci et al., 2008b |
| Cox11 | Rhizobium meliloti | Solution NMR | CFCF | Apo | 1SP0 | Banci et al., 2004 |

the cytoplasm is either bound by glutathione (GSH) or is directly picked up by copper chaperones, which can deliver copper to their specific target proteins (Kim et al., 2008). For example, the cytosolic chaperone ATOX1 delivers copper to the Golgi compartment via the P-type ATPases -ATP7A and ATP7B. These ATPases are localized to the trans-Golgi network (TGN), where they pump copper into the lumen of the TGN to facilitate its insertion into copper-dependent enzymes of the secretory pathway (Vulpe et al., 1993, Petrukhin et al., 1994, Klomp et al., 1997). Another cytosolic chaperone, CCS, delivers copper specifically to copper/zinc superoxide dismutase (SOD1) (Culotta et al., 1997). Notably, these pathways of organelle- and protein-specific copper delivery are highly conserved. For example, the yeast homolog of human ATOX1 is Atx1 and CCS is Ccs1.

Unlike copper delivery to the Golgi compartment, copper delivery to the mitochondria is not well characterized. According to the current model, copper enters the mitochondria bound to a non-proteinaceous ligand (Cobine et al., 2004). The identity of this copper ligand has remained a mystery even 15 years after its discovery (Cobine et al., 2004, Cobine et al., 2006). The copper-ligand (Cu-L) is transported across the IM into the mitochondrial matrix via Pic2 or Mrs3, where it is stored (Vest et al., 2013; Vest et al., 2016). Indirect experimental evidence suggests that this matrix localized Cu-L pool is used for metallation of COX1 and COX2 subunits (Cobine et al., 2006).

**Diseases of copper metabolism**

Copper is an essential cofactor for many enzymes involved in vital cellular functions, including mitochondrial respiration, iron acquisition, reactive oxygen species (ROS) scavenging, melanin synthesis, neuropeptide maturation, blood coagulation, and

connective tissue maturation (Kim et al., 2008). Most of these cuproenzymes harness the redox active nature of copper, i.e. its ability to rapidly cycle between its $Cu^{2+}$ and $Cu^{+}$ redox states. The same redox active nature of copper makes it highly toxic when unbound because it can undergo fenton-like reactions, producing ROS and damaging the cells (Jomova et al., 2011). Therefore, living organisms tightly regulate cellular copper levels with almost zero free copper in the cytoplasm (Rae et al., 1999). A total of 2 to 3 mg of copper uptake is recommended daily, which most adults obtain through food consumption (Chambers et al., 2010). Uptake of copper into the cells takes place through CTR1, which is expressed in most tissues, including the apical membrane of intestinal cells (Nose et al., 2006). A P-type copper ATPase, ATP7A, is trafficked to the basolateral membrane of intestinal enterocytes to pump copper from into the blood (Monty et al., 2005). Genetic mutations in *ATP7A* results in Menkes disease, leading to copper accumulation in enterocytes and copper deficiency in almost all organs of the body, including the brain (Danks et al., 1972). Therefore, the loss of ATP7A function results in copper deficiency not only in the proteins that receive copper in the trans-golgi network, including lysyl oxidase, dopamine β-hydroxylase, and tyrosinase, but also in cytochrome *c* oxidase, the most critical enzyme for cellular respiration (Maehara et al., 1983). Patients with Menkes disease suffer from copper deficiency in the brain, skeletal muscle, and heart, resulting in CcO deficiency in these organs (Maehara et al., 1983, Kodama et al., 1989). Menkes patients often suffer from neurological abnormalities, mental retardation and connective tissue disorders (Kodama et al., 1999). Another important P-type copper ATPase ATP7B, is expressed specifically in hepatocytes, where it regulates release of stored copper

(Bingham et al., 1998). Loss-of-function mutations in the *ATP7B* gene results in Wilson disease, an autosomal recessive disorder leading to accumulation of copper mainly in the liver and brain (Gow et al., 2000).

In addition to the Menkes and Wilson's diseases, mutations in the mitochondrial copper chaperones or assembly factors involved in the delivery of copper to cytochrome *c* oxidase, results in mitochondrial disorders. For example, Valnot *et al.* reported four patients with compound heterozygous mutations in the *SCO1* gene, which resulted in a mitochondrial disease due to CcO deficiency (Valnot et al. 2000a). *SCO1* patients display neurological disorders, hypertrophic cardiomyopathy, encephalopathy and lactic acidosis (Valnot et al. 2000a, Leary et al., 2013a). Similarly, patients with mutations in the *SCO2* display CcO deficiency leading to fatal infantile cardioencephalomyopathy (Papadopoulou et al., 1999, Jaksch et al., 2000). Along with the most prevalent E140K mutation in *SCO2*, new compound heterozygous mutations were reported by Verdijk et al. (2008) and more recently by Tran-Viet et al. (2013) in patients who showed cardiac and vision anomalies (Verdijk et al., 2008; Tran-Viet et al., 2013). The bases of the clinical heterogeneity of ubiquitously expressed proteins *SCO1* and *SCO2*, both of which participate in copper metallation of CcO, remain elusive.

Besides SCO1 and SCO2, COA6 is also a protein involved in copper delivery to CcO, and mutations in it result in mitochondrial disease. Two patients have been reported with COA6 mutations, one with compound heterozygous mutations (W59C, E87X) and another with a homozygous missense mutation (W66R), both result in CcO

deficiency and the infantile cardioencephalomyopathy (Calvo et al., 2012, Baertling et al., 2015).

**Therapeutic approaches for the treatment of copper deficiency disorders**

Copper deficiency disorders are often the result of inherited or acquired mutations in copper trafficking proteins. As mentioned in the previous section, mutations in SCO1, SCO2, and COA6, all proteins involved in the copper delivery to CcO result in rare mitochondrial disorders (Baertling et al., 2015; Papadopoulou et al., 1999; Valnot et al., 2000). It has been shown that exogenous copper supplementation rescues CcO deficiency in SCO2 patient myoblast cells (Jaksch et al., 2001) as well as in *coa6Δ* yeast cells and COA6 human patient fibroblasts (Baertling et al., 2015; Ghosh et al., 2014). Taken together, these findings suggest that restoration of copper delivery to mitochondria could restore CcO activity by bypassing SCO2 and COA6 functions. However, the use of direct copper supplementation, i.e., subcutaneous injections of copper-histidine, as a therapeutic agent was not successful in a patient with a SCO2 mutation (Freisinger et al., 2004). Even though this treatment partially rescued hypertrophic cardiomyopathy, it failed to rescue other clinical outcomes or survival of the patient (Freisinger et al., 2004). Therefore, there is a need for pharmacological agents that can bind copper and deliver it into cells to restore copper homeostasis more efficiently. Such agents could be used as human therapeutics for copper deficiency. In this regard, copper ionophores can be used to transport copper across biological membranes to bypass physiological barriers and reestablish copper homeostasis.

# CHAPTER II

# ELESCLOMOL RESTORES MITOCHONDRIAL FUNCTION IN GENETIC MODELS OF COPPER DEFICIENCY*

## Disclaimer

Chapter II is a reprint of a paper published in the journal *PNAS* for which I am the first author. I performed all the experimental work described in this chapter except for the following figures. Haarin Chun at the Department of Animal and Avian Sciences, University of Maryland, College Park performed experiments described in Figure 2.8 A-C. Dr. Andrew J. Latimer, Eugene Bell Center for Regenerative Biology and Tissue Engineering, Marine Biological Laboratory, Woods Hole, performed experiments described in Figure 2.10 and 2.11. Jennifer J. Rahn, Department of Drug Discovery and Biomedical Sciences, Medical University of South Carolina, performed experiments described in the Figure 2.12. I also greatly appreciate the help of Shrishiv Timbalia and Alison Vicary, of the Department of Biochemistry and Biophysics at Texas A&M University, in performing yeast growth assays described in Figure 2.3 and Figure 2.1 and 2.2, respectively.

---

*This chapter is adapted from the work which was originally published in Proceedings of the National Academy of Sciences of the United States of America. Soma S, Latimer AJ, Chun H, Vicary AC, Timbalia SA, Boulet A, Rahn JJ, Chan SSL, Leary SC, Kim BE, Gitlin JD, Gohil VM. Elesclomol restores mitochondrial function in genetic models of copper deficiency. *Proc Natl Acad Sci U S A*. 2018; 115(32):8161-8166. Copyright (2018) National Academy of Sciences.

**Summary**

Copper is an essential cofactor of cytochrome *c* oxidase (CcO), the terminal enzyme of the mitochondrial respiratory chain. Inherited loss-of-function mutations in several genes encoding proteins required for copper delivery to CcO result in diminished CcO activity and severe pathology in affected infants. Copper supplementation restores CcO function in patient cells with mutations in two of these genes, *COA6* and *SCO2,* suggesting a potential therapeutic approach. However, direct copper supplementation has not been therapeutically effective in human patients, underscoring the need to identify highly efficient copper transporting pharmacological agents. Utilizing a candidate-based approach, we identified an investigational anti-cancer drug, elesclomol (ES), that rescues respiratory defects of *COA6* deficient yeast cells by increasing mitochondrial copper content and restoring CcO activity. ES also rescues respiratory defects in other yeast mutants of copper metabolism, suggesting a broader applicability. Low nanomolar concentrations of ES reinstate copper-containing subunits of CcO in a zebrafish model of copper deficiency and in a series of copper deficient mammalian cells, including those derived from a *SCO2* patient. These findings reveal that ES can restore intracellular copper homeostasis by mimicking the function of missing transporters and chaperones of copper, and may have potential in treating human disorders of copper metabolism.

## Introduction

Copper is an essential micronutrient required for the assembly and activity of cytochrome *c* oxidase (CcO), the terminal enzyme of the mitochondrial respiratory chain that catalyzes the reduction of molecular oxygen and drives mitochondrial energy production (Smith et al., 2017; Timon-Gomez et al., 2018). CcO is a highly conserved, multimeric inner mitochondrial membrane protein complex that has two copper-containing subunits, Cox1 and Cox2, which together form its catalytic core (Timon-Gomez et al., 2018). Copper delivery to mitochondria and its insertion into these copper-containing subunits is an intricate process that requires multiple metallochaperones and ancillary proteins (Smith et al., 2017). Failure to deliver copper to Cox1 and Cox2 disrupts CcO assembly and results in a respiratory deficiency.

Cytosolic copper is delivered to the mitochondrial matrix via the recently identified yeast protein Pic2 (Vest et al., 2013), where it is stored in a ligand bound form (Cobine et al., 2004). This mitochondrial matrix copper pool is the main source of copper ions that are inserted into the CcO subunits in the mitochondrial inter-membrane space (IMS) (Cobine et al., 2004). Mobilization of copper from the mitochondrial matrix to the IMS for its delivery to copper sites in CcO subunits requires a number of evolutionarily conserved proteins (Baker et al., 2017). The precise molecular functions of these proteins have remained unsolved, except for the metallochaperones Cox17, Sco1, Sco2 and Cox11, which have been shown to transfer copper to CcO subunits in a bucket-brigade fashion (Baker et al., 2017). Specifically, Cox17 receives copper from the mitochondrial matrix and transfers it to Cox11 and Sco1/Sco2 (Horng et al., 2004), which then metallate copper

sites on Cox1 and Cox2, respectively (Hiser et al., 2000; Leary et al., 2004). Recently two other proteins, Coa6 and Cox19, have also been shown to be part of this copper delivery pathway in the IMS (Bode et al., 2015; Ghosh et al., 2016; Pacheu-Grau et al., 2015; Stroud et al., 2015).

In humans, inherited partial loss-of-function mutations in SCO1, SCO2 and COA6 result in a CcO deficiency and are associated with hepatopathy, metabolic acidosis, cardiomyopathy and neurological defects in affected patients (Baertling et al., 2015; Papadopoulou et al., 1999; Valnot et al., 2000). Copper supplementation rescues CcO deficiency in myoblasts from patients with mutations in SCO2 (Jaksch et al., 2001) and restores CcO activity in COA6 deficient yeast and human patient cell lines (Baertling et al., 2015; Ghosh et al., 2016), suggesting that efficient delivery of copper to mitochondria could restore CcO activity by bypassing SCO2 and COA6 functions. In an attempt to translate these observations in a clinical setting, subcutaneous injections of copper-histidine were administered to a patient with a SCO2 mutation. While copper supplementation improved the patient's hypertrophic cardiomyopathy, it did not improve other clinical outcomes or survival (Freisinger et al., 2004). Thus, a more effective mechanism for restoration of copper homeostasis will be required for human therapeutics. This study employed yeast *coa6Δ* cells to identify compounds that can efficiently transport copper across biological membranes and restore mitochondrial respiratory chain function over a broad range of concentrations. This approach identified elesclomol (ES), which was shown to re-establish subcellular copper homeostasis in copper deficient cells, highlighting its therapeutic potential for human diseases of copper metabolism.

**Results**

A targeted search for copper-binding agents identifies elesclomol as the most potent pharmacological agent in rescuing respiratory defects of yeast *coa6Δ* cells

We tested a number of copper-binding pharmacological agents (Helsel and Franz, 2015) for their ability to rescue respiratory deficient growth of *coa6Δ* cells. Among all the compounds tested, ES was unique in that it rescued respiratory growth at low nanomolar concentrations without exhibiting overt toxicity over a broad range of concentrations (Fig. 2.1). ES rescued the respiratory growth of *coa6Δ* cells with an $ED_{50}$ of 0.8 nM (Fig. 2.2). ES-mediated growth rescue of *coa6Δ* cells was also observed on solid growth medium containing a non-fermentable carbon source (Fig. 2.3A). Consistent with the rescue of respiratory growth, ES supplementation restored the oxygen consumption rate of *coa6Δ* cells to that of wild type cells (Fig. 2.3B). To determine the biochemical basis for the observed respiratory rescue of *coa6Δ* cells, we measured the assembly and activity of CcO-containing mitochondrial respiratory chain supercomplexes by native-polyacrylamide gel electrophoresis blotting and in-gel activity assay, respectively. ES supplementation restored the abundance and activity of CcO-containing supercomplexes to near wild type levels (Fig. 2.3C-F). We next tested the efficacy of ES to rescue *COA6* mutations observed in human patients by heterologous expression of yeast-human chimeric proteins with patient mutations (W26C, W33R and E54X) in yeast *coa6Δ* cells (Fig. 2.4A). Similar to *coa6Δ* cells, 10 nM ES or 10 μM copper supplementation rescued yeast *coa6Δ* cells expressing patient mutations (Fig. 2.4B). These results show that ES is

at least 1000 times more potent than copper in rescuing the respiratory growth defect of yeast *coa6Δ* cells.

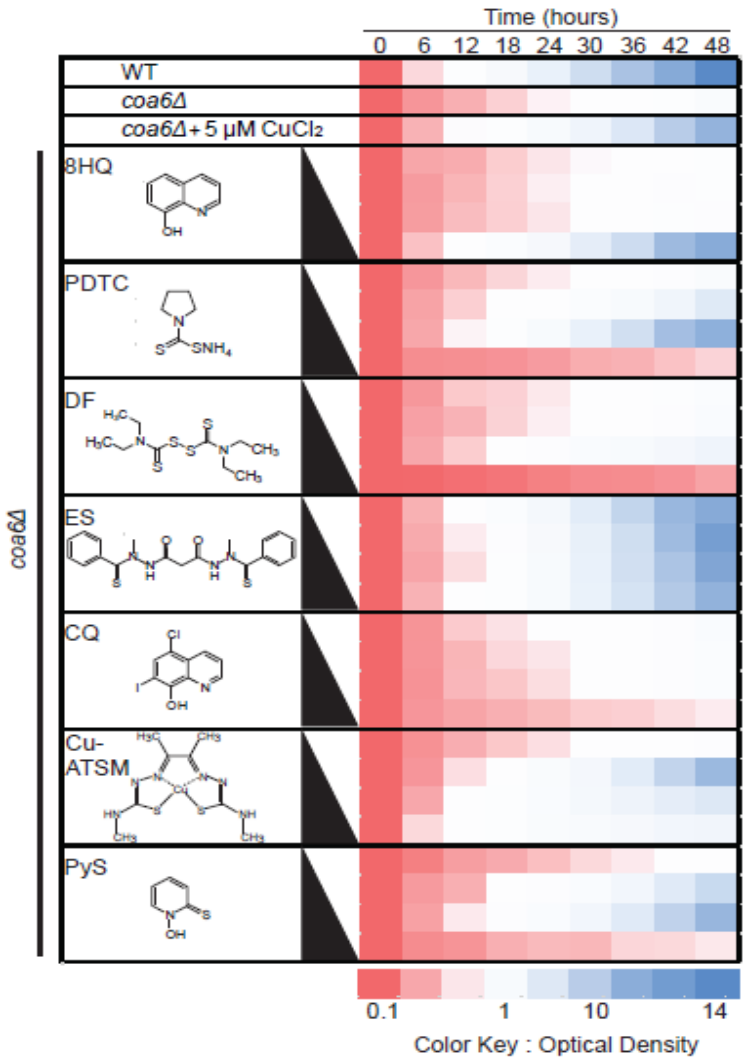


**Figure 2.1 A comparative analysis of copper binding agents identifies ES as the most potent pharmacological agent in rescuing respiratory growth deficiency of yeast *coa6Δ* cells.**

The respiratory growth of *coa6Δ* cells in YPGE supplemented with either 5µM copper chloride ($CuCl_2$) or with increasing concentrations (10nM to 10µM) of 8-hydroxyquinoline (8HQ), ammonium pyrrolidine dithiocarbamate (PDTC), disulfiram (DF), elesclomol (ES), clioquinol (CQ), diacetylbis(N(4)-methylthiosemicarbazonato) copper (II) (Cu-ATSM), and pyrithione (PyS) was measured at 37°C at the indicated time points. The data are representative of two independent measurements.

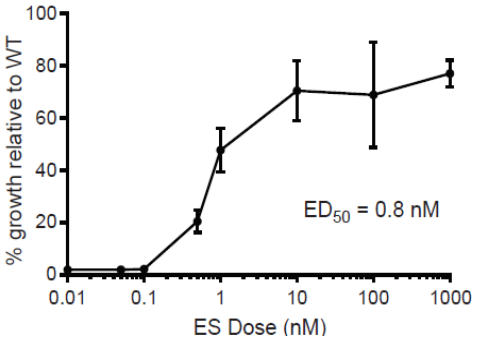


**Figure 2.2 Determination of the median effective dose ($ED_{50}$) of elesclomol.**
Yeast *coa6Δ* cells were cultured in YPGE medium at 37°C in the presence of increasing concentrations (0.01nM to 1µM) of ES. The cell density was measured spectrophotometrically after 58 hours of growth at 600nm. The data represent the average ± SD from three independent measurements.

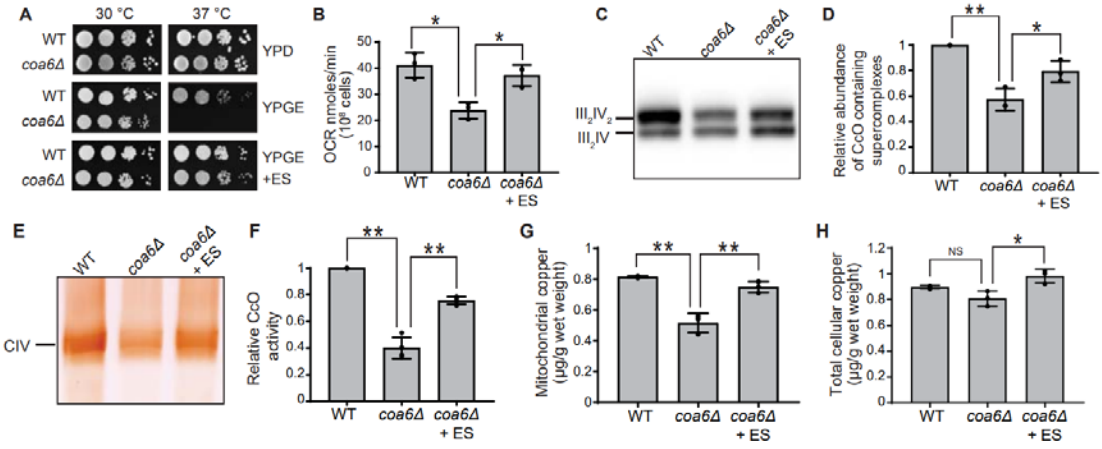


**Figure 2.3 ES supplementation rescues CcO assembly defects by restoring mitochondrial copper levels of *coa6Δ* cells.**
(A) Serially diluted wild type (WT) and *coa6Δ* cells were seeded on the indicated plates and incubated at 30°C and 37°C for 2 days (YPD) or 4 days (YPGE) before imaging. (B-F) WT, *coa6Δ* and *coa6Δ* cells supplemented with 20 nM ES were cultured in YP galactose medium until early stationary growth phase followed by - (B) oxygen consumption rate (OCR) measurement, (C) BN-PAGE/Western analysis of mitochondrial respiratory chain super complexes containing Complex IV (CIV, also called CcO), (D) Quantification of super complexes, (E) in-gel activity staining for Complex IV, (F) Quantification of CcO activity, (G) mitochondrial copper levels and (H) total cellular copper content. Error bars represent mean ± SD (n=3, two-tailed unpaired Student's t-test *p< 0.05, **p< 0.005). Data shown in (A, C and E) are representative of at least three independent experiments.

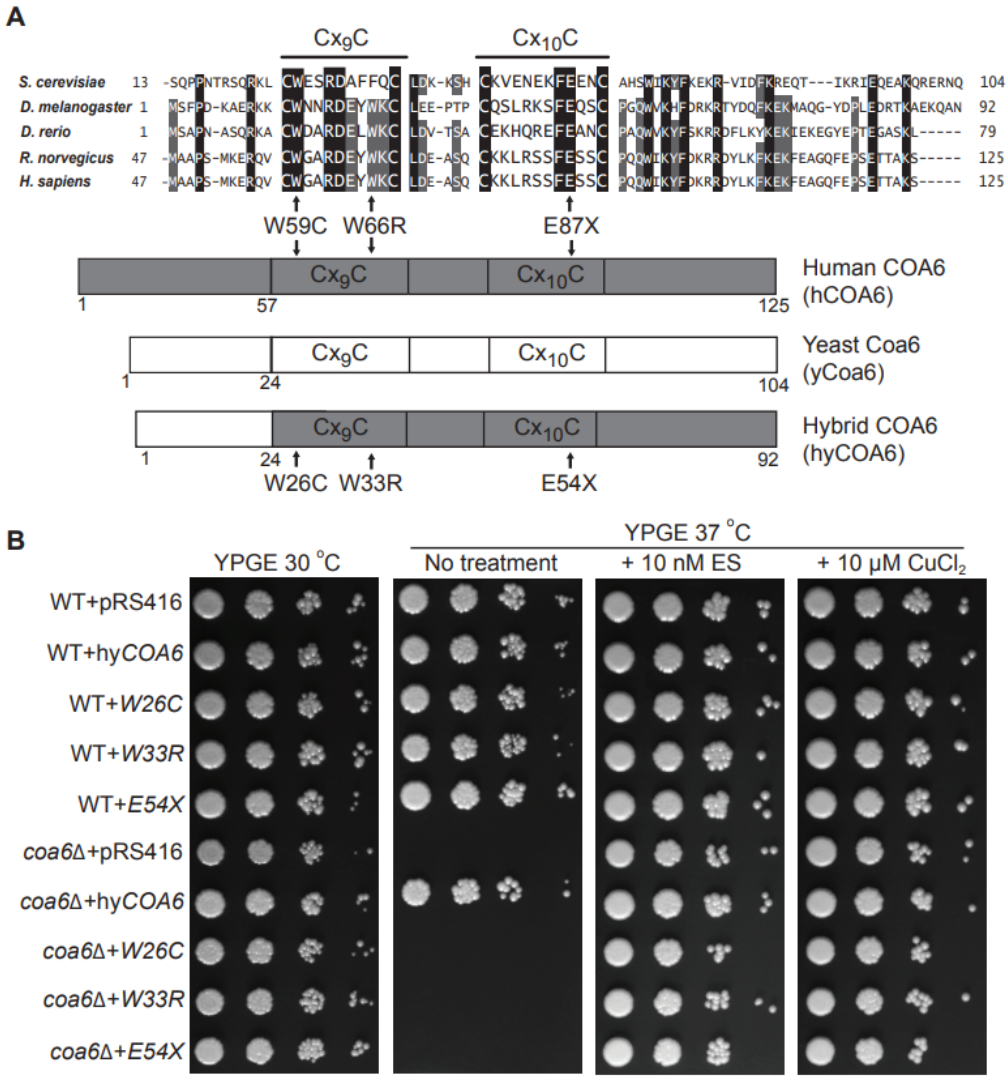


**Figure 2.4 ES supplementation restores respiratory growth of yeast cells expressing pathogenic *COA6* variants.**

(A) Sequence alignment of the conserved region of COA6 across indicated model organisms. Horizontal lines above $Cx_9C$ and $Cx_{10}C$ residues show the conserved $Cx_9Cx_nCx_{10}C$ motif. Schematic representation of yeast-human hybrid (hyCOA6) protein, where the sequence from yeast Coa6 is shown in white, and the sequence from human COA6 is shown in gray. Arrows indicate amino acid residues that were mutated in human COA6 patients and the corresponding residues in the hyCOA6 protein. (B) WT and *coa6Δ* cells transformed with pRS416 empty vector or pRS416 vector expressing either hyCOA6 or hyCOA6 harboring patient mutations (W26C, W33R and E54X) were serially diluted and seeded on YPGE plates alone or those supplemented with either 10 nM ES or 10 µM copper chloride. Images were taken after 3 days for cells grown at 30°C and 5 days for cells grown at 37°C.

A previous study has shown that ES scavenges copper from the culture medium, enters the cell as an ES-copper complex, and selectively accumulates in mitochondria where it dissociates from copper (Nagai et al., 2012). Consistent with this concept, we observed an almost complete rescue of mitochondrial copper levels in *coa6Δ* cells supplemented with ES (Fig. 2.3G). ES supplementation also moderately increased total cellular copper levels (Fig. 2.3H). To further corroborate that ES increases mitochondrial copper levels by actively transporting extracellular copper into the cells, we decreased copper availability in the extracellular compartment by co-treatment with ES and a known copper chelator, bathocuproine disulfonate (BCS). As expected, BCS treatment resulted in reduced respiratory growth of wild type cells, which was rescued by co-treatment with ES, suggesting that ES is also able to overcome pharmacological copper deficiency by outcompeting BCS (Fig. 2.5A). Moreover, ES mediated rescue of *coa6Δ* was diminished in the presence of BCS (Fig. 2.5B). To determine whether ES is able to bypass a mitochondrial copper transporter, Pic2, we performed ES supplementation in *pic2Δ* and *coa6Δpic2Δ* cells. Although under the conditions tested we did not observe a respiratory growth defect of *pic2Δ* cells, ES did rescue *coa6Δpic2Δ* cells, suggesting that this compound can deliver copper to the mitochondria independent of Pic2 function (Fig. 2.5C). These results imply that ES mediated rescue of CcO function is driven by its ability to transport extracellular copper to the mitochondria of *coa6Δ* cells.

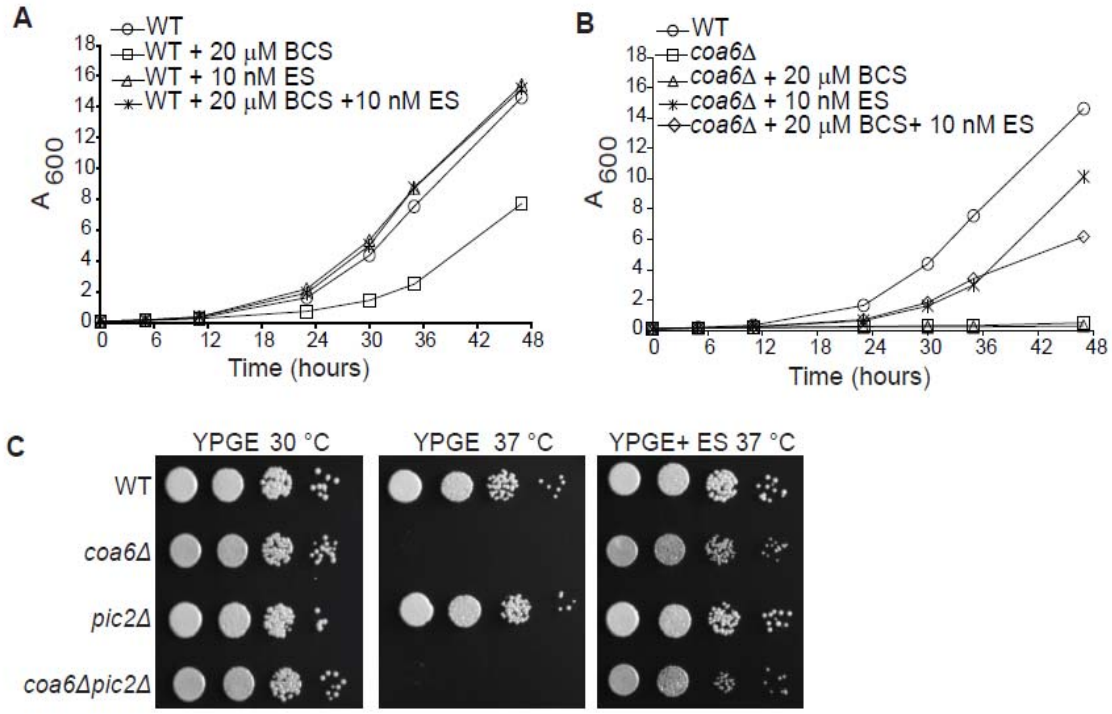


**Figure 2.5 Elesclomol rescue of respiratory growth of *coa6Δ* cells is dependent on copper availability but is independent of Pic2, a putative mitochondrial copper transporter.**
(A) BY4741 wild type (WT) and (B) *coa6Δ* cells were cultured in YPGE medium at 37 °C in the presence of 10nM ES, 20μM of the copper chelator bathocuproine disulfonic acid (BCS), or a combination of both. The cell density was measured spectrophotometrically at the indicated time points at 600nm. The data are representative of two independent experiments. (C) Serially diluted WT, *coa6Δ, pic2Δ, and coa6Δpic2Δ* double mutants were seeded on YPGE plates with and without 10nM ES supplementation and incubated at the indicated temperatures for 4 days before imaging. The data are representative of two independent experiments.

ES rescues many different yeast mutants with impaired copper metabolism

To test the specificity of ES mediated rescue, we shortlisted a number of yeast mutants of genes required for maintaining cellular and mitochondrial copper homeostasis (Baker et al., 2017; Smith et al., 2017; Timon-Gomez et al., 2018). We prioritized genes based on their evolutionary conservation, presence of pathogenic mutations in humans

and/or the existence of a related mouse phenotype (Fig. 2.6A). These yeast mutants showed a pronounced respiratory deficient growth phenotype in non-fermentable media at 37°C after two days of growth, which became less evident after four days of growth (Fig. 2.6B). Most of the yeast mutants were rescued with ES supplementation, albeit to different degrees, reflecting their distinct roles in cellular and mitochondrial copper homeostasis (Fig. 2.6B). ES failed to rescue *sco1Δ* cells, possibly because of the specific role of Sco1 as a metallochaperone in inserting copper into the Cox2 subunit of CcO (Fig. 2.6). We noticed that a higher concentration of ES is required to rescue *ctr1Δ* cells (Fig. 2.7), which is consistent with the severe reduction in copper levels in cells lacking Ctr1 (Lee et al., 2001). Overall, these results suggest the broad applicability of ES in ameliorating defects of cellular and mitochondrial copper homeostasis.

A

| Yeast gene | Human gene | Role in copper metabolism | Clinical phenotypes of human disease or animal model (OMIM) |
|---|---|---|---|
| *COA6* | *COA6* | Required for copper delivery to COX2 | Fatal infantile cardioencephalomyopathy (614772) |
| *SCO1* | *SCO1* | Transfer of copper to $Cu_A$ site in COX2 | Neonatal hepatopathy and hypertrophic cardiomyopathy (603644) |
| *SCO2* | *SCO2* | Oxidoreductase required for copper transfer to COX2 | Neonatal encephalo-cardiomyopathy (604272) |
| *COX12* | *COX6B1* | Cytochrome c oxidase subunit | Encephalomyopathy and hypertrophic cardiomyopathy (124089) |
| *CTR1* | *CTR1* | High-affinity copper transporter | *Ctr1*$^{-/-}$ mice are embryonic lethal (603085) |
| *ATX1* | *ATOX1* | Delivery of cytosolic copper to ATP7A and ATP7B | Failure to thrive and increased perinatal mortality in *Atox1*-null mice (602270) |
| *CCS1* | *CCS* | Copper delivery to Cu/Zn SOD | Congenital cataracts, hearing loss, and neurodegeneration (603864) |
| *GSH1* | *GSX1* | Catalyzes the first step in glutathione biosynthesis | Growth retardation and infertility in *Gsh1*-null mice (616542) |
| *CCC2* | *ATP7A*<br>*ATP7B* | Copper transporting P-type ATPase | Menkes disease, occipital horn syndrome and spinal muscular atrophy (300011)<br>Wilson disease - liver disease and neurological defects (606882) |
| *GEF1* | *CLCN5*<br>*CLCN7* | Voltage-gated chloride channel | Dent disease - chronic kidney failure (300008)<br>Osteopetrosis - bone defect (602727) |

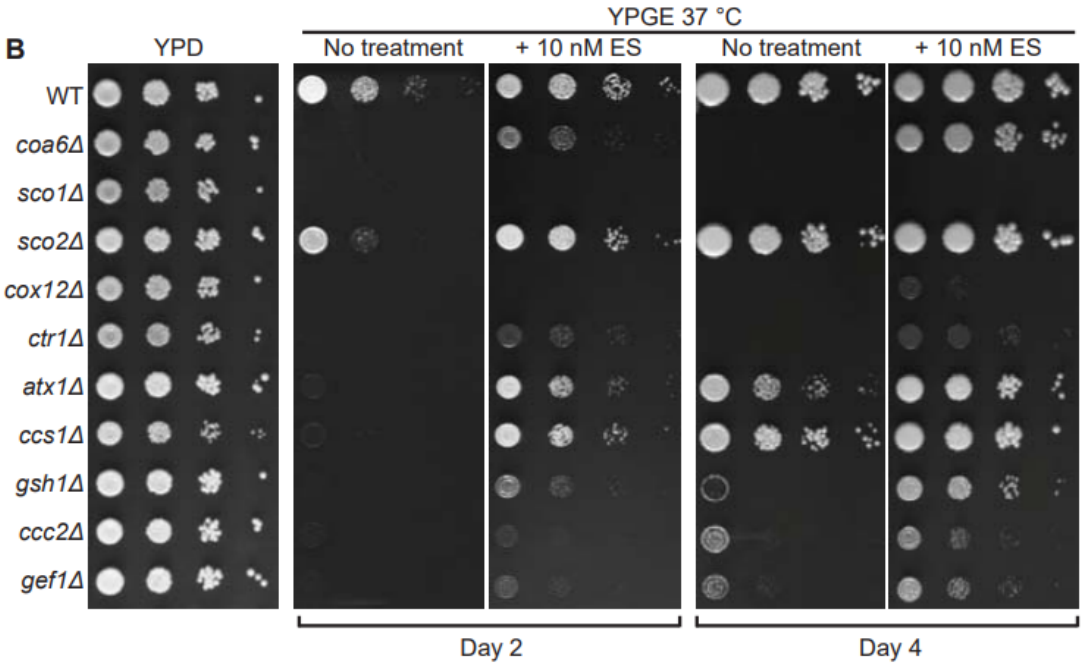


**Figure 2.6 ES can rescue the respiratory growth deficiency of yeast mutants of copper metabolism.**
(A) List of yeast genes and their human orthologs implicated in cellular and mitochondrial copper metabolism, and the clinical phenotypes associated with mutations in the human or murine genes. (B) Serially diluted WT cells and the indicated mutants were spotted on YPD, YPGE, and YPGE supplemented with 20 nM of ES. The plates were incubated at 37°C and allowed to grow for 2 days (YPD) or 2 & 4 days (YPGE) before imaging.

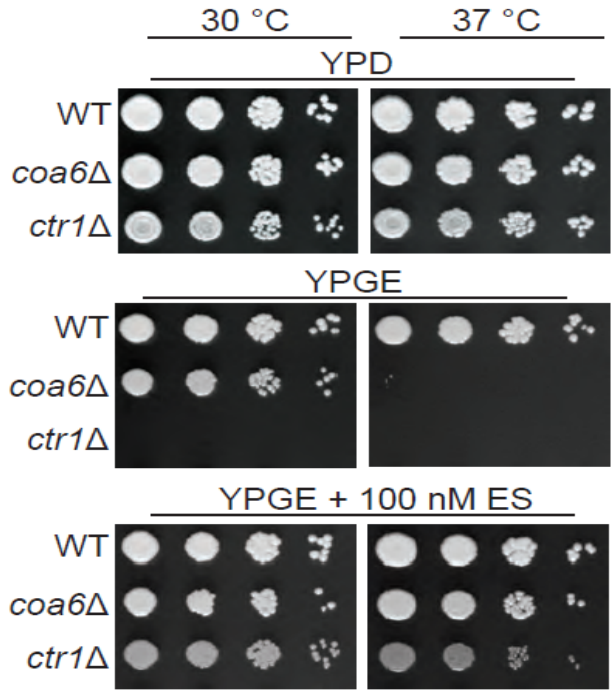


**Figure 2.7 Respiratory growth rescue of *ctr1Δ* cells is more pronounced with 100 nM elesclomol supplementation.**
Serially diluted WT, *coa6Δ*, and *ctr1Δ* cells were cultured under the indicated growth conditions for 4 days before imaging. The data are representative of three independent experiments.

ES supplementation rescues levels of CcO subunits in mammalian cell lines with genetic defects in copper metabolism

To expand upon our findings in yeast and to test the efficacy of ES in mammalian cell culture models of copper deficiency, we constructed a *Ctr1* knockout rat H9c2 cardiomyocyte cell line by CRISPR/Cas9. The *Ctr1*$^{-/-}$ cell line was validated by demonstrating the loss of Ctr1 protein (Fig. 2.8A). As expected, the loss of Ctr1 led to a ~4-fold decrease in the levels of intracellular copper (Fig. 2.8B) and a concomitant reduction in the levels of the CcO subunit COX4 (Fig. 2.8C). Notably, *Ctr1*$^{-/-}$ cells exhibited elevated levels of CCS, the copper chaperone of SOD1, which is known to

increase during copper deficiency (Fig. 2.8C). We used this validated *Ctr1*$^{-/-}$ cell line to test the efficacy of ES in rescuing COX1, a copper-containing subunit of CcO. The loss of Ctr1 resulted in reduced levels of COX1 that were rescued by ES in a dose dependent manner (Fig. 2.8D). Similarly, we also observed a dose dependent rescue of COX1 levels in *Ctr1*$^{-/-}$ mouse embryonic fibroblasts (MEFs) (Fig. 2.8E) (Lee et al., 2002). However, we noticed ES toxicity at higher doses, which was reflected in reduced COX1 levels in control MEFs (Fig. 2.8E). Finally, we tested the efficacy of ES in rescuing CcO defects in *SCO2* patient fibroblasts that were previously shown to have a COX2 deficiency (Jaksch et al., 2001). Unlike copper supplementation, ES treatment was able to partially rescue the steady state levels of COX2 in a dose and time dependent manner (Fig. 2.8F). Notably, the ES toxicity occurs at a concentration 20X higher than the dose that rescued COX2 levels (Fig. 2.9A). Consistent with the known anti-carcinogenic activity of ES, we observed much more pronounced toxicity in immortalized cell lines (Fig. 2.9A) when compared to primary cultures of the same cell type (Fig. 2.9B). Together, these results suggest that a low nano-molar concentration of ES is efficacious in rescuing mitochondrial copper deficiency and restoring CcO levels in mammalian cell lines with genetic defects in copper homeostasis.

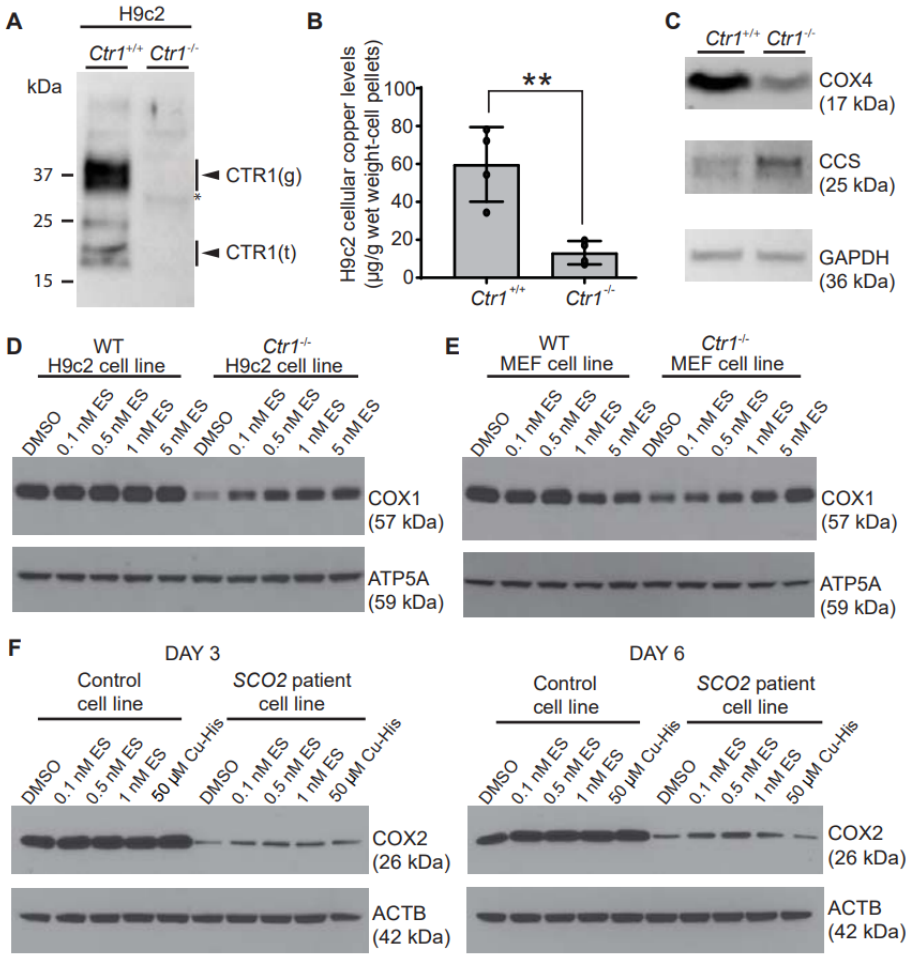


**Figure 2.8 ES supplementation rescues the steady state levels of copper-containing subunits of CcO in mammalian cell lines with genetic defects in copper metabolism**. (A)Immunoblot analysis of CTR1 in *Ctr1*$^{+/+}$ and *Ctr1*$^{-/-}$ H9c2 cells. The arrowheads labeled g and t indicate the full-length glycosylated and truncated forms of CTR1, respectively. (B) Total copper levels measured by ICP-MS in H9c2 cells. Data are presented as mean ± SD (n=4, two-tailed unpaired Student's t-test (*$p < 0.001$). (C) Immunoblot analysis of CCS, COX4 and GAPDH protein levels in *Ctr1*$^{+/+}$ and *Ctr1*$^{-/-}$ H9c2 cells. GAPDH serves as a loading control. (D) The *Ctr1*$^{+/+}$ and *Ctr1*$^{-/-}$ H9c2 rat cardiomyocytes and (E) mouse embryonic fibroblasts were cultured for 3 days with the indicated doses of ES followed by Western analysis of COX1 protein levels. ATP5A is used as loading control. (F) Control (MCH46) and *SCO2* patient cell lines were cultured for three or six days in the presence of the indicated concentrations of ES or a copper-histidinate (Cu-His) complex in DMEM with 10% FBS. The cellular COX2 levels were detected by SDS-PAGE/Western blot analysis. β actin (ACTB) was used as a loading control.

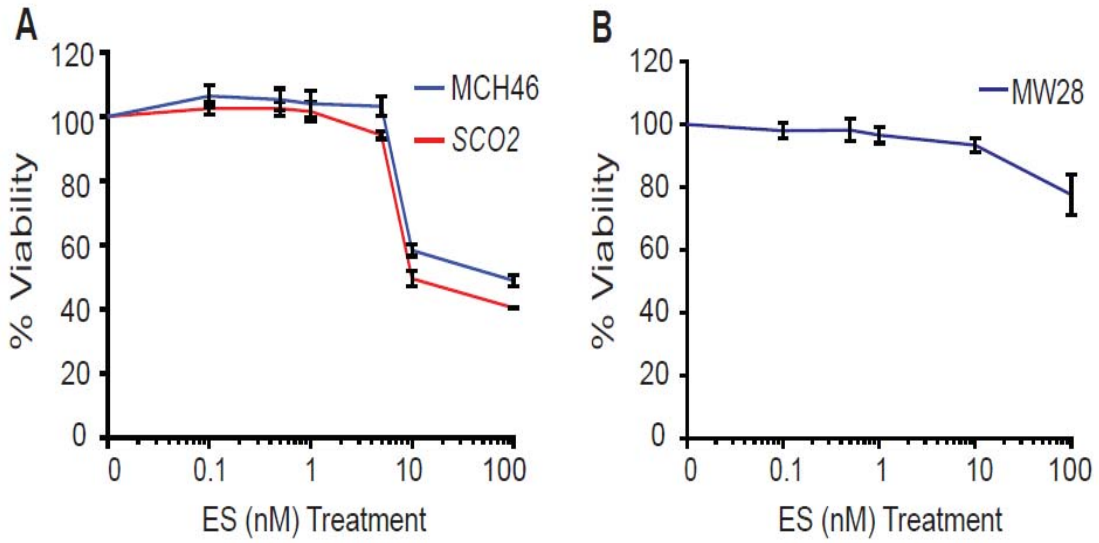


**Figure 2.9 Cell viability of immortalized and primary human fibroblasts cell lines treated with increasing concentrations of elesclomol.**
(A) Immortalized control (MCH46) and *SCO2* patient fibroblasts and (B) primary human skin fibroblasts (MW28) cultured in the DMEM glucose – containing media were treated with increasing concentrations of ES for 36 hours. Cell viability was measured by quantifying total cellular ATP levels by Cell-Titre GLo assay (Promega). Data are expressed as mean ± SD (n=3)

ES supplementation rescues copper deficiency phenotypes in zebrafish models

To determine whether ES can rescue phenotypes associated with copper deficiency in an intact developing vertebrate animal model, we utilized zebrafish embryos with a null mutation in the gene encoding the plasma membrane copper importer Ctr1. We chose zebrafish because of the ability to quickly monitor the pigmentation defect that arises due to the copper requirement of tyrosinase, an enzyme that catalyzes the critical step in melanin biosynthesis. Wild type zebrafish embryos have a characteristic melanin pigmentation pattern visible at 48 hours post fertilization (hpf) (Fig. 2.10A). To determine

if ES can rescue copper deficiency phenotypes in zebrafish, we incubated zebrafish embryos from heterozygous *Ctr1* crosses in 10 nM ES and compared these to untreated embryos. We found that the expected ~25% of untreated embryos from *Ctr1* heterozygous crosses lacked melanin deposition (16/59) (Fig. 2.10B), whereas all of the ES treated embryos from the same crosses were pigmented (49/49) (Fig. 2.10C). Similarly, we also observed rescue of the pigmentation defect at 100 nM ES but the equivalent dose of copper failed to rescue this defect (Fig 2.11). *Ctr1*$^{-/-}$ mutants also exhibited a CcO assembly defect likely due to mitochondrial copper deficiency. To determine whether ES can rescue the observed CcO assembly defect, we grew clutches of embryos from heterozygous *Ctr1* crosses in the presence of ES until 10 days post-fertilization (dpf) and measured levels of Cox1 in their mitochondrial extracts. Compared to wild type embryos, the *Ctr1*$^{-/-}$ mutants exhibited a severe reduction in Cox1 levels that was almost completely rescued by treatment with ES (Fig. 2.10D).

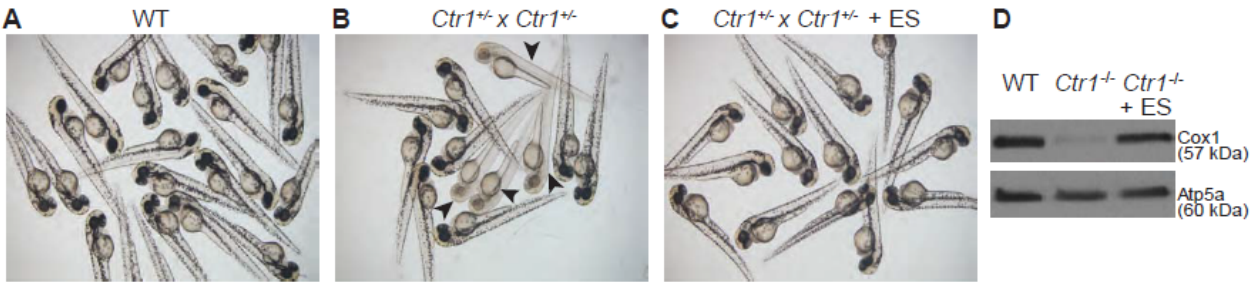


**Figure 2.10 ES supplementation rescues pigmentation and the Cox1 deficiency of Ctr1 knockout zebrafish.**
(A-C) Clutches of embryos from a WT zebrafish and from a cross of a pair of *Ctr1*$^{+/-}$ heterozygous zebrafish were imaged at 48hpf following treatment with and without 10 nM ES. Arrows in (B) indicate homozygous *Ctr1*$^{-/-}$ embryos with a pigmentation defect. (D) Mitochondria were isolated from 10-day post fertilization WT zebrafish and homozygous *Ctr1*$^{-/-}$ zebrafish treated with and without 10 nM ES. Mitochondrial samples were subjected to SDS-PAGE and immunoblotted using the Complex IV specific antibody anti-Cox1. The mitochondrial protein Atp5a was used as a loading control**.**

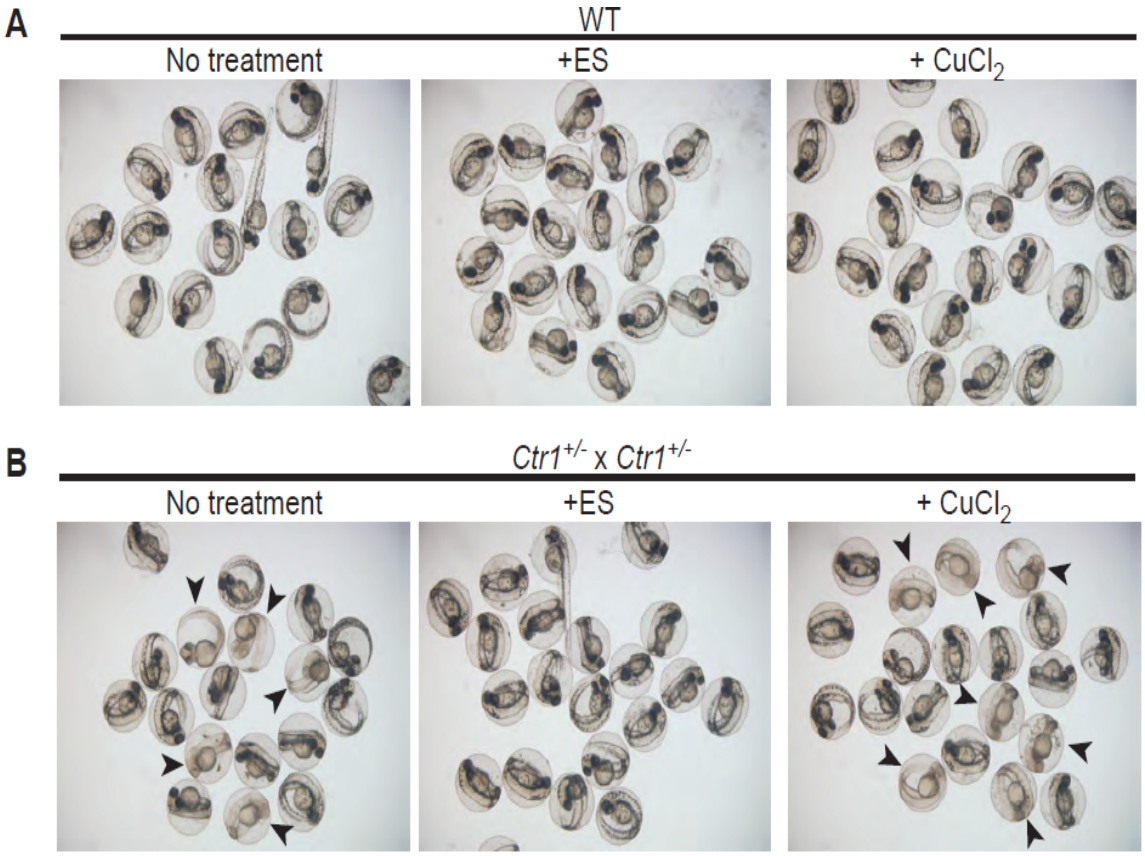


**Figure 2.11 ES supplementation rescues pigmentation of Ctr1 knockout zebrafish while equivalent concentration of copper fails to rescue this defect.**
**(**A) Clutches of embryos from a WT zebrafish and (B) from a cross of a pair of *Ctr1*$^{+/-}$ heterozygous zebrafish were imaged at 48hpf following treatment with and without 100 nM elesclomol (ES) or 100 nM copper chloride (CuCl2). Arrowheads in (B) indicate homozygous *Ctr1*$^{-/-}$ embryos with a pigmentation defect. Notably, not a single embryo with pigmentation defect was observed upon ES treatment.

To further establish the potential of ES to treat metabolic diseases involving defective copper delivery to the mitochondrion, we tested the efficacy of ES in rescuing phenotypes associated with *Coa6* knockdown in zebrafish embryos (Ghosh et al., 2014). First, we determined the maximal tolerable dose of ES for zebrafish embryos to be 100 nM (Fig. 2.12A). Consistent with the mechanism of action of ES, we observed that co-supplementation of 100 nM ES with 100 nM of copper resulted in 100% lethality (Fig.

2.12B). As shown previously, zebrafish embryos injected with the *zfcoa6* translation blocking morpholino exhibited pronounced morphological defects characterized by pericardial edema, smaller heads and eyes and curved tails (Ghosh et al., 2014). The severity of these phenotypes was scored at four different time points (24, 48, 72, and 96 hpf) (Fig. 2.12C) and we observed rescue with 100 nM ES treatment as early as 48 hpf (Fig. 2.12D). Given that one of the most striking features of Coa6 deficiency in this model is a pronounced cardiac edema and a decreased heart rate (Ghosh et al., 2014), we next determined whether ES treatment as able to rescue these phenotypes. Indeed, 100 nM ES treatment prevented pericardial edema and significantly increased the heart rate of Coa6 knockdown zebrafish embryos at both 72 and 96 hpf, without altering the heart rate of control embryos (Fig. 2.12E & F). These results demonstrate the efficacy of ES in rescuing phenotypes associated with copper deficiency in intact living vertebrate animals.

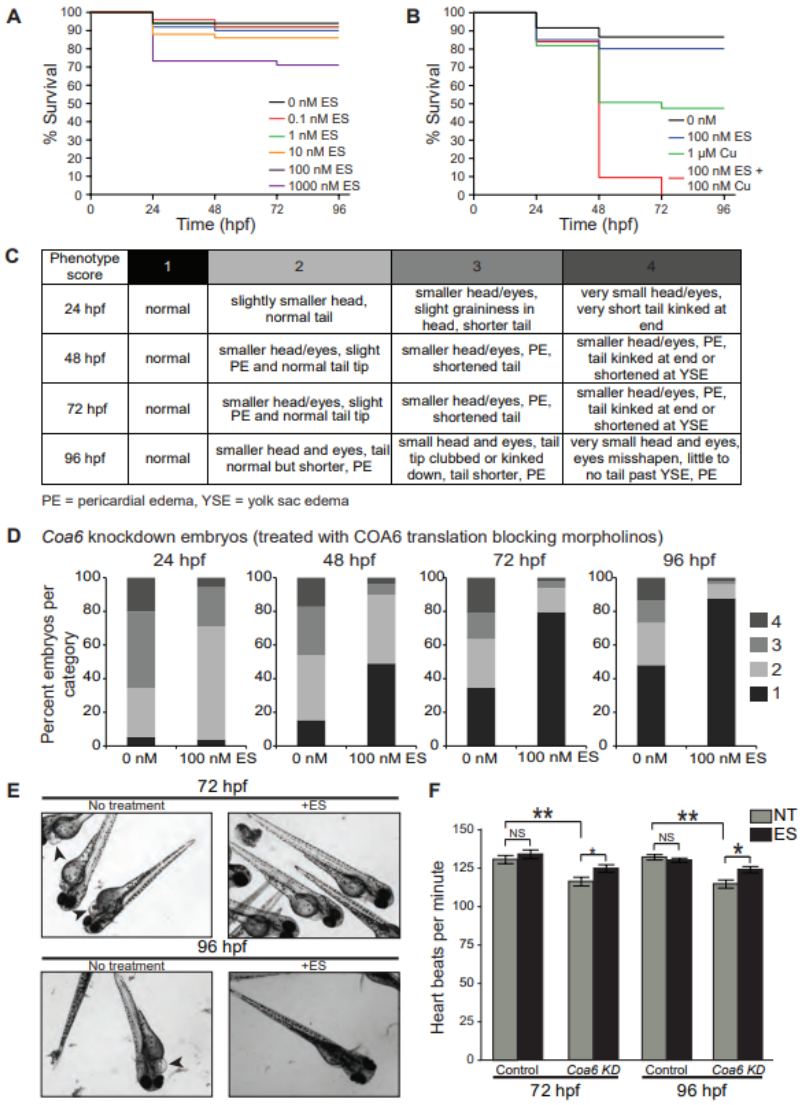


C

| Phenotype score | 1 | 2 | 3 | 4 |
|---|---|---|---|---|
| 24 hpf | normal | slightly smaller head, normal tail | smaller head/eyes, slight graininess in head, shorter tail | very small head/eyes, very short tail kinked at end |
| 48 hpf | normal | smaller head/eyes, slight PE and normal tail tip | smaller head/eyes, PE, shortened tail | smaller head/eyes, PE, tail kinked at end or shortened at YSE |
| 72 hpf | normal | smaller head/eyes, slight PE and normal tail tip | smaller head/eyes, PE, shortened tail | smaller head/eyes, PE, tail kinked at end or shortened at YSE |
| 96 hpf | normal | smaller head and eyes, tail normal but shorter, PE | small head and eyes, tail tip clubbed or kinked down, tail shorter, PE | very small head and eyes, eyes misshapen, little to no tail past YSE, PE |

PE = pericardial edema, YSE = yolk sac edema




**Figure 2.12 ES treatment improves morphological defects observed in Coa6 knockdown embryos.**

(A) Zebrafish embryos were treated with indicated concentrations of ES and (B) copper, and combination of both at 3 hours post fertilization (hpf). The surviving fish were counted at the indicated time points. (n ≥30 for each treatment). (C) Table describing phenotype scores (1-4) at different time points in zebrafish embryo development. (D) Phenotypic scores of untreated and ES treated *Coa6* knockdown zebrafish embryos at the indicated time points (hpf, hours post fertilization). Batches of 50 fertilized embryos injected with either translation blocking or mismatch control morpholinos were treated with or without 100 nM ES at 3 hpf, before making observations at the indicated time points. (n≥30 for each time point and treatment). (E) Representative images of untreated and ES treated *Coa6* knockdown zebrafish embryos at 72 and 96 hpf. The arrow heads indicate cardiac edema. (F) Heart rate of zebrafish embryos treated with either mismatch control morpholino or the *Coa6* translation blocking morpholino were measured at the indicated time point. (n≥30 per group; data represent mean ± SEM).

## Discussion

Mitochondrial disorders of copper metabolism represent a subset of inborn errors of mitochondrial energy metabolism for which no therapy currently exists (Lightowlers et al., 2015). A previous attempt to use direct copper supplementation as a therapeutic approach was unsuccessful (Freisinger et al., 2004), possibly due to stringent regulation of systemic copper levels. Thus, there is an unmet need for developing better copper delivery agents. With this goal in mind, we tested a number of clinically used pharmacological agents on a yeast mitochondrial disease model of *COA6* deficiency and identified ES as the most potent and best tolerated compound capable of restoring mitochondrial function. Subsequent experiments on other yeast, murine, human and zebrafish models established broad applicability of ES in treating cellular and mitochondrial copper deficiency. ES has undergone multiple human clinical trials where it has exhibited a favorable toxicity profile (Hedley et al., 2016; O'Day et al., 2013); thus, our findings offer an exciting possibility of repurposing this anti-cancer drug for the treatment of disorders of copper metabolism.

Pharmacological interventions that alter the subcellular concentration and distribution of metals in a targeted manner could be of therapeutic benefit. For example, co-administration of copper with disulfiram, a Food and Drug Administration approved drug, increased the activity of CcO in the brains of a mouse model of Menkes disease, a genetic disorder characterized by systemic copper deficiency (Bhadhprasit et al., 2012). Similarly, $Cu^{II}$-ATSM has been shown to be efficacious in a transgenic mouse model of

amyotrophic lateral sclerosis (Roberts et al., 2014). However, a comparative study on the efficacy of these clinically used copper complexes in a model of copper deficiency is lacking. Therefore, our study identifying ES as the most potent pharmacological agent among many of the clinically used copper chelators and ionophores represents an important advance (Fig. 2.1). The physicochemical properties of ES, including its binding affinity, its specificity for copper, and the redox potential of the ES-copper complex, allow it to mimic a copper metallochaperone (Yadav et al., 2013). Higher affinity of ES for copper (II) compared to copper (I) allows it to scavenge copper from the extracellular environment where copper is more likely to exist in an oxidized state (Yadav et al., 2013). ES is unlikely to strip copper from intracellular proteins, because of the higher prevalence of copper in the reduced state in the intracellular environment.

Although a previous study shows selective enrichment of the ES-copper complex in the mitochondria (Nagai et al., 2012), the rescue of yeast *atx1Δ* and *ccc2Δ*, which have impaired copper homeostasis in the Golgi compartment (Smith et al., 2017), suggests that ES is also able to deliver copper to other subcellular compartments (Fig. 2.6). Indeed, the rescue of the pigmentation defect observed in *Ctr1*$^{-/-}$ zebrafish caused by a defective secretory pathway enzyme also indicates that ES could increase copper levels in other organelles (Fig. 2.10). Finally, the rescue of the respiratory growth defect of *ccs1Δ* cells, which are deficient in a metallochaperone for the cytosolic protein Sod1 suggests that ES is also able to elevate cytosolic copper levels (Fig. 2.6). While the mechanism by which ES is able to deliver copper to different subcellular compartments is not clear, it is possible that some of the ES-copper complexes dissociate before reaching mitochondria, thereby

releasing free copper in the cytoplasm. Alternatively, excess mitochondrial copper may 'leak' out of the mitochondria and become available to other organelles. Notwithstanding the mechanism, this interesting observation suggests that ES could be efficacious in the treatment of more common disorders of copper deficiency, including Menkes disease.

## Materials & Methods

Reagents

Copper chloride, tetraethylthiuram disulfide (disulfiram; DF), 8-hydroxyquinoline (8HQ), 5-chloro-7-iodo-8-quinolinol (clioquinol; CQ), ammonium pyrrolidinedithiocarbamate (PDTC), diacteylbis(N(4)-methylthiosemicarbazonato) copper (II) (Cu-ATSM), 2-mercaptopyridine N-oxide (pyrithione; PyS) and dimethyl sulfoxide (DMSO) were purchased from Sigma-Aldrich. Elesclomol (ES) was purchased from Selleckchem. The yeast-human hybrid (hyCOA6) gene construct was codon optimized for yeast and synthesized using GeneArt® Gene Synthesis (Life Technologies). The hybrid gene hyCOA6 was cloned into pRS416 plasmid under the control of the yeast Coa6 native promoter. *COA6* patient mutations were introduced by site-directed-mutagenesis (Agilent Technologies QuikChange Lightning) using hyCOA6 as a template. All the primers used in this study are listed in Fig. 2.13. All the constructs were sequenced verified.

| Name | Sequence (5' → 3') |
|---|---|
| **Site Directed mutagenesis primers** | |
| Hy*COA6* W26C Forward | agtattcatctctagcaccgcaacacaattttctttggg |
| Hy*COA6* W26C Reverse | cccaaagaaaattgtgttgcggtgctagagatgaatact |
| Hy*COA6* W33R Forward | ttttcgtccaaacatttccggtattcatctctagcaccc |
| Hy*COA6* W33R Reverse | gggtgctagagatgaataccggaaatgtttggacgaaaa |
| Hy*COA6* E54X Forward | cattgttgtggacaagaagattagaaagaggatctcaacttctta |
| Hy*COA6* E54X Reverse | taagaagttgagatcctctttctaatcttcttgtccacaacaatg |

**Figure 2.13 Primers used in this study.**

Yeast strains and culture conditions

*Saccharomyces cerevisiae* strains used in this study are listed in Fig. 2.14. The authenticity of yeast strains was confirmed by PCR as well as by replica plating on dropout plates. Yeast cells were cultured in standard growth media including YPD (1% yeast extract, 2% peptone and 2% glucose), YPGal (2% galactose), YPGE (3% glycerol + 1% ethanol) or synthetic media (0.17% yeast nitrogen base, 0.5% ammonium sulfate, 0.2% dropout amino acid mix, 2% dextrose) (SC glucose). For qualitative growth measurement, 10-fold serial dilutions of overnight cultures were spotted on YPD or YPGE plates and incubated at 30°C and 37°C for 2 to 4 days. Growth in liquid media was measured spectrophotometrically at 600 nm.

| Strain | Genotype | Source |
|---|---|---|
| BY4741 WT | MAT a, *his3Δ1*, *leu2Δ0*, *met15Δ0*, *ura3Δ0* | Greenberg lab |
| BY4741 *coa6Δ* | MAT a, *his3Δ1*, *leu2Δ0*, *met15Δ0*, *ura3Δ0*, *coa6Δ:: KanMX4* | Open Biosystems |
| BY4741 *sco1Δ* | MAT a, *his3Δ1*, *leu2Δ0*, *met15Δ0*, *ura3Δ0*, *sco1Δ:: KanMX4* | Open Biosystems |
| BY4741 *sco2Δ* | MAT a, *his3Δ1*, *leu2Δ0*, *met15Δ0*, *ura3Δ0*, *sco2Δ:: KanMX4* | Open Biosystems |
| BY4741 *cox12Δ* | MAT a, *his3Δ1*, *leu2Δ0*, *met15Δ0*, *ura3Δ0*, *cox12Δ:: KanMX4* | Open Biosystems |
| BY4741 *ctr1Δ* | MAT a, *his3Δ1*, *leu2Δ0*, *met15Δ0*, *ura3Δ0*, *ctr1Δ:: KanMX4* | Open Biosystems |
| BY4741 *atx1Δ* | MAT a, *his3Δ1*, *leu2Δ0*, *met15Δ0*, *ura3Δ0*, *atx1Δ:: KanMX4* | Open Biosystems |
| BY4741 *ccs1Δ* | MAT a, *his3Δ1*, *leu2Δ0*, *met15Δ0*, *ura3Δ0*, *ccs1Δ:: KanMX4* | Open Biosystems |
| BY4741 *gsh1Δ* | MAT a, *his3Δ1*, *leu2Δ0*, *met15Δ0*, *ura3Δ0*, *gsh1Δ:: KanMX4* | Open Biosystems |
| BY4741 *ccc2Δ* | MAT a, *his3Δ1*, *leu2Δ0*, *met15Δ0*, *ura3Δ0*, *ccc2Δ:: KanMX4* | Open Biosystems |
| BY4741 *gef1Δ* | MAT a, *his3Δ1*, *leu2Δ0*, *met15Δ0*, *ura3Δ0*, *gef1Δ:: KanMX4* | Open Biosystems |
| BY4741 *pic2Δ* | MAT a, *his3Δ1*, *leu2Δ0*, *met15Δ0*, *ura3Δ0*, *pic2Δ:: KanMX4* | Open Biosystems |
| STY11 *pic2Δcoa6Δ* | MAT a, *his3Δ1*, *leu2Δ0*, *met15Δ0*, *ura3Δ0*, *pic2Δ::KanMX4,coa6Δ::NatMX4* | Ref (10) |

**Figure 2.14 Yeast strains used in this study**

Mammalian cell culture

The human control MCH46 and *SCO2* patient fibroblasts as well as the rat H9c2 control and *Ctr1*$^{-/-}$ cardiomyocytes were cultured in high glucose Dulbecco's modified Eagle's medium (DMEM) supplemented with 10% fetal bovine serum (Sigma) and 1 mM sodium pyruvate (Life Technologies). The mouse embryonic fibroblasts were cultured in DMEM 10% FBS, 1 mM sodium pyruvate, 1x minimum essential medium non-essential amino acids (MEM NEAA; Life Technologies 11140), 50 µg/mL uridine, and 1x Pen Strep Glutamine (Life Technologies 10378). All cell lines were cultured under 5% $CO_2$ at 37 °C and were treated with different concentrations (0.1 to 5 nM) of ES for 3-6 days

before harvesting. Whole cell protein was extracted in lysis buffer (BP-115, Boston BioProducts) supplemented with protease inhibitor cocktail (cOmplete Mini EDTA-free; Roche Diagnostics) and the protein concentrations were determined by BCA assay (Thermo Scientific).

Construction of a Ctr1 knockout rat H9c2 cell line

A CRISPR/Cas9 mediated *Ctr1* knockout rat H9c2 cell line was generated by using lentiCRISPR v2 plasmid (Addgene, # 52961). A guide RNA (gRNA) sequence targeting exon 1 of the *Ctr1* gene was identified using the online CRISPR design tool (http://crispor.tefor.net). Forward (5' CACCGTGGTGATGTTGTCGTCCGTG 3') and reverse (5' AAACCACGGACGACAACATCACCAC 3') oligonucleotides were inserted into lentiCRISPR v2 plasmid. The transfection was performed using PolyJet (SignaGen Laboratories). Two days after transfection, cells were plated on a 96-well plate containing 5 μg/mL puromycin selection media. Each colony formed from single cells was isolated and established in medium without puromycin. Disruption of the *Ctr1* gene was confirmed by genomic DNA sequencing.

Oxygen consumption measurement

For measurements of respiration rates, cells were grown to late log phase in YPGal medium and then washed, counted and resuspended in fresh YPGal medium at $10^8$ cells/ml. The rate of oxygen consumption was then measured at 30°C using the Oxytherm (Hansatech, Norfolk, UK). Cyanide-sensitive respiration was calculated after the addition of 1 mM KCN, and the cyanide-insensitive respiration was subtracted from the total

respiration.

SDS-PAGE, BN-PAGE and immunoblotting

Sodium dodecyl sulfate polyacrylamide gel electrophoresis (SDS-PAGE) and Blue Native PAGE (BN-PAGE) were performed to separate denatured and native protein complexes, respectively. For SDS-PAGE, mitochondrial lysate (20 μg) was separated on NuPAGE 4–12% Bis-Tris gels (Life Technologies, Carlsbad, CA) and transferred onto polyvinylidene fluoride (PVDF) membranes using a Trans-Blot SD semi-dry transfer cell (Bio-Rad, Hercules, CA). For BN-PAGE, yeast mitochondria were solubilized in buffer containing 1% digitonin (Life Technologies) by incubating for 15 min at 4°C. Clear supernatant was collected after a 20,000 × *g* (30 min, 4°C) spin, 50x G-250 sample additive was added, and 20 μg of protein was loaded on a 3–12% native PAGE Bis-Tris gel (Life Technologies). Following wet transfer, the membrane was probed with the following primary antibodies: for yeast proteins - Cox2, 1:50,000 (110 271; Abcam) and porin, 1:50,000 (110 326; Abcam), for mammalian proteins – COX1 (14705; Abcam), COX2 (110258; Abcam), CTR1, COX4 (A21348; Thermo Fisher Scientific), CCS (FL-274; Santa Cruz Biotechnology), GAPDH (G9545, sigma), ATP5A (14748; Abcam), and β-actin (A2228; Sigma). Secondary antibodies (1:5000) were incubated for 1 h at room temperature, and membranes were developed using Western Lightning Plus-ECL (PerkinElmer, Waltham, MA).

In-gel activity measurements

In-gel activities for mitochondrial respiratory chain complexes were performed

using Clear native (CN)–PAGE to avoid interference of Coomassie blue with activity measurements (Wittig et al., 2007). Mitochondria solubilized in 1% digitonin were resolved by gel electrophoresis on a 4–16% Native PAGE Bis-Tris gel (Life Technologies) using a cathode buffer containing 0.05% dodecyl maltoside (DDM) and 0.05% deoxycholate (DOC). For measuring CcO activity, 90 μg of protein was loaded on the gel, followed by incubation in staining solutions as described (Wittig et al., 2007).

Cellular and mitochondrial copper measurements

Cellular and mitochondrial copper levels were measured using the Perkin Elmer DRC II Inductively Coupled Plasma – Mass Spectrometer (ICP-MS). Intact yeast cells and isolated mitochondrial pellets were washed with 100 μM EDTA containing water, weighed, and digested with 40% nitric acid (TraceSELECT, Sigma) at 90°C for 18 h. Samples were diluted in ultrapure metal-free water (TraceSELECT, Sigma) and analyzed by ICP-MS. Copper standard solutions were prepared by appropriate dilutions of commercially available mixed metal standards (BDH Aristar Plus). Copper concentrations in mammalian cells were also measured by ICP-MS.

Zebrafish experiments

All zebrafish studies were approved by the Marine Biological Laboratory Institutional Animal Care and Use Committee (#16-38). Wild type AB strain and *Ctr1* heterozygous zebrafish were maintained and crossed using standard methods. Embryos were staged and raised in Egg Water at 28.5°C. For drug treatments, embryos from *Ctr1* heterozygous crosses were incubated in 10 nM ES diluted in Egg Water beginning at 3

hours post-fertilization (hpf). For imaging live embryos at 48hpf, representative embryos of each sample were anesthetized in Tricaine and imaging was performed on an Olympus SZX12 stereomicroscope. For immunoblots, zebrafish mitochondrial protein was prepared from 10dpf larvae. Mitochondrial lysate was separated by SDS-PAGE on 4-15% Mini-PROTEAN TGX Gels (Bio-Rad) followed by Western blot analysis using anti-Cox1 at 1:5000 (anti-MTCO1; Abcam; ab14705) and anti-Atp5a at 1:5000 (Abcam; ab110273). The morpholino-based experiments were performed as described previously (Ghosh et al., 2014).

# CHAPTER III

# SOLUTION STRUCTURE OF COA6 PROVIDES INSIGHTS INTO $CU_A$ SITE FORMATION IN MITOCHONDRIAL CYTOCHROME C OXIDASE

**Disclaimer**

I performed all the experimental work described in this chapter except for the following figures. Dr. Alok Ghosh, of the Department of Biochemistry and Biophysics at Texas A&M University performed experiments described in Fig. 3.8B. Aren Boulet, of the Department of Biochemistry, University of Saskatchewan, Saskatoon, performed experiments described in Fig. 3.4D&E, 3.10F and 3.11. Marcos Morgada, of the Instituto de Biología Molecular y Celular de Rosario, Consejo Nacional de Investigaciones Científicas y Técnicas, Facultad de Ciencias Bioquímicas y Farmacéuticas, Universidad Nacional de Rosario, performed experiments described in Fig. 3.5, 3.10B-E. Dr. James Ames, of the Department of Chemistry, University of California, Davis, performed experiments described in Fig. 3.6E. Nathaniel Dziuba of the Department of Biochemistry and Biophysics at Texas A&M University performed experiments described in Fig. 3.8D&F and 3.9. I also greatly appreciate Dr. Mandar Naik, of the Department of Biochemistry and Biophysics at Texas A&M University, help in performing NMR experiments described in Fig.3.1D-F, 3.2A-D, 3.3 and 3.6A-D.

**Summary**

Insertion of copper into the mitochondrial cytochrome *c* oxidase (CcO) serves as a paradigm of how metal centers are formed in integral membrane proteins. The formation of $Cu_A$ site on CcO *in vivo* requires concerted actions of SCO1, SCO2, and a recently discovered COA6 protein, however; molecular function of COA6 in this process has remained unclear. We address this by solving the solution structure of COA6, which revealed a CHCH domain typically found in the redox-active proteins of the mitochondrial inter membrane space. Consistent with its redox role, COA6 function is redundant in the reducing environment. Interaction mapping and redox potential determination of COA6 and its client proteins are consistent with our demonstration of thiol-disulfide reductase activity of COA6 towards SCO1 and COX2 proteins in the metallation of $Cu_A$ site. Overall, our results provide a mechanism of how coordinated activities of metallochaperone and thiol-disulfide reductases form the $Cu_A$ site.

## Introduction

Copper (Cu) is a redox-active metal that plays an essential role in cellular physiology by acting as a catalytic cofactor in enzymatic reactions (Kim et al., 2008). One of the most critical Cu-containing enzymes is the inner mitochondrial membrane localized cytochrome *c* oxidase (CcO), a multimeric heme-Cu oxidase that is the main site of cellular respiration (Ferguson-Miller and Babcock, 1996). CcO activity and assembly depends on the formation of its two Cu centers -$Cu_A$ and $Cu_B$ on COX2 and COX1 subunits, respectively (Tsukihara et al., 1995). These Cu centers provide a molecular conduit for the transfer of electrons from reduced cytochrome *c* to oxygen, the terminal step in mitochondrial respiration.

The high reactivity and thiophilic nature of Cu present peculiar problems in the transport and insertion of Cu to its target enzymes. Free Cu can drive the production of deleterious hydroxyl radicals (Halliwell and Gutteridge, 1984) and can displace other metal ions from proteins preventing its own delivery to its target cuproprotein (Foster et al., 2014; Macomber and Imlay, 2009). Moreover, the correct oxidation state of cysteines of its target protein is necessary for Cu binding (Abriata et al., 2008). Not surprisingly, the metallation of the CcO is a complex process that requires several evolutionarily conserved proteins (Soto et al., 2012; Timon-Gomez et al., 2018). For example, delivery of Cu to the $Cu_A$ site, a cysteine-bridged dinuclear Cu center, requires at least four proteins– COX17, SCO1, SCO2, and COA6 – all of which are localized to the IMS or are in the inner mitochondrial membrane with their soluble domain facing the IMS (Vogtle et al., 2017). These proteins are part of a relay system, where Cu is sequentially transferred from

COX17 to SCO1 to the $Cu_A$ site on COX2 (Horng et al., 2004; Banci et al., 2008a; Morgada et al., 2015). Structural and functional analyses of yeast and human COX17 and SCO1 proteins have shown that they coordinate Cu through their cysteinyl residues (Abajian et al., 2004; Abajian and Rosenzweig 2006; Banci et al., 2006; Banci et al., 2008a) and act as metallochaperones (Banci et al., 2008a; Horng et al., 2004; Morgada et al., 2015). Human SCO2 has been shown to act as thiol-disulfide reductase of SCO1 *in vivo* and COX2 *in vitro*, (Leary et al., 2009; Morgada et al., 2015). These findings show that in addition to the metallochaperone activity of COX17 and SCO1, a thiol-disulfide reductase activity is essential for inserting Cu into the $Cu_A$ site.

Recently, we reported that Cytochrome Oxidase Assembly factor 6, COA6, a poorly characterized CcO assembly factor, is the novel member of the Cu delivery pathway to the CcO (Ghosh et al., 2014). Subsequent biochemical and genetic interactions studies showed that COA6 interacts with SCO1, SCO2, and COX2 and has an overlapping function with SCO2 in the biogenesis of COX2, findings that placed it in the Cu delivery pathway to the $Cu_A$ site of CcO (Ghosh et al., 2016; Pacheu-Grau et al., 2015; Stroud et al., 2015). Loss of COA6 function in many organisms results in severe CcO deficiency and underlies human disease, demonstrating its critical and conserved role in this pathway (Baertling et al., 2015; Calvo et al., 2012). However, how COA6 interacts with multiple protein partners, what is their relative affinity, and what is the precise biochemical function of COA6 in $Cu_A$ site maturation has remained open questions.

Here, we address these questions by a combination of NMR-based structural determination and *in vitro* and *in vivo* mechanistic biochemistry. We show that COA6

adopts a coiled-coil-helix-coiled-coil-helix (CHCH) domain, preferentially interacts with SCO1 and exhibit thiol-disulfide reductase activity both *in vitro* and *in vivo*, with SCO1 and COX2 being the most likely target. Collectively, our data suggest a model where COA6 and SCO2 act as thiol-disulfide reductases in a step-wise transfer of Cu from Cox17 to the $Cu_A$ site.

**Results**

Human COA6 is a helical protein with a coiled-coil-helix-coiled-coil-helix domain

Using yeast genetics, we recently placed a previously uncharacterized CcO assembly factor, Coa6, in the Cu delivery pathway to the Cox2 subunit of CcO (Ghosh et al., 2014; Ghosh et al., 2016). Consistent with our findings in the yeast model system, other groups revealed requirement of human COA6 in COX2 biogenesis via its physical interaction with Cu metallaochaperones – SCO1 and SCO2 (Pacheu-Grau et al., 2015, Stroud et al., 2015). While these biochemical and genetic interactions studies linked COA6 function to the maturation of the $Cu_A$ site, the precise molecular function of COA6 remained elusive.

To uncover the molecular function of COA6, we first solved the solution structure of human COA6 isoform 3 (COA6). We chose isoform 3 for structural determination because it encompasses the most well conserved region of COA6 and contains the primary structure that functionally complements the yeast *coa6Δ* cells (Ghosh et al., 2014; Ghosh et al., 2016). We sub-cloned human COA6 in the bacterial expression

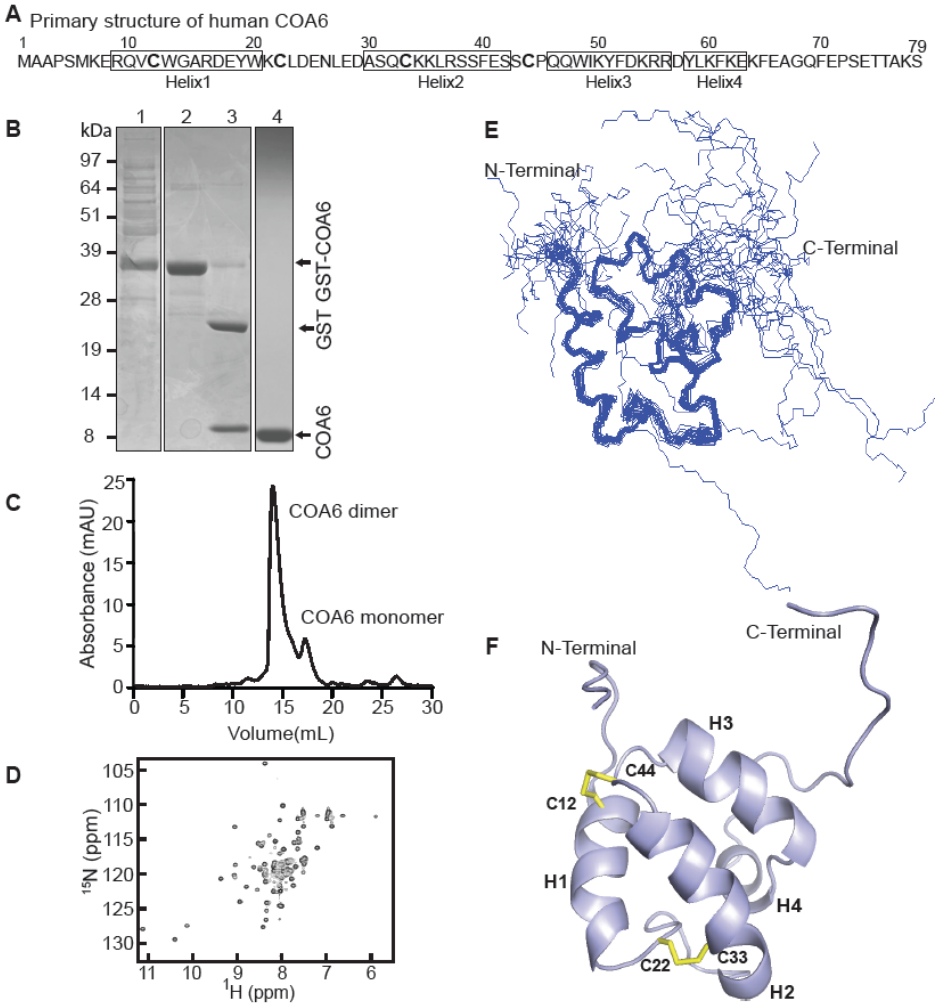


**Figure 3.1 Solution structure of human COA6.**
(A) Primary structure of human COA6. (B) SDS-PAGE analysis of the samples obtained during COA6 purification steps: lane 1, supernatant of lysate from *E. coli* expressing COA6-GST fusion protein; lane 2, eluate containing COA6-GST from GST binding column; lane 3, COA6-GST after cleaving GST tag with thrombin; lane 4, purified COA6 sample from gel filtration chromatography. (C) Elution profile of purified COA6 from Superdex 75 gel filtration column. (D) $^{1}H$-$^{15}N$ HSQC spectrum of human COA6. (E) Ensemble of the 20 NMR solution structures of COA6 by backbone representation. (F) Ribbon representation of human COA6 based on the lowest energy conformer of solution structures. Human COA6 has four helixes labeled as H1, H2, H3 and H4, and the two disulfide bonds between H1 and H2 are shown in yellow.

**Table 3.1 NMR and refinement statistics for solution structure of COA6**

| | |
|---|---|
| **NMR distance and dihedral constraints** | |
| Distance restraints | |
| Total NOE | 554 |
| Intra-residue | 163 |
| Inter-residue | 284 |
| Sequential ($\|i-j\|=1$) | 177 |
| Nonsequential ($\|i-j\|>1$ ) | 214 |
| Hydrogen bonds | 32 |
| Total dihedral angle restraints | 108 |
| ϕ (TALOS+) | 54 |
| ψ (TALOS+) | 54 |
| **Structure statistics** | |
| Violations (mean and s.d.) | |
| Distance constraints (Å) | 0.01 ± 0.03 |
| Dihedral angle constraints (º) | 0.37 ± 0.88 |
| Max. dihedral angle violation (º) | 6.18 |
| Max. distance constraint violation (Å) | 0.43 |
| Deviations from idealized geometry | |
| Bond lengths (Å) | 0.008 |
| Bond angles (º) | 0.6 |
| Ramachandran Plot | |
| Most favored | 79.6% |
| Additionally allowed | 17.2% |
| Generously allowed | 3.2% |
| Disallowed | 0.1% |
| Average pairwise r.m.s. deviation* (Å) | |
| Protein structured region (residues 9 to 64) | |
| Heavy | 1.35 |
| Backbone | 0.54 |

*Pairwise r.m.s. deviation was calculated among 20 refined structures.

system for recombinant expression of the 79 amino acid long COA6 (Fig. 3.1A). The recombinant COA6 was expressed as a GST fusion protein, which was then cleaved with thrombin protease to release free COA6 (Fig. 3.1B). Gel-filtration analysis of COA6 suggests that it predominantly exists as an ~18 kDa dimer (Fig. 3.1C). We utilized isotope-enriched COA6 samples for structure determination by using distance and angle restraints

obtained from 2D and 3D heteronuclear nuclear magnetic resonance (NMR) spectra. The $^{1}H$-$^{15}N$ heteronuclear signal quantum correlation (HSQC) spectra of COA6 show well-dispersed resonances, indicative of a well-folded protein (Fig. 3.1D). In the $^{1}H$-$^{15}N$ HSQC of human COA6, 67 out of the expected 79 $^{15}N$ backbone amide resonances were detected and approximately 90% of all detectable carbon, nitrogen and hydrogen nuclei were assigned. A number of peaks in the center of HSQC spectra were not fully resolved possibly because of monomer:dimer equilibrium of hCOA6. In order to determine if dimerization of COA6 is affected by its concentration, we acquired the $^{15}N$ HSQC spectrum of COA6 at varying protein concentrations (Fig. 3.2A), which showed fast-picoseconds motions in the C-terminus of COA6 (Fig. 3.2B). Analysis of chemical shift perturbation of lowest to highest COA6 concentration (Fig. 3.2B) indicates that the residues in the C-terminus of COA6, which exhibited significant chemical shift perturbations, are likely involved in dimerization. Notably, the dimerization of COA6 is independent of strong reducing agent as determined by analyzing the $^{1}H$-$^{15}N$ HSQC and gel filtration chromatography of COA6 with and without 1mM TCEP (Fig. 3.2 C-E).

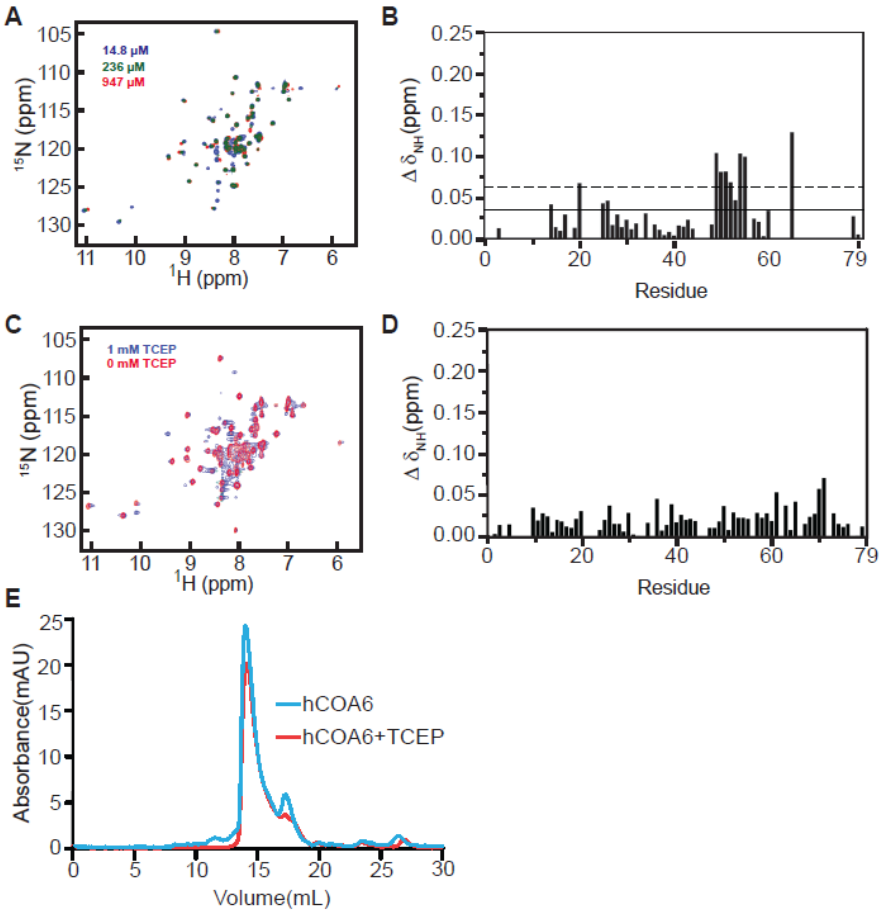


**Figure 3.2 Human COA6 forms a homodimer that is stable in the presence of a strong reducing agent.**
(A) Overlay of the $^{1}$H-$^{15}$N HSQC spectra of human COA6 at three different concentrations of TCEP: 14.8 µM (blue), 236 µM (green), and 947 µM (red). (B) Average chemical shift deviation of $^{15}$N-labeled COA6 at 947 µM TCEP when compared to treatment with 14.8 µM TCEP. Horizontal solid line represents the mean and dashed line represents mean + SD of chemical shift perturbation for all the residues. (C) Overlay of the $^{1}$H-$^{15}$N HSQC spectra of human COA6 with and without 1mM TCEP. (D) Average chemical shift deviation of $^{15}$N-labeled COA6 upon addition of 1mM TCEP. (E) Elution profile of COA6, with and without TCEP treatment, from Superdex 75 gel filtration column.

The ensemble of 20 different COA6 structures indicates that the N and C termini of COA6 are unstructured, which may contribute to target recognition (Fig. 3.1E). Overall,

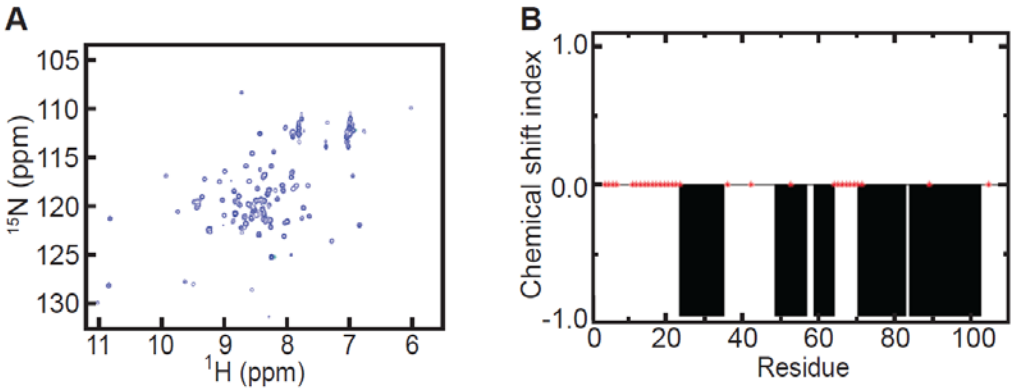


**Figure 3.3 Yeast Coa6 is a helical protein.**
(A) $^{1}$H-$^{15}$N HSQC spectrum of yeast Coa6. (B) The chemical shift index is shown as a function of residue number. Negative values represent an α-helical propensity, while positive values are indicative of participation in a β-strand. Red asterisks (*) denotes the residues which were unassigned.

the ensemble of 20 COA6 structures is in excellent agreement with the experimental restraints (Table 3.1). The lowest energy conformer of COA6 shows that it is an all-helical protein with four helices where the first two helices, H1 and H2, are stabilized by two disulfide bonds (Fig. 3.1F). COA6 exhibits a coiled-coil-helix-coiled-coil-helix (CHCH) domain found in many mitochondrial IMS proteins that are proposed to have a role in redox chemistry. To further determine if the structural features of COA6 are conserved in yeast Coa6, we analyzed $^{1}$H-$^{15}$N HSQC and chemical shift index (CSI) of recombinant yeast Coa6 and found that yeast Coa6 is also a helical protein (Fig. 3.3A&B).

Mapping COA6 patient mutations on hCOA6 structure

Mutations in the *COA6* have been identified in two human mitochondrial disease patients, one with compound heterozygous mutations (W59C, E87X) (Calvo et al., 2012) and the other with a homozygous missense mutation (W66R) (Baertling et al., 2015). These three mutated residues are conserved from yeast to humans (Fig. 3.4A). In order to understand

how these mutations, affect COA6 function, we mapped the patient mutations residues on COA6 structure. The truncation mutation (E87X) is expected to lose CHCH domain because large part of the protein from helix 2 onwards is deleted (Fig. 3.4B). Other two mutations, W59C and W66R, are on the 1st helix of COA6 where side chains of both of these tryptophan residues faces the solvent and away from the structure, which suggest that these residues likely participate in the interaction with target proteins (Fig. 3.4B). In order to test the effect of these mutations on COA6 function, we introduced patient mutations in yeast-human chimeric protein (hyCOA6). As expected from our previous study the respiratory growth of *coa6Δ* cells was restored by the wild copy of hyCOA6 (Ghosh et al., 2016) but not when it harbors patient mutations suggesting that patient mutations disrupt the function of COA6 (Fig. 3.4C). To study the effect of mutations within the context of human cells, we overexpressed the wild type and mutant alleles of *COA6* in COA6 patient cell lines and found that allele with W66R mutation fails to rescue CcO activity, however, expression of W59C mutation leads to a partial recovery of CcO activity (Fig. 3.4D), a result consistent with the previous report (Stroud et al., 2015). Surprisingly, both the mutations led to undetectable COA6 (Fig. 3.4E). This apparent discrepancy could be due to inability of COA6 antibody to detect mutant protein. However, consistent with the partial rescue of CcO activity, we observed mild rescue of COX2 protein levels (Fig. 3.4E). It seems that in most cell types residual levels of the partially functional W59C allele are not sufficient to support CcO assembly and mitochondrial respiration because *coa6Δ* cells expressing the W59C variant do not exhibit

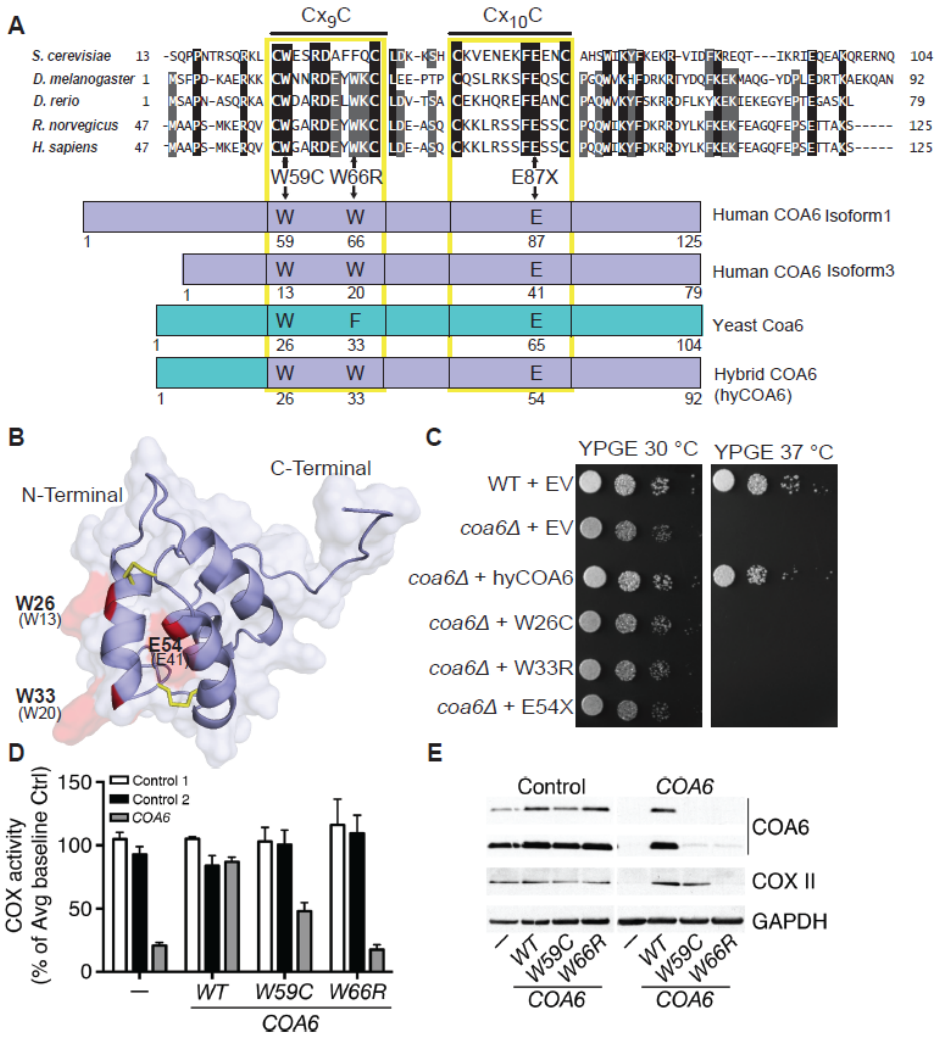


**Figure 3.4 Mapping COA6 patient mutations on COA6 structure.**
(A) Sequence alignment of the conserved region of COA6 across indicated model organisms. Horizontal lines above $Cx_9C$ and $Cx_{10}C$ residues show the conserved $Cx_9Cx_nCx_{10}C$ motif. Schematic representation of yeast-human hybrid (hyCOA6) protein, where the sequences from yeast Coa6 and human COA6 are shown in cyan and blue, respectively. Arrows indicate amino acid residues that were mutated in human COA6 patients and the corresponding residues in the hyCOA6 protein. (B) COA6 patient mutations mapped on COA6 structure in red. (C) WT and *coa6Δ* cells transformed with empty vector (EV) or vector expressing either hyCOA6 or hyCOA6 harboring patient mutations (W26C, W33R and E54X) were serially diluted and seeded on YPGE plates. Cells were grown at 30°C and 37°C for 5 days. (D) Human control 1, control 2 and COA6 patient cell lines were transduced with cDNAs expressing either WT or patient mutations of COA6 followed by measurement of COX activity. (E) SDS-PAGE/western blot depicting COA6, COXII and GAPDH (loading control) levels in protein lysate from the Control 1 and COA6 cell lines as indicated in Figure D.

respiratory growth (Fig. 3.4C) and human patient with the W59C mutation exhibits a severe CcO deficiency in cardiac tissue (Calvo et al., 2012). Taken together, these data provide structural basis for pathogenicity of human patient mutations and suggest critical roles of conserved tryptophans in COA6 protein stability.

SCO1 displays stronger interaction with COA6 than SCO2

In order to elucidate the molecular function of COA6, it is important to identify its true interacting partners. Previous studies from yeast and human cell lines have identified *in vivo* interaction of COA6 with COX2 and SCO proteins (Ghosh et al., 2016; Pacheu-Grau et al., 2015; Stroud et al., 2015). However, there is some discrepancy in the results obtained in these studies – while one group identified interaction of human COA6 only with SCO2 (Pacheu-Grau et al., 2015), the other group showed that human COA6 interacts only with SCO1. Interestingly, we found that yeast Coa6 interacts with both SCO1 and SCO2 (Ghosh et al., 2016).

To resolve these discrepancies, we used size-exclusion chromatography (SEC) to perform a competitive binding analysis of COA6 with SCO1 and SCO2. First, we determined the elution profiles of each protein alone. The shape of the COA6 elution profile (Fig. 3.5A) suggests equilibrium between the monomeric and dimeric forms (~17kDa), which is consistent with our NMR data, while the soluble domains of SCO1 and SCO2 behave as monomeric 20 kDa and 17.6 kDa proteins, respectively (Fig. 3.5B & 3C). We then obtained elution profiles for different mixtures of these proteins. An equimolar mixture of COA6 and SCO1 led to the formation of a complex of ~27 kDa, and the absence of the peak corresponding to COA6 alone indicating that all of the

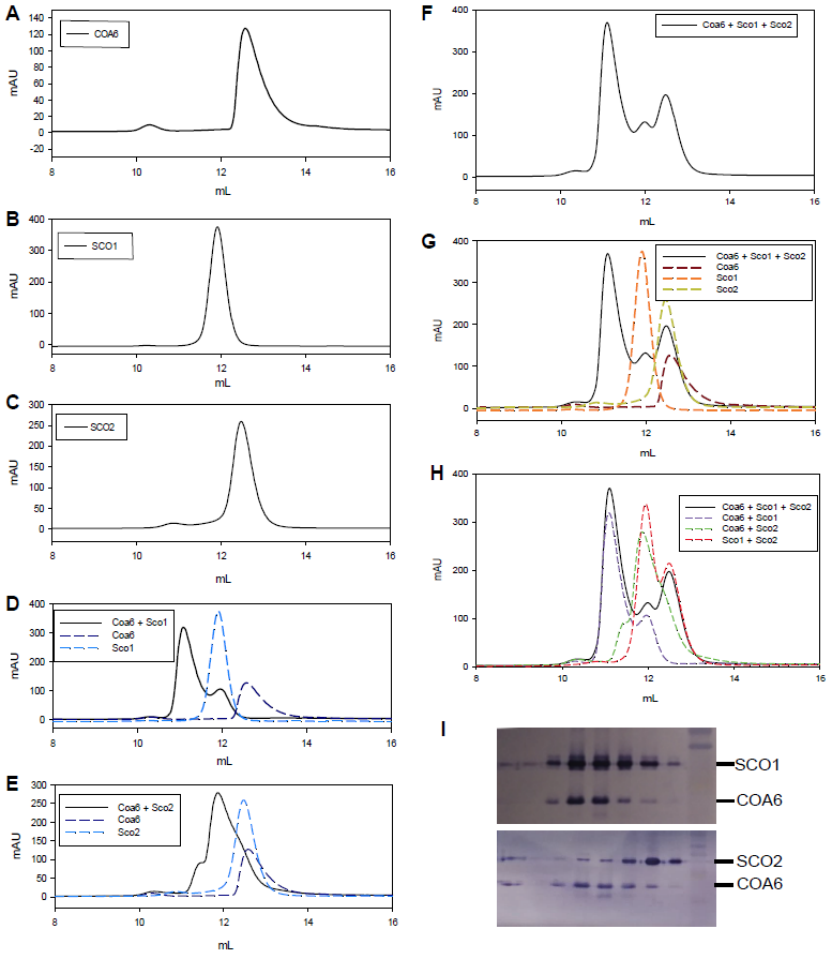


**Figure 3.5 Human COA6 exhibits stronger interaction with SCO1 than SCO2.** (A-C) Size exclusion chromatography elution profiles of (A) COA6, (B) SCO1, and (C) SCO2. (D-H) Elution profiles of the indicated mixtures of proteins (solid lines), compared to simulations of the indicated individual proteins or mixtures of two proteins (dotted lines). (I) SDS-PAGE/western blot analysis of different fractions from size exclusion chromatography shown in (F), probed with COA6, SCO1, and SCO2 antibodies.

COA6 is part of the complex (Fig. 3.5D). The excess SCO1 appears as a shoulder on the chromatogram (Fig. 3.5D). Based on the apparent molecular weight of the complex, COA6 seems to interact with SCO1 in a monomeric form. Similarly, an equimolar mixture of COA6 and SCO2 led to the formation of two species of complexes, with apparent molecular weights of ~24 kDa and ~ 22 kDa. These could consist of SCO2 complexed

with the dimer and monomer of COA6, respectively. We also observed a shoulder around 18 kDa, which corresponds to excess SCO2 or COA6 dimer (Fig. 3.5E). To determine the competitive binding of SCO1 and SCO2 with COA6, a mixture with all these three proteins was prepared and analyzed using SEC, which identified three distinct peaks in the elution profile (Fig. 3.5F). Through curve fitting, we compared this elution profile with each of the individual protein traces (Fig. 3.5G) or the mixtures of two proteins (Fig. 3.5H), and found that the high molecular weight peak corresponds to the SCO1:COA6 complex and the remaining two peaks correspond to SCO1 and SCO2 alone. To further investigate the constituents of the elution profile we performed SDS-PAGE/western analysis of each of the elution fractions and probed for the SCO proteins and COA6. We found that the majority of COA6 co-elutes with SCO1 (Fig. 3.5I). These *in vitro* data strongly suggest that SCO1 is the most likely interacting partner of COA6.

Mapping the interaction surfaces of COA6 and SCO1

To identify the interaction surfaces of COA6 and SCO1 proteins we compared HSQC spectra of $^{15}$N-labeled COA6 obtained in the presence and absence of unlabeled SCO1. The comparison of the two spectra identified pronounced chemical shift perturbations in the C-terminal residues of COA6, specifically residues 49-55 present in the helix 3 and the residues 65-69 that form a beta hairpin turn (Figures 3.6A and B). Interestingly, most of these COA6 residues are non-polar, suggesting a hydrophobic interaction between COA6 and SCO1. To obtain complementary information about the interaction surfaces on SCO1 protein, we performed a reciprocal experiment, where

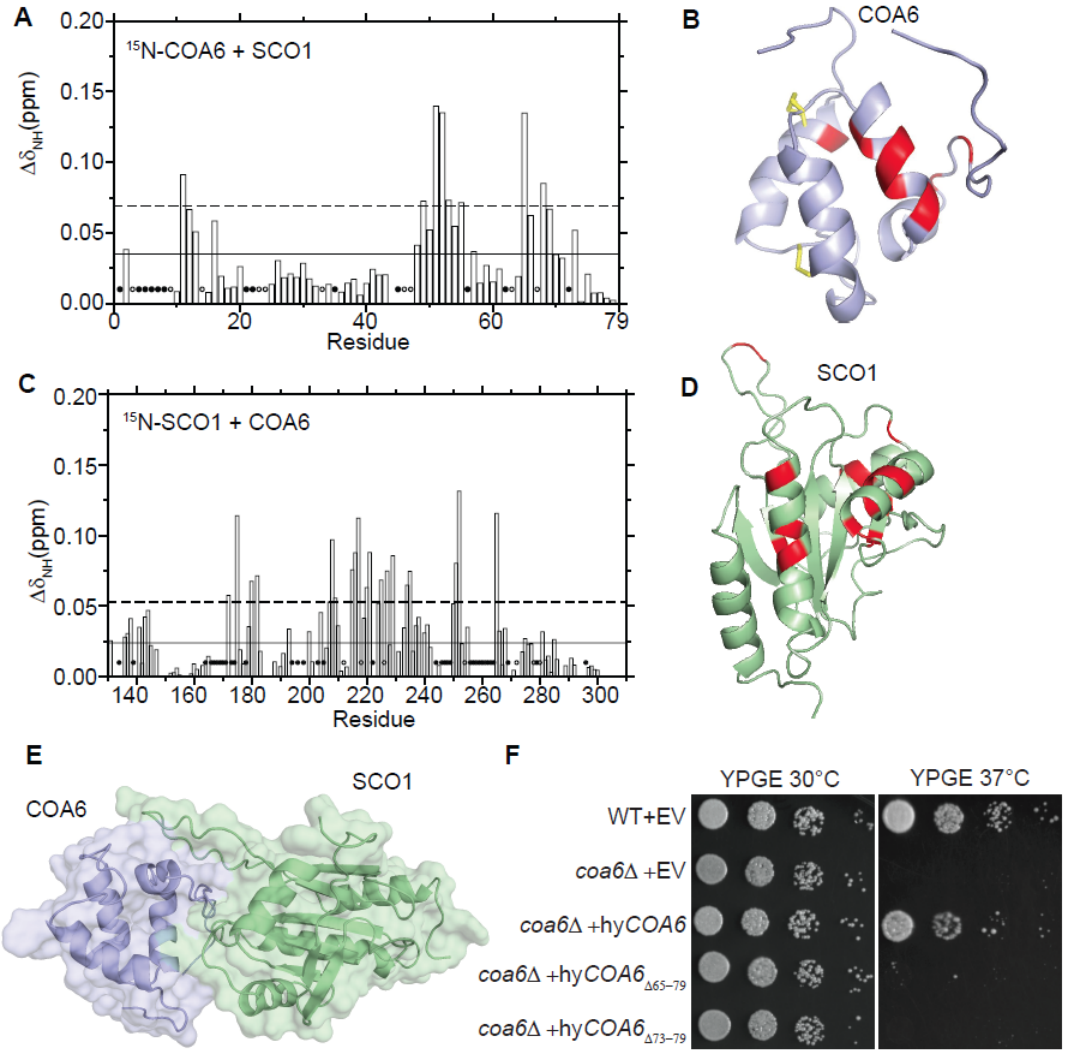


**Figure 3.6 Mapping the interactions between COA6 and SCO1 proteins.**
(A) Average chemical shift perturbation of $^{15}$N-labeled COA6 upon addition of equimolar unlabeled SCO1. Horizontal solid line, mean chemical shift perturbation; dashed line, mean + SD of chemical shift perturbation for all residues; solid circles, unassigned residues; open circles, residues with broadened peaks upon complex formation. (B) COA6 residues with significant chemical shift perturbations are colored in red on a ribbon representation of COA6. (C) Chemical shift perturbation of $^{15}$N-labeled SCO1 residues upon addition of equimolar unlabeled COA6, as displayed in (A). (D) SCO1 residues with significant chemical shift perturbations are colored in red on a ribbon representation of SCO1. (E) A HADDOCK docking model of COA6 and SCO1 complex generated using chemical shift perturbation (CSP) data. (F) WT and *coa6Δ* cells transformed with empty vector.

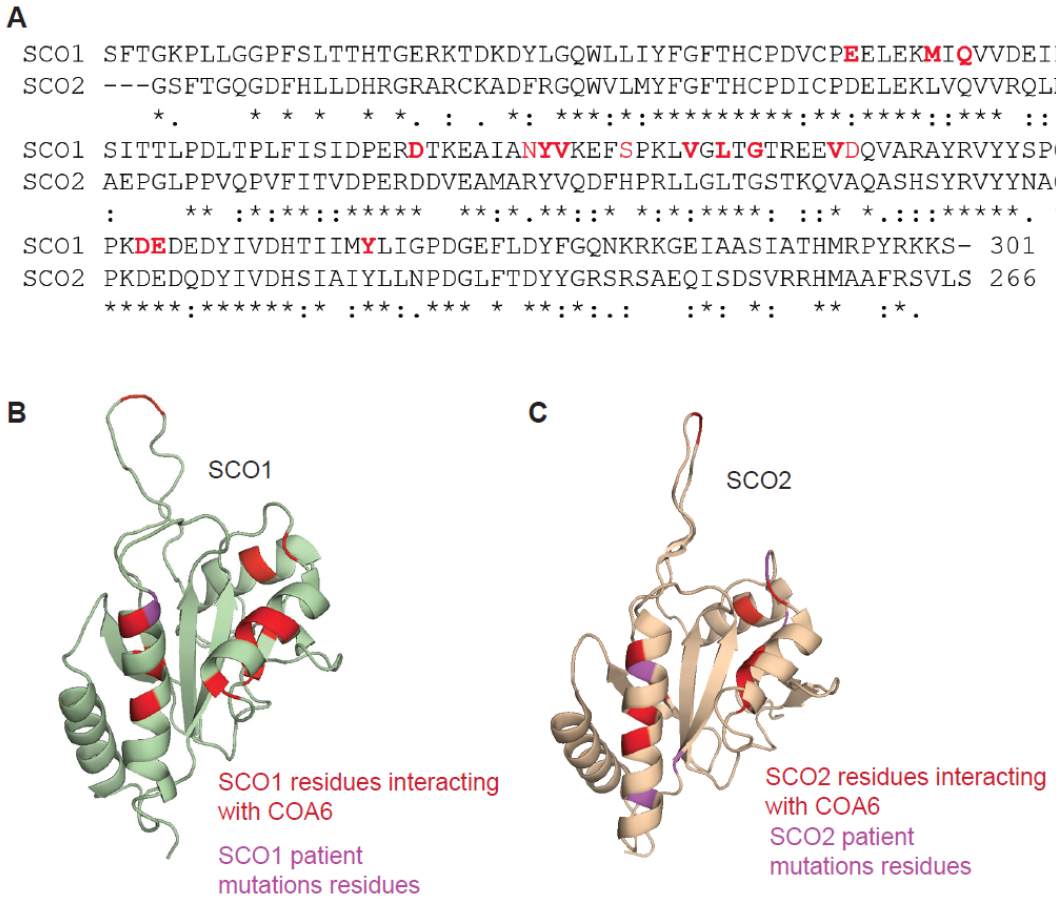


**Figure 3.7 Patient mutation residues of SCO1 and SCO2 are close to COA6 interacting residues.**
A) Alignment of human SCO1 and SCO1 polypeptides (sizes, in amino acids, at right). The amino acids shown in red and bold are the conserved among the SCO proteins and involved in the interaction with COA6. B) Structure of SCO1 (PDB:2GVP) and SCO2 (PDB:2RLI) are shown where residues that interact with COA6 are shown in red and the patient mutations are shown in purple.

HSQC spectra of $^{15}$N-labeled SCO1 was obtained in the presence and absence of unlabeled COA6, which identified a number of non-polar residues present on the same face of the SCO1 (Fig. 3.6C and D). Interestingly, this interaction surface of SCO1 with COA6 is highly conserved in SCO2 protein, suggesting that COA6 likely interacts with SCO protein through their similar surfaces. Using the chemical shift perturbation data, we have

generated a hypothetical docking model for COA6-SCO1 complex using High Ambiguity Driven protein-protein Docking (HADDOCK). As shown in the model, the C-terminal end of COA6 docks into a deep crevice formed by a flap in SCO1 that resembles a clamshell opening (Fig. 3.6E). The docking results show that the interaction between COA6 and SCO1 is mainly driven by hydrophobic interactions, which are stabilized by salt bridge formation with R55 on COA6 forming an intermolecular salt bridge with D171 on SCO1.

The docking results suggest that the C-terminal unstructured region of COA6 is important for the interaction between COA6 and SCO1. In order to test this model, we generated two truncated forms of COA6 by deleting residues 64-79 (COA6Δ64-79) and residues 72-79 (COA6Δ72-79) from the C-terminus. Both the truncations abrogate COA6 function, likely due to a loss of interaction with SCO1 (Fig. 3.6F). Additional evidence in support of the docking model and the interacting surfaces of COA6 and SCO1 comes from human patient data - the most commonly reported pathogenic variants in SCO1 (P174L) and SCO2 (E140K) both are close to COA6 interacting residues (Fig. 3.7) (OMIM *6033644 and *604272).

COA6 function can be bypassed in a reducing environment.

The presence of CHCH domain in COA6 structure suggests that it may play a redox role because a number of mitochondrial IMS protein with this domain are redox active and the CHCH fold has been suggested to represent the most minimal oxidoreductase domain (Banci et al., 2009). We utilized hypoxia treatment to uncover the potential *in vivo* redox role of COA6 in Cu delivery to CcO (Koritzinsky et al.,

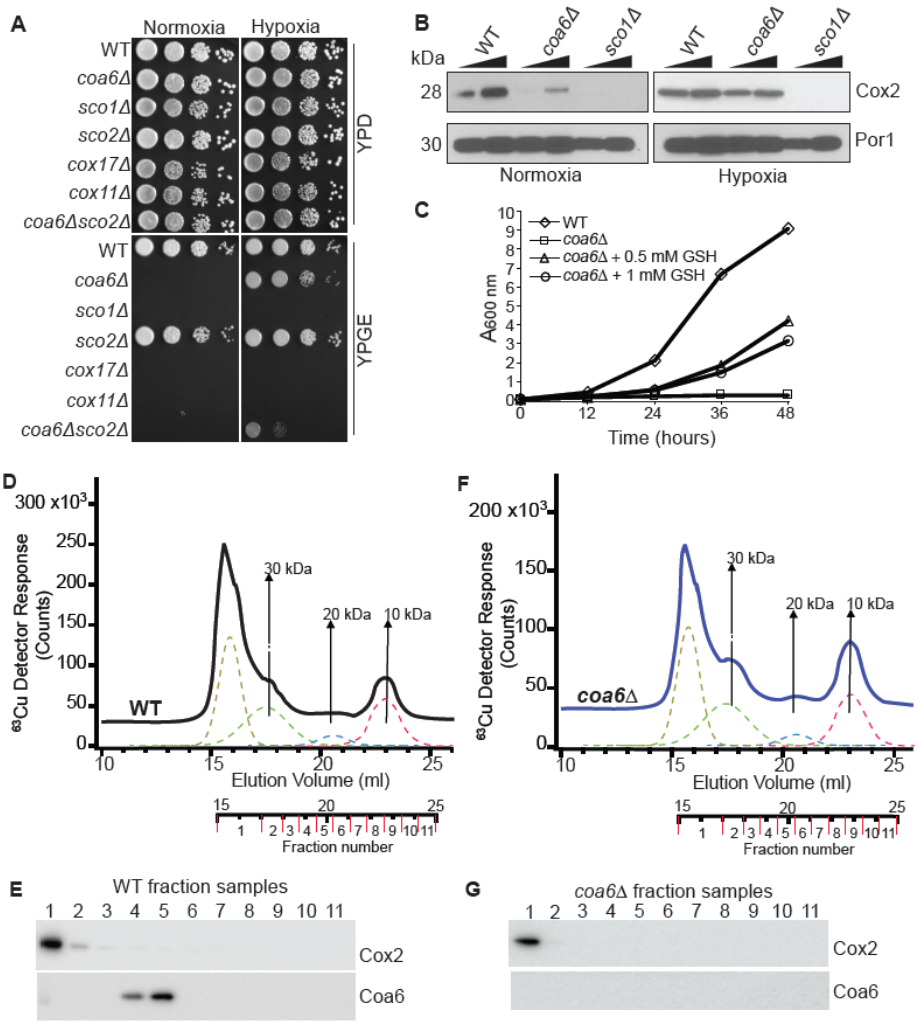


**Figure 3.8 Reducing environment specifically rescues respiratory growth of *coa6Δ* cells.**

(A) Serially diluted wild type (WT), *coa6Δ*, *sco1Δ, sco2Δ*, *cox17Δ*, *cox11Δ* and *coa6Δsco2Δ* cells were spotted on YP Dextrose (YPD) and YP Glycerol Ethanol (YPGE) plates and grown in normoxic or hypoxic (4% $O_2$) conditions. (B) SDS-PAGE/western blot depicting Cox2 levels and Por1 was used as loading control. (C) Wild type and *coa6Δ* cells were cultured in YPGE medium at 37°C in the presence or absence of reduced GSH at indicated concentrations. The cell density was measured spectrophotometrically at the indicated time points at 600 nm. (D-F) Copper traces from online LC-ICP-MS of WT sample shown in black (D) and *coa6Δ* sample shown in blue (F), while dotted lines indicate simulated curves generated by peak fitting. (E-F) SDS-PAGE/western blot depicting Cox2 and Coa6 levels in different fractions of WT and *coa6Δ* from online LC-ICP-MS.

2013). Hypoxic treatment (4% $O_2$) is expected to counter the oxidizing environment of mitochondrial IMS and would provide an *in vivo* condition to test the redox function of COA6. To this end, we cultured *coa6Δ* and other mutants of Cu delivery pathway in hypoxia in both fermentable and respiratory media and found that the respiratory growth of *coa6Δ* was almost fully rescued in the hypoxic conditions (Fig. 3.8A). Notably, the respiratory growth of *sco1Δ*, *cox17Δ*, and *cox11Δ* cells, which lack proteins with established Cu metallochaperone activity were not rescued under hypoxic conditions, a finding that suggests that hypoxia cannot replace metallochaperone function and is likely more specific in rescuing the deficiency of redox-related protein (Fig. 3.8A). Indeed, consistent with the established thiol-reductase role of SCO2 in the Cu delivery process, we also observed a partial rescue of *coa6Δsco2Δ* cells (Fig.3.8A). Since yeast lacking Sco2 do not have a clear respiratory growth-related phenotype, we were not able to test the effect of hypoxia on *sco2Δ* directly (Fig. 3.8A). The respiratory growth defect of *coa6Δ* cells has been attributed to a decrease in the levels of Cox2, which undergoes rapid turnover when Cu delivery is impeded (Ghosh et al., 2014; Pacheu-Grau et al., 2015). Therefore, to test whether Cu delivery to Cox2 is restored under hypoxic conditions, we measured Cox2 abundance in *coa6Δ* cells and found that it was indeed the case (Fig. 3.8B). Moreover, exogenous supplementation of reduced GSH also partially rescued respiratory growth of *coa6Δ* cells, further suggesting a redox role of Coa6 in the Cu delivery process (Fig. 3.8C).

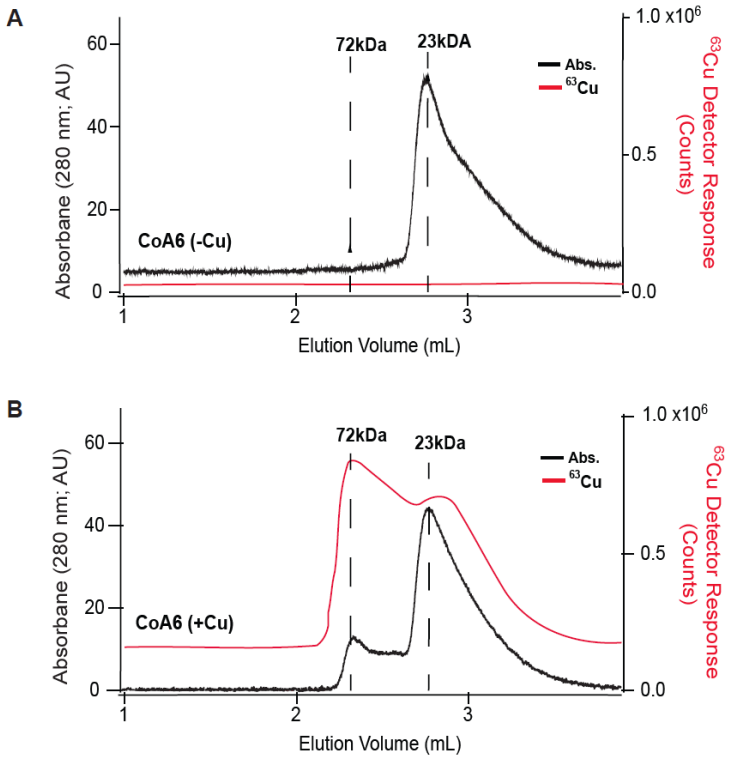


**Figure 3.9 Purified recombinant COA6 only binds copper when reconstituted with copper.**
(A) $^{63}Cu$ and protein traces of recombinant COA6 analyzed by LC-ICP-MS. (B) $^{63}Cu$ and protein traces of recombinant COA6 reconstituted with $CuSO_4$ and reduced glutathione.

Previous work has shown that human COA6 can bind Cu with high affinity *in vitro* (Stroud et al., 2015) suggesting a possible metallochaperone-like function. However, since we did not detect Cu in our structural studies with purified COA6, we wanted to determine Cu-binding properties of COA6. We utilized a custom-built online liquid chromatography-inductively coupled plasma- mass spectrometry (LC-ICP-MS) device, which allows simultaneous detection of Cu and protein in elution fractions obtained following size-exclusion chromatography. When purified COA6 was applied to this LC-ICP-MS system, we detected a major peak at $A_{280}$ corresponding to the COA6 dimer (Fig.

3.9A). The $A_{280}$ peak was not symmetrical suggesting contributions from COA6 monomer (Fig. 3.9A). We did not detect any $^{63}Cu$ peaks in the chromatogram indicating that recombinant COA6 does not bind endogenous Cu from *E. coli* (Fig. 3.9A). When purified COA6 was reconstituted with $CuSO_4$ and reduced glutathione as described previously (Stroud et al., 2015), we detected two major $A_{280}$ peaks corresponding to a dimer as well as less intense higher molecular weight species that likely corresponds to an aggregate of COA6 and Cu (Fig. 3.9B). Indeed, Cu peak was detected in the same fractions as COA6, with excess Cu found in the high-molecular weight COA6 aggregates (Fig. 3.9B). Thus, upon reconstitution in the presence of reduced glutathione, COA6 can bind Cu but whether this represents the physiological form remained uncertain. To address this concern, we decided to test whether Cu can bind Coa6 *in vivo* by analyzing the yeast mitochondrial fractions containing Coa6. Lysates from anaerobically purified mitochondria from the WT and *coa6Δ* cells were subjected to LC-ICP-MS to identify Cu-specific peaks. We detected four $^{63}Cu$ peaks, including one associated with the void volume and others associated with masses of ca. 30 kDa, 20 kDa and 10 kDa in the WT mitochondria (Fig. 3.8D). Notably, these $^{63}Cu$ peaks do not correspond to the fractions containing Coa6 (Fig. 3.8E) and the $^{63}Cu$ peaks in WT were nearly identical to those of *coa6Δ* samples in the region associated with the 30 kDa, 20 kDa and 10 kDa copper peaks (Fig. 3.8D-G). The lack of any difference in the $^{63}Cu$-detected WT and *coa6Δ* mitochondrial lysates suggests that Coa6 does not bind Cu under physiological conditions in yeast cells. Together, these results suggest that Coa6 likely has a redox function in Cu delivery and unlikely to be a metallochaperone.

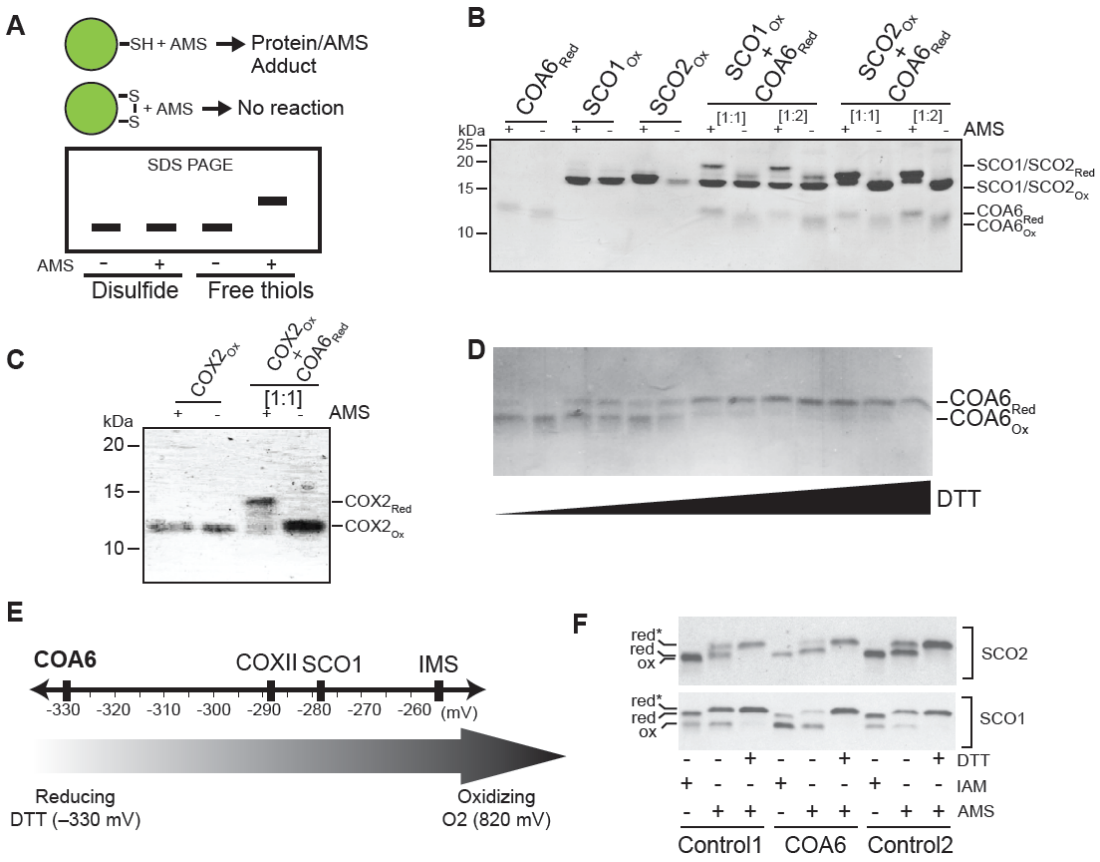


**Figure 3.10 COA6 acts as a thiol disulfide reductase of SCO and COX2 proteins.** (A) A schematic of how AMS reacts with reduced protein thiols resulting in protein-AMS adducts which increases the mass of the protein and retards its migration in SDS-PAGE (B-C) Migration patterns of purified recombinant human COA6, SCO1, SCO2, and COX2 proteins with and without AMS treatment on non-reducing SDS-PAGE. 1h co-incubation of reduced COA6 with oxidized SCO1, SCO2, or COX2 was followed by AMS treatment and SDS-PAGE. SCO and COA6 proteins were used at 1:1 and 1:2 stoichiometries. COX2 and COA6 proteins were used at a 1:1 stoichiometry. (D) SDS-PAGE analysis of COA6 protein subjected to increasing concentration of DTT followed by the treatment with alkylating agent AMS to irreversibly modify cysteines containing reduced thiols. (E) A schematic representation of redox potential of COA6 with previously determined redox potential values of COXII, SCO1, and the mitochondrial inter-membrane space (IMS). (F) Isolated mitochondria from two controls (Control 1 and Control 2) and COA6 mutant human fibroblasts were incubated in the presence or absence of the reductant dithiothreitol (DTT), followed by treatment with alkylating agents iodoacetamide (IAM) or AMS to irreversibly modify cysteines containing reduced thiols. Species of SCO1 and SCO2 containing oxidized (ox) cysteines were then resolved from those with reduced (red) cysteines by non-reducing SDS–PAGE and detected by immunoblotting with the indicated antibodies. Red* refers to reduced thiols that were modified in the presence of AMS.

COA6 acts as a thiol-disulfide reductase of SCO and COX2 proteins

Previous work on the biogenesis of prokaryotic $Cu_A$ center of heme-Cu oxidases has identified the requirement of both Cu metallochaperones and thiol-reductases (Abriata et al., 2007). In the case of COA6, the presence of CHCH domain, its redundancy in hypoxic environment, and previously reported overlapping function with SCO2, argues for its thiol-reductase activity. To directly test whether COA6 can reduce disulfide bonds of Cu-coordinating cysteines of its interacting partners, we utilized a thiol-alkylating reagent, 4-acetamido-4'-maleimidylstilbene-2,2'-disulfonic acid (AMS), that selectively reacts with free thiols on proteins to form a protein-AMS adduct, increasing the protein mass by ~0.5 kDa per free thiol. This additional molecular weight leads to an upward shift on an SDS-PAGE gel (Fig. 3.10A). Utilizing this assay, we observed that a 1h co-incubation of reduced COA6 with either of the oxidized SCO proteins led to the appearance of two SCO-specific bands in the AMS-treated samples (Fig. 3.10B). This observation suggests that COA6 is able to reduce the disulfides of SCO proteins, generating free sulfhydryl groups that react with AMS. Similarly, we found that COA6 can also reduce cysteines of COX2 (Fig. 3.10C).

To determine whether reduction of COX2 and SCO proteins is thermodynamically favorable, we determined the redox potential of COA6 using the DTTRed:DTTOx redox couple, and found it to be -330 mV at pH 7.0, which is lower than that of SCO1 (-280 mV) and COX2 (-290 mV) (Fig. 3.10D and E). Thus, the observed reduction of disulfide bonds in SCO1 and COX2 by COA6 is thermodynamically favorable.

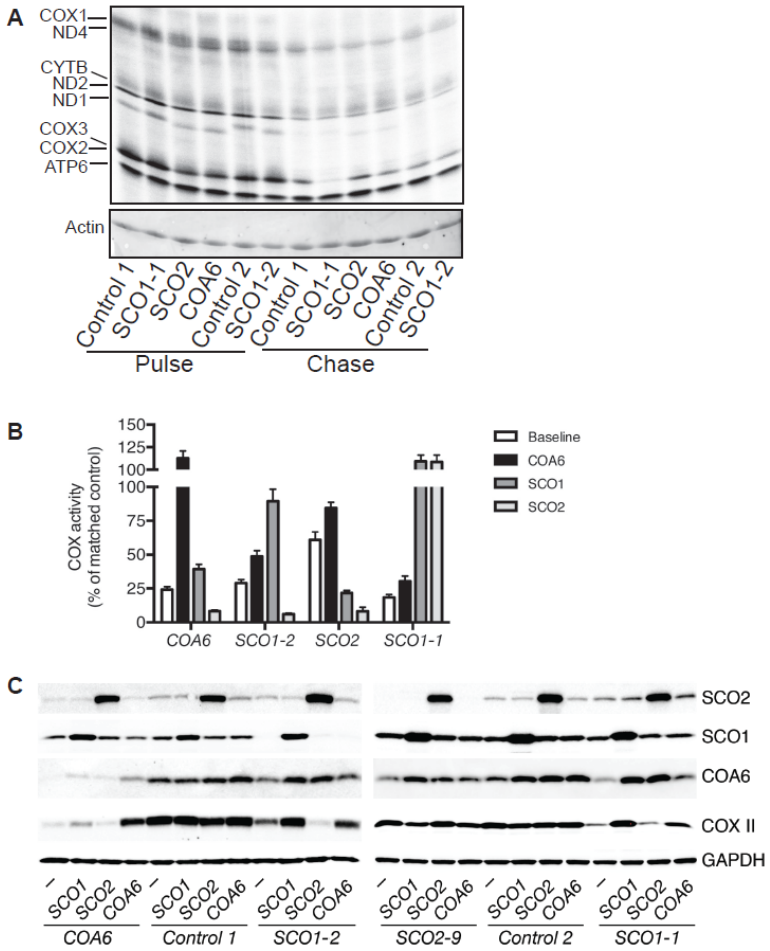


**Figure 3.11 *COA6* overexpression partially rescues the CcO deficiency in *SCO1* and *SCO2* patient backgrounds.**
(A*) In vivo* labeling of mitochondrial translation products in indicated control and patient cell lines. Samples were pulse-chased and analyzed by SDS-PAGE and digital autoradiography. (B) Cytochrome c oxidase acitvity (COX) in the COA6, SCO1, and SCO2 patient cell lines alone (baseline) or when over expressing *COA6* or *SCO1* or *SCO2*. (C) SDS-PAGE/western blot depicting COA6, SCO1, SCO2, COXII and GAPDH (loading control) levels in protein lysate from the *Control 1*, *Control* 2, *SCO1*, *SCO2* and *COA6* cell lines alone or when over expressing *COA6* or *SCO1* or *SCO2* as indicated.

Redox potential of SCO2 has been previously shown to be lower than -300 mV (Banci et al., 2007) possibly similar to even lower than COA6 and thus electron transfer from COA6 to SCO2 may not be thermodynamically favorable. To corroborate these *in vitro* findings,

we tested the redox state of the cysteinyl thiols of SCO proteins *in vivo* in COA6 patient cell lines using the alkylating agents AMS and iodoacetamide (IAM). As shown previously, in control fibroblast cell lines, SCO1 and SCO2 proteins exist as mixed populations consisting of species with either oxidized or reduced thiols as apparent by the presence of two bands in AMS-treated conditions (Fig. 3.10F) (Leary et al., 2009). The relative ratio of reduced to oxidized cysteinyl thiols of SCO1 in control cells lines is higher compared to the COA6 patient cell line, where oxidized species of SCO1 predominates (Fig. 3.10F). The difference in the ratio of oxidized to reduced species of SCO2 between the control and COA6 patient cell lines are not apparent (Fig. 3.10F). Together, these findings provide further evidence for thiol-disulfide reductase activity of COA6 *in vivo* and SCO1 being the target of this activity (Fig. 3.10F).

In order to determine how the redox function of COA6 affects the synthesis and stability of COX2 we performed pulse-chase labeling of mitochondrial DNA-encoded proteins in control and *COA6*, *SCO1* and *SCO2* patient cell lines. As determined by pulse labeling, COX2 synthesis was slightly reduced in COA6 and SCO2 but not in SCO1 patient cell lines (Fig. 3.11A). During chase, COX2 stability is dramatically reduced in SCO1 patient cell lines resulting from the rapid turnover of apo COX2, whereas COX2 levels in COA6 are more similar to SCO2 patient cells (Fig. 3.11A). These results are expected if COA6 has similar biochemical function to that of SCO2, which has previously been shown to have thiol-disulfide reductase activity (Leary et al., 2009; Morgada et al., 2015). Consistent with the idea that COA6 potentiates SCO1 function and has overlapping

function with SCO2, we found that overexpressing COA6 in SCO1 and SCO2 patient cell lines partially rescues CcO activity and COX2 levels (Fig. 3.11B and C).

**Discussion**

A large body of data has established that Cu insertion in the evolutionarily conserved dinuclear $Cu_A$ center in the COX2 subunit of CcO occurs in the mitochondrial IMS (Baker et al., 2017; Timon-Gomez et al., 2018). This topology poses two challenges: First, the Cu-coordinating cysteines of COX2 must be prevented from forming disulfide bonds in the oxidizing environment of the IMS. Second, the Cu metallochaperone responsible for delivering Cu to the $Cu_A$ site must be present in the IMS with its Cu coordinating thiols kept in the reduced state in order for Cu to bind. Thus, building the $Cu_A$ site is necessarily a two-step process that involves reducing thiol-disulfides of newly synthesized apoCOX2 followed by Cu transfer from a metallochaperone. To this end, here, we show that COA6 is a CHCH domain-containing protein that facilitates $Cu_A$ site maturation by exhibiting thiol-disulfide reductase activity towards apoCOX2 and SCO1, the metallochaperone that inserts Cu into the reduced apoCOX2. Thus, COA6 likely plays a dual role in $Cu_A$ maturation by maintaining Cu-coordinating cysteines of COX2 and its metallochaperone SCO1 in the correct oxidation state that allows Cu binding.

We have recently shown that *in vitro* metallation of $Cu_A$ site can be achieved by the combined action of -SCO1 and SCO2 proteins, where SCO1 transfers two Cu(I) equivalents to COX2 and thus, performs the metallochaperone function; and SCO2 reduces cysteine residues of COX2 making it competent for Cu binding (Morgada et al., 2015). Thus, *in vitro*, two orthologous SCO proteins are sufficient to form $Cu_A$ center;

however, genetic and protein-protein interaction data from multiple groups suggested that the final step in the metallation of $Cu_A$ center requires combined activities of at least three proteins, SCO1, SCO2 and COA6 (Ghosh et al., 2016; Pacheu-Grau et al., 2015; Stroud et al., 2015). To address this, disconnect between the *in vitro* and *in vivo* data, we decided to focus on determining the function of COA6, the most recently discovered member of this pathway. We considered three potential functions of COA6 -a Cu metallochaperone, a thiol-disulfide reductase and an adaptor protein that brings together SCO1, SCO2, and COX2.

Human COA6 being a small soluble 79 amino acid protein is highly amenable to NMR-based structure determination. Thus, we utilized NMR to solve the solution structure of human COA6 and identified a CHCH domain (Fig. 3.1F), which has been proposed to be the most "minimal" oxidoreductase domain described so far (Banci et al., 2009). One of the prototypical members of this family of CHCH-domain containing proteins is the mitochondrial IMS protein MIA40, which facilitates import of the mitochondrial IMS proteins by promoting oxidative folding of its client proteins (Banci et al., 2008). It has been proposed that MIA40 structurally resembles its own substrates, indeed prior work has shown that COA6 import into the mitochondrial IMS is dependent on MIA40 system (Vogtle et al., 2012). Consistent with its potential redox role, we found that COA6 function can be bypassed in reducing conditions (Fig. 3.8 A-C), which suggests that it may exhibit thiol-disulfide reductase activity. Indeed, our *in vitro* and *in vivo* experiments provided further support to this idea and identified SCO1 and COX2 as COA6 client proteins (Fig. 3.10). Having two client proteins for a thiol-disulfide reductase

in not unusual, a bacterial periplasmic protein thioredoxin TlpA was shown to act as a specific reductant for metallochaperone Sco1 and also CoxB, a bacterial equivalent of COX2 (Abicht et al., 2014; Mohorko et al., 2012). Thus, COA6 appears to be a functional homolog of bacterial TlpA, and represents an example of convergent evolution because there is no sequence homology between these two proteins. The oxidizing environment of the bacterial periplasmic space and the mitochondrial IMS (Hermann et al., 2009), where SCO1 and $Cu_A$ site resides, perhaps necessitates presence of TlpA and COA6 to reduce Cu-binding cysteines of its target proteins.

Our findings beg the questions as to why do you need three proteins – COA6, SCO1 and SCO2 *in vivo*, when two proteins, SCO1 and SCO2 are sufficient to form a $Cu_A$ center? In the *in vitro* experiments the redox states of SCO1 and SCO2 were set to favor Cu delivery to $Cu_A$ site, however, *in vivo* the appropriate redox states of these proteins need to be continuously regenerated for them to function. Thus, after delivering Cu to the $Cu_A$ site, SCO1 cysteines are likely to be more prone to oxidation in the oxidizing environment of the mitochondrial IMS and, have to be reduced to bind Cu for the next round of Cu delivery to apoCOX2. In this setting, COA6 function could be critical. Previously, it was shown that COX17, a metallochaperone that transfers Cu to SCO1, was also responsible for transferring electrons and reducing Cu-binding cysteines of SCO1 (Banci et al., 2008a). However, the redox potential of the S-S/2SH redox couple of COX17 (-198mV) does not thermodynamically favor electron transfer to SCO1 (-277mV) (Banci et al., 2008a) but apparently, a Cu-bound COX17 was able to overcome this thermodynamic barrier *in vitro*. Based on these observations and our findings, it appears

that COA6 is a more likely electron donor for SCO1 *in vivo*. In support of this, a recent report has identified SCO1-COA6-COX2 assembly module in yeast CcO biogenesis (Franco et al., 2018).

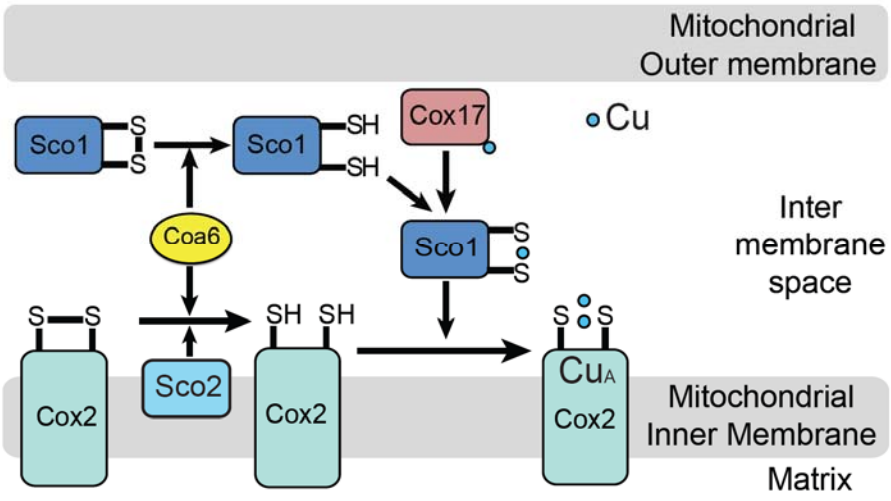


**Figure 3.12 A proposed model depicting putative function of COA6 in the $Cu_A$ site biogenesis.**

There is some discrepancy in the literature in terms of COA6 interacting partners, one group has shown specific interaction of COA6 with SCO2 both in yeast and human cells (Pacheu-Grau et al., 2015), whereas other group found interaction only between COA6 and SCO1 in human cells (Stroud et al., 2016). Now, our study utilizing competitive binding of purified human SCO1, SCO2, and COA6 proteins clearly shows that COA6 preferentially interacts with SCO1 (Fig. 3.5). Interestingly, the COA6 binding site of SCO1 is conserved in SCO2 suggesting that under certain conditions, when SCO2 levels exceed SCO1, it may bind COA6 (Fig. 3.5 and 3.7). Consistent with this idea, we find that overexpression of SCO2 in human SCO1 patient cell lines diminished CcO activity and COX2 levels, possibly by sequestering COA6 and preventing its interaction

with partially functional SCO1 protein (Fig. 3.11). Moreover, most commonly reported human patient mutations in SCO1 (P174L) (Valnot et al., 2000) and SCO2 (E140K) (Papadoupolous et al., 1999) are close to COA6 interacting surface providing clues to the molecular basis of these pathogenic mutations (Fig. 3.7). Future work is required to find out whether these mutations impair their interactions with COA6.

Previous studies had shown that purified COA6 can bind Cu, raising the possibility that it may act as a metallochaperone (Pacheu-Grau 2015; Stroud 2015). Here we find that unlike other Cu binding proteins, SCO1 and SCO2, which contain Cu upon purification from *E. coli* cultured in Cu supplemented media (Nittis et al., 2001 and Horng et al., 2005) recombinant COA6 did not contain Cu (Fig. 3.9A). We only observed Cu binding when recombinant COA6 was reconstituted with Cu and glutathione as described previously (Stroud et al., 2015). Importantly, we also did not detect COA6 in Cu-enriched mitochondrial fractions suggesting that either COA6 does not bind Cu *in vivo* or is present in too small a fraction that contributes to mitochondrial cupro-proteome (Fig. 3.8D-G). Moreover, unlike SCO2, which requires Cu for its redox activity, COA6 exhibits thiol-disulfide reductase activity in the absence of Cu (Fig. 3.10B and C). Thus, endogenous COA6 is unlikely to bind Cu and act as a metallochaperone.

By combining both *in vivo* and *in vitro* approaches, our study demonstrates that the mechanism of mitochondrial $Cu_A$ biogenesis requires combined activities of COA6, SCO1, and SCO2, where COA6 facilitates Cu delivery to the $Cu_A$ site by keeping Cu-binding cysteines of SCO1 and COX2 in a reduced state (Fig. 3.12). This model is consistent with the previous report, which documented a synthetic lethal interaction

between *coa6Δ* and *sco2Δ* yeast mutants (Ghosh et al., 2016) because both COA6 and SCO2 exhibit thiol-disulfide reductase activities and likely have a common target in COX2 (Fig. 3.12). In conclusion, our study provides molecular insights into the mitochondrial $Cu_A$ site biogenesis by unraveling the structure and function of COA6.

## Methods

Cloning and expression

*E.coli* codon optimized human *COA6* isoform3 was cloned into pGEX4t-1 vector using BamHI and XhoI restriction endonucleases to generate N-terminal, GST-fused *COA6*. *E.coli* codon optimized yeast *COA6* was cloned into a pET28a using XhoI and EcoRI restriction endonucleases to generate N-terminal, His-GFP-fused *COA6*. The resultant plasmids were then transformed into *E.coli* BL 21(DE3) cells. Human COA6 and yeast Coa6 expression was induced by the addition of 0.5 mM isopropyl-D-thiogalactopyranoside (IPTG) at an optical density of 600 nm ($OD_{600}$) of 0.6, and the cells were grown at 37°C and 16°C for 4 hr and 12 hr respectively. $^{15}N/^{13}C$ labeled proteins for NMR structural characterization were expressed in cells grown in minimal medium, which contained 3 g/liter $KH_2PO_4$, 6.8 g/liter $Na_2HPO_4$, 0.1 mM $CaCl_2$, 2 mM $MgCl_2$, 1x Basal Medium Eagle (BME) vitamin solution (Sigma), 1 g/liter $^{15}N$-ammonium chloride and 4 g/liter $^{13}C$-D-glucose (Sigma). Protein expression was induced using 0.5 mM IPTG at an $OD_{600}$ between 0.8 to 1, and the cells expressing human COA6 and yeast Coa6 were grown at 37 °C and 16 °C for 6 hr and 15 hr respectively.

Protein purification

To purify human COA6, cells were resuspended in lysis Buffer (50 mM Tris (pH 7.4), 150 mM NaCl, 1 mM PMSF and 0.1 % Triton X100) and lysed by repeated sonication on ice for a total of 4 min. The lysate was clarified by centrifugation at 40,000 g for 30 min at 4°C and the supernatant was applied to a GST binding column pre-equilibrated with 50 mM Tris (pH 7.4), 150 mM NaCl. GST-COA6 was eluted using 50 mM Tris (pH 7.4), 150 mM NaCl, and 10 mM reduced glutathione. Eluted GST-COA6 was subjected to thrombin digestion (20 units of thrombin for 100 mg of GST-COA6 protein) for 12 hr at room temperature. To further purify, COA6 from the flow through was injected onto HiPrep Sephacryl S-100 column pre-equilibrated with 20 mM Tris (pH 7.4), 150 mM NaCl.

To purify yeast Coa6, cells were resuspended in lysis Buffer containing 20 mM Tris (pH 8), 500 mM NaCl, 1 mM PMSF and 6 mM imidazole and sonicated on ice for a total of 4 min. The lysate was clarified by centrifugation at 40,000 g for 30 min at 4°C and the supernatant was applied to a HisTrap HP column pre-equilibrated with 20 mM Tris (pH 8), 500 mM NaCl, and 6 mM imidazole. His-GFP-Coa6 was eluted using 20 mM Tris (pH 8), 500 mM NaCl, and 400 mM imidazole. Eluted His-GFP-Coa6 was subjected to TEV digestion for 12 hr at 4°C. Yeast Coa6 was further purified by using Superdex 200 column pre-equilibrated with 20 mM Tris (pH 7.4), 500 mM NaCl. Human SCO1 and SCO2 were purified as described before (Banci et al., 2006; Banci et al., 2007).

NMR Spectroscopy

NMR data were acquired in Shigemi tubes on 0.015 – 0.947 mM COA6 sample buffered in 20 mM Tris, 150 mM NaCl, 10% (v/v) $D_2O$; pH 7.4. All NMR experiments used for the structure calculation were carried out at 25°C on the Bruker Avance 800 MHz, 600 MHz, or 500 MHz NMR spectrometers equipped with a 5 mm triple-resonance cryoprobe and single-axis pulsed field gradient by using standard pulse programs provided by the instrument manufacturer. NMR data were acquired and processed by using software Topspin, version 3.2 (Bruker, Germany), and were further analyzed in Sparky, version 3.112 (University of California, San Francisco).

$^{1}H$, $^{13}C$, and $^{15}N$ resonance assignments for Coa6 were indirectly referenced according to the IUPAC recommendations (Markley et al., 1998). The protein backbone resonance assignments were achieved through analysis of the 3D-triple resonance experiments and the aliphatic side-chain resonances were primarily assigned using 3D-HCCH-COSY and $^{15}N$-edited TOCSY-HSQC acquired with 60 ms mixing time. The aromatic side-chains were assigned using 2D-homo-nuclear TOCSY and NOESY spectra and verified with 2D-experiments $^{13}C$-HMQC and (HB)CB(CGCD)HD. The NOE distance restraints were based on 3D-experiments, $^{13}C$-edited NOESYHSQC and $^{15}N$-edited NOESY HSQC, each acquired with a 150 ms mixing time. Semi-automated NOE cross-peak assignments were performed by using the CYANA software package (Guntert et al., 2015) and were manually checked for correctness in an iterative manner. Dihedral angle restraints were predicted from the backbone chemical shifts using the program TALOS+ (Shen et al. 2009). Sixteen slowly exchanging backbone amide protons

identified in H/D exchange experiment were predicted to belong in α-helical regions by the chemical shift index analysis (Wishart et al., 1994) and the NOESY patterns. Thus 32 corresponding distance restraints for HN-O and N-O atoms were imposed in the final structure calculation to depict the H-bonds (Williamson et al., 1985). Isotope-filtered NOESY experiments (3D-$^{13}$C,$^{15}$N-filtered/edited NOESY HSQC) were performed on a sample prepared by mixing 1:1 ratio of unlabeled and $^{13}$C,$^{15}$N-labeled sample to identify inter-subunit contacts between COA6 dimer. These experiments failed to observe any cross peaks due to the weak dimerization constant and were not used in further analysis.

COA6 subunit structure calculation was performed using CYANA, version 3.96, following a torsion angle molecular dynamics protocol (Guntert et al., 1997). A total of 200 random conformers were annealed in 15,000 steps for 7 cycles, and 20 structures with the lowest target functions after the final cycle were selected for water refinement, which was performed using software X-plor NIH version, 2.50 (Schwieters et al., 2003). The structure ensemble was validated with the Protein Structure Validation Software suite 1.5 (Bhattacharya et al., 2007)

$^{15}$N relaxation experiments were performed on $^{15}$N-labeled COA6 samples at 25°C on the 600 MHz spectrometer. Ten $^{15}$N longitudinal relaxation rate constant (R1) experiments were performed in random order, with relaxation delays of 10 (duplicate), 90, 190, 320, 470 (duplicate), 660, 936, 1500 ms. Similarly, the transverse relaxation rate constant (R2) experiments were performed with relaxation delays of 0 (duplicate), 16.9, 33.9, 50.9 (duplicate), 67.8, 84.8, 118.7, 186.6 ms. Both rate constants were calculated using the program Curvefit, assuming a monoexponential decay of the peak intensities.

The errors in the peak intensities were calculated from the two duplicate experiments. The steady-state heteronuclear [$^{1}$H]-$^{15}$N NOE experiment was carried out in an interleaved manner, with and without proton saturation and repeated thrice. The NOE effect was calculated as an average ratio of the peak intensities.

Online LC-ICP-MS

Cu binding to the purified COA6 and the yeast mitochondrial extracts was measured by using an online LC-ICP-MS system. A bio-inert HPLC system (Agilent Technologies, 1260) was kept inside a chilled and refrigerated glove box (MBraun, labmaster 130) and was connected to an ICP-MS (Agilent Technologies, 7700x) via a PEEK tubing coming from the diode array of the LC system in the glove box for detection. The HPLC system was composed of a pump (G5611A), diode array (G4212B), fraction collector (G5664A), and manual injector. The ICP-MS was interfaced with the LC system via a micromist nebulizer that was attached to a Scott-type spray chamber. The ICP-MS was tuned each day prior to analyzing samples and all samples were analyzed with the ICP-MS configured in helium collision mode. The instrument was tuned as previously described (Dziuba, et al., 2018).

Samples were analyzed either with a dual Superdex Peptide 10/300 GL (GEHealthcare) columns connected in series or with a Bio SEC-3 (Agilent Technologies) column. All samples were passed through either a Titan regenerated cellulose 0.2 μm filter (Thermo scientific), a 0.2 μm cellulose acetate filter (VWR). The Superdex peptide columns used a mobile phase of 20 mM Tris pH 7.4 and 10 mM NaCl at a flow rate of 0.350 mL/min for a total of 160 min per run and a loop of 300 uL. The Bio SEC-3 column

used a mobile phase of 20 mM Tris pH 7.4 and 150 mM NaCl at a flow rate of 0.4 mL/min for a total of 10 min per run and a loop of 20 µL. The diode array was set for detection and data collection at the 280 nm wavelength for samples. Cyanocobalamin (1.3 kDa) from Fisher BioReagents; cytochrome c (12 kDa), carbonic Anhydrase (30 kDa), albumin (66 kDa) and apoferritin (443 kDa) from Sigma were used as molecular weight references.

Gel filtration chromatography

The apparent molecular weight of COA6 was determined using gel filtration chromatography. COA6 (100 µM) was loaded onto a Superdex 75 10/300 GL column equilibrated with 20 mM Tris, pH 7.4 and 150 mM NaCl at a flow rate of 0.3 ml/min. Aprotinin (6.5 kDa), cytochrome c (12.4 kDa), carbonic anhydrase (29 kDa) and albumin (66 kDa) were used as molecular weight references (Sigma, MWGF70).

Haddock docking calculation of COA6/SCO1 complex

The molecular docking of COA6 and SCO1 was performed using the Haddock d-level 2.2 web server as described (van Zundert and Bonvin, 2014). Chemical shift perturbation data were used as structural restraints (referred to as ambiguous interaction restraints (AIR)). The docking calculation used the NMR structure of COA6 determined in this study and the crystal structure of SCO1 (PDB ID: 2GVP) as input structures for the docking calculation. A total of 26 AIR restraints were used based on chemical shift perturbation data for COA6 (Fig. 3.6A) and SCO1 (Fig. 3.6C). Initial docking calculations generated 200 structures (with lowest energy) that were then used for subsequent simulated

annealing and water refinement. The final docked structures (10 lowest energy structures) had an overall RMSD of 1.8 Å.

Yeast strains, plasmids and culture conditions

All strains used in this study are listed in Table 3.3 and all the primers used in this study are listed in Table 3.2. Yeast cells were grown in YP (1% yeast extract, 2% bactopeptone) medium with 2% dextrose (YPD) or 3% glycerol + 1% ethanol (YPGE) as carbon sources. Synthetic media was prepared with 0.17% yeast nitrogen base, 0.5% ammonium sulfate, 0.2% dropout amino acid mix and contained 2% dextrose as a carbon source. Solid media was prepared by additionally adding 2% agar. Growth was measured spectrophotometrically at 600 nm in liquid medium or by spotting on solid plates. For hypoxic growth conditions on solid media, indicated plates were incubated in hypoxia incubator chamber (STEMCELL Technologies), which was purged with certified gas mixture (4% oxygen, 5% carbon dioxide and 91% nitrogen). For hypoxic growth conditions in liquid media media, synthetic complete raffinose liquid media which constitutes 2% raffinose and 1x TEM (0.5% Tween80, 2.4 µg/ml ergosterol, 55.6 µg/ml methionine) was kept in glove box with nitrogen gas for 24 hrs before cultured with the indicated strains, followed by incubation at 30°C at 225 rpm.

**Table 2.2 Primers used in this study**

| Name | Sequence (5' to 3') |
|---|---|
| **Protein expression primers** | |
| Human COA6 isoform 3 Forward | GGGCCAGGATCCATGGCAGCACCGAGCATGAAA |
| Human COA6 isoform 3 Reverse | GGGCCACTCGAGTTAGCTTTTTGCGGTGGTTTC |
| Yeast Coa6 Forward | TAGCGAAAATCTGTATTTTCAGGGTAGCGAATTC ATGGGCTTATTTTCATTTGATGGTGGC |
| Yeast Coa6_Stop Reverse | GTGGTGGTGGTGGTGCTCGAGTCACTGATTTCGT TCCCTCTGTTTAG |
| Yeast Coa6 Reverse | GTGGTGGTGGTGGTGCTCGAGCTGATTTCGTTCC CTCTGTTTAG |
| **Site Directed mutagenesis primers** | |
| *HyCOA6* W26C Forward | AGTATTCATCTCTAGCACCGCAACACAATTTTCT TTGGG |
| *HyCOA6* W26C Reverse | CCCAAAGAAAATTGTGTTGCGGTGCTAGAGATG AATACT |
| *HyCOA6* W33R Forward | TTTTCGTCCAAACATTTCCGGTATTCATCTCTAGC ACCC |
| *HyCOA6* W33R Reverse | GGGTGCTAGAGATGAATACCGGAAATGTTTGGA CGAAAA |
| *HyCOA6* E54X Forward | CATTGTTGTGGACAAGAAGATTAGAAAGAGGAT CTCAACTTCTTA |
| *HyCOA6* E54X Reverse | TAAGAAGTTGAGATCCTCTTTCTAATCTTCTTGTC CACAACAATG |
| **Primers for Human COA6** | |
| COA6-F | AAAAAGCAGGCTACCATGGGCCCGGGAGGTCCC TT |
| COA6-R | AGAAAGCTGGGTCTAGGATTTTGCAGTTGTTTCT GA |
| COA6 W59C-F | GAAAGACAGGTCTGCTGTGGGGCCCGGGATGAG TAC |
| COA6 W59C-R | GTACTCATCCCGGGCCCCACAGCAGACCTGTCTT TC |
| COA6 W66R-F | GCCCGGGATGAGTACCGGAAGTGTTTAGATG |
| COA6 W66R-R | CATCTAAACACTTCCGGTACTCATCCCGGGC |
| **Protein truncation primers** | |
| *HyCOA6* SacI Forward | CCCCTGGAGCTCGCAAAGACGCGCAGCCAAAAA |
| *HyCOA6_64* BamH1 Reverse | GCGCGCGGATCCCTTTTCTTTGAACTTCAAGTAG TCTCT |
| *HyCOA6_72* BamH1 Reverse | GCGCGCGGATCCTGGTTCGAATTGACCGGCTTCG AACTT |

**Table 3.3 *Saccharomyces cerevisiae* strains used in this study**

| Yeast Stains | Genotype | Source |
|---|---|---|
| BY4741 WT | *MATa, his3Δ1, leu2Δ0, met15Δ0, ura3Δ0* | Greenberg lab |
| BY4741 *coa6Δ* | *MATa, his3Δ1, leu2Δ0, met15Δ0, ura3Δ0 coa6Δ::kanMX4* | Open Biosystems |
| BY4741 *sco1Δ* | *MATa, his3Δ1, leu2Δ0, met15Δ0, ura3Δ0 sco1Δ::kanMX4* | Open Biosystems |
| BY4741 *sco2Δ* | *MATa, his3Δ1, leu2Δ0, met15Δ0, ura3Δ0 sco2Δ::kanMX4* | Open Biosystems |
| BY4741 *cox11Δ* | *MATa, his3Δ1, leu2Δ0, met15Δ0, ura3Δ0 cox11Δ::kanMX4* | Open Biosystems |
| BY4741 *cox17Δ* | *MATa, his3Δ1, leu2Δ0, met15Δ0, ura3Δ0 cox17Δ::kanMX4* | Open Biosystems |
| STY10 *sco2Δcoa6Δ* | *MAT a, his3Δ1, leu2Δ0, ura3Δ0, lys2Δ0, sco2Δ::KanMX4, coa6Δ::NatMX4* | Ghosh et al., 2016 |

Mammalian Cell Culture

Primary fibroblasts from control, *COA6* (Baertling et al., 2015), *SCO1-1* (R149X/P174L; Valnot et al., 2000), *SCO1-2* (V93X/M294V; Leary et al., 2013) and *SCO2-9* (Leary et al., 2013) were immortalized as previously described (Leary et al., 2004). Fibroblasts were transduced at 40–60% confluency with retrovirus produced by the Phoenix amphotrophic packaging cell line, and selected in media containing hygromycin or puromycin to yield stable overexpression cell lines (Leary et al., 2004). Both fibroblasts and the packaging cells were grown in high-glucose DMEM containing 10% bovine growth serum (ThermoFisher) at 37°C in an atmosphere of 5% $CO_2$ and tested to ensure that they were *Mycoplasma*-free (Lonza MycoAlert) before harvesting.

SDS-PAGE and western blotting

For yeast samples- SDS-polyacrylamide gel electrophoresis (SDS-PAGE) mitochondria (20 μg) were separated and blotted onto a polyvinylidene difluoride membrane. Membranes were treated for 1 h in blocking buffer containing 5% nonfat milk dissolved in Tris-buffered saline with 0.1% Tween 20 (TBST-milk), followed by overnight incubation with primary antibody in TBST-milk at 4°C. Primary antibodies were used at the following dilutions: Cox2, 1:100,000 (Abcam 110271); Coa6, 1:5000 and Porin, 1:50,000 (Abcam 110326).

For human cell line- Whole cells were homogenized on ice in STE buffer (250 mM sucrose, 10 mM Tris-HCl, pH 7.4, and 1 mM EDTA) supplemented with a 1× protease inhibitor cocktail (Roche, Indianapolis, IN) and 0.5 mM phenylmethylsulfonyl

fluoride (PMSF; Sigma-Aldrich) and centrifuged twice at 4°C for 10 min at 600 × *g* to obtain a postnuclear supernatant. A crude mitochondrial fraction was then obtained by centrifugation at 4°C for 10 min at 8000 × *g* and used for non-reducing SDS–PAGE analyses as previously described (Leary et al. 2009). Whole cells were extracted in a RIPA extraction buffer [50 mM Tris (pH 7.4), 150 mM NaCl, 1% Triton X-100, 0.5% sodium deoxycholate, 0.1% SDS, 1 mM EDTA and 1x Complete protease inhibitor cocktail (Roche)], adjusted to a final concentration of 5 mg/ml, incubated on ice for 30 min and then centrifuged at 4 °C for 10 min at 14 000 ×*g* and used for reducing SDS-PAGE analyses (Boulet et al., 2018).

For both reducing and nonreducing SDS–PAGE gels, equal amounts of protein were separated on precast gels (BioRad), transferred to nitrocellulose membrane, blocked for 2 h in Tris buffered saline supplemented with Tween 20 [TBST; 25 mM Tris (pH 7.4), 137 mM NaCl, 2.5 mM KCl and 0.05% Tween 20] containing 5% milk (US Biologicals), and incubated overnight at 4 °C in primary antibody. Membranes were then washed six times for 5 min in TBST, incubated for 60 min in the appropriate horseradish peroxidase conjugated secondary antibody (BioRad, 1: 2500) in TBST containing 5% milk, and washed again in TBST as above. Membranes were developed using a homemade luminol-enhanced chemiluminescence solution, and visualized with the BioRad ChemiDoc™ MP Imaging System.

Redox state determination

*In vitro* redox state of the cysteine residues in protein and protein mixtures were investigated by nonreducing SDS/PAGE after reaction of the samples with and without AMS as described previously (Morgadaa et al., 2015). Reduced and oxidized samples and protein mixtures were (20–40 μM) treated in an anaerobic environment with 1% (wt/vol) SDS and 10 mM AMS for 1 hr at 37°C, and resolved by 17% nonreducing SDS/PAGE.

Redox potential determination

The reduction potential of the cysteine residues in COA6 was estimated by monitoring the redox state of thiols in COA6, using AMS and non-reducing SDS/PAGE after titrating with varying concentrations of dithiothreitol.

In vitro labeling of mitochondrial translation products

Cells were labeled in 6 cm dishes as described in detail elsewhere (Sasarman and Leary 2009). Briefly, cells were incubated in chloramphenicol (Sigma) prior to labeling to inhibit mitochondrial translation and allow for the accumulation of nuclear-encoded respiratory chain subunits. 400 μCi of a [$^{35}$S]-methionine and cysteine mixture (Easy Tag™ EXPRESS) was added for 60 min to cells in methionine- and cysteine-free DMEM containing 10% dialyzed fetal bovine serum (Gibco) and anisomycin (Sigma), to reversibly inhibit cytoplasmic translation. Total cellular protein (50 μg) was resuspended in sample loading buffer containing β-mercaptoethanol, sonicated and run on a 12–20%

gradient gel. Gels were subsequently transferred to nitrocellulose under semi-dry conditions and the [$^{35}$S]-labeled mitochondrial translation products were detected through digital autoradiography.

# CHAPTER IV

# MITOCHONDRIAL DISEASE GENES COA6, COX6B AND SCO2 HAVE OVERLAPPING ROLES IN COX2 BIOGENESIS*

## Disclaimer

The work described in this chapter comprises of a paper published in the journal *Human Molecular Genetics,* to which I contributed as a third author. The summary is a reprint of the publication abstract and the rest of the sections are as published. My contributions to this chapter are described in the figures 4.7 and 4.8.

## Summary

Biogenesis of cytochrome *c* oxidase (CcO), the terminal enzyme of the mitochondrial respiratory chain, is a complex process facilitated by several assembly factors. Pathogenic mutations were recently reported in one such assembly factor, *COA6,* and our previous work linked Coa6 function to mitochondrial copper metabolism and expression of Cox2, a copper-containing subunit of CcO. However, the precise role of Coa6 in Cox2 biogenesis remained unknown. Here we show that yeast Coa6 is an orthologue of human COA6, and like Cox2, is regulated by copper availability, further implicating it in copper delivery to Cox2. In order to place Coa6 in the Cox2 copper delivery pathway, we performed a comprehensive genetic epistasis analysis in the yeast *Saccharomyces cerevisiae* and found that simultaneous deletion of Coa6 and Sco2, a mitochondrial copper metallochaperone,

---

* This chapter is adapted from the work which was originally published in Human Molecular Genetics. Ghosh A, Pratt AT, Soma S, Theriault SG, Griffin AT, Trivedi PP, Gohil VM. Mitochondrial disease genes COA6, COX6B and SCO2 have overlapping roles in COX2 biogenesis. Hum Mol Genet. 2016; 25 (4):660-671. by permission of Oxford University Press.

or Coa6 and Cox12/COX6B, a structural subunit of CcO, completely abrogates Cox2 biogenesis. Unlike Coa6 deficient cells, copper supplementation fails to rescue Cox2 levels of these double mutants. Overexpression of Cox12 or Sco proteins partially rescues the *coa6Δ* phenotype, suggesting their overlapping but non-redundant roles in copper delivery to Cox2. These genetic data are strongly corroborated by biochemical studies demonstrating physical interactions between Coa6, Cox2, Cox12 and Sco proteins. Furthermore, we show that patient mutations in Coa6 disrupt Coa6–Cox2 interaction, providing the biochemical basis for disease pathogenesis. Taken together, these results place COA6 in the copper delivery pathway to CcO and, surprisingly, link it to a previously unidentified function of CcO subunit Cox12 in Cox2 biogenesis.

**Introduction**

Defects in the function and formation of the mitochondrial respiratory chain (MRC) manifest clinically in mitochondrial diseases, one of the most common classes of inborn errors of metabolism (Vafai and Mootha, 2012). A subset of MRC disorders can be attributed to the deficiency of MRC complex IV, commonly known as cytochrome c oxidase (CcO). CcO is the terminal enzyme of the MRC that catalyzes the reduction of molecular oxygen to water and generates an electrochemical gradient that drives mitochondrial adenosine triphosphate (ATP) synthesis. CcO is an evolutionarily conserved multi-subunit enzyme complex whose catalytic core is composed of three subunits: Cox1, Cox2 and Cox3, which are encoded by mitochondrial DNA in both yeast and humans (Soto et al., 2012). The other structural subunits, which are encoded by

nuclear DNA, surround the catalytic core to form the CcO holoenzyme. In addition to the protein subunits, CcO contains several cofactors including two copper centers ($Cu_A$ and $Cu_B$), two heme groups (heme *a* and *a3*), a magnesium ion and a zinc ion (Tsukihara et al., 1996). The assembly of a fully mature, catalytically active CcO is an extremely complex process that requires a number of assembly factors to bring together the mitochondrial and nuclear DNA encoded subunits with their metal cofactors.

CcO biogenesis is a modular process that begins with the independent maturation of the core subunits Cox1, Cox2 and Cox3, followed by the addition of other nuclear-encoded subunits (Fornuskova et al., 2010; McStay et al., 2013). There are ~40 assembly factors discovered to date that facilitate different steps of CcO assembly (Soto et al., 2012). For example, 22 assembly factors are required for the expression and membrane insertion of the catalytic core subunits, 9 assembly factors are required for copper delivery to copper A ($Cu_A$) and copper B ($Cu_B$) site in Cox2 and Cox1 subunits, respectively, and 4 factors are required for heme biosynthesis and insertion into the catalytic core (Soto et al.,2012 ). Unlike assembly factors required for the expression and insertion of mitochondrial DNA-encoded catalytic subunits, all the factors required for copper delivery and heme insertion to the Cox1 and Cox2 subunits are conserved in yeast and humans (Soto et al., 2012).

Patients suffering from CcO deficiency exhibit multi-systemic and tissue-specific disorders, primarily affecting organs with higher energy demands including the brain, skeletal muscle and heart (Ghezzi and Zeviani, 2012; Shoubridge, 2001). CcO deficiency leads to early onset, autosomal recessive disorders with fatal clinical outcomes (Ghezzi and Zeviani, 2012; Shoubridge, 2001). The combination of human genetics and

knowledge of CcO assembly factors from *Saccharomyces cerevisiae* has led to the discovery of multiple CcO disease genes. While a few mutations can be attributed to the structural subunits of CcO, including COX1, COX2, COX3, COX4 and COX6B (Abdulhag et al., 2015; Massa et al., 2008; Shoubridge, 2001; Shteyer et al., 2009), the majority of patient mutations are found in genes encoding assembly factors including LRPPRC, TACO1, FASTKD2, PET100, COX10, COX14, COX15, COX20, SURF1, SCO1, SCO2, COA3, COA5 and COA6 (Antonicka et al., 2003; Baertling et al., 2015; Calvo et al., 2012; Ghezzi et al., 2008; Gohil et al., 2010; Huigsloot et al., 2011; Jaksch et al., 2000; Lim et al., 2014; Mootha et al., 2003; Ostergaard et al., 2015; Papadopoulou et al., 1999; Stiburek et al., 2009; Szklarczyk et al., 2013; Valnot et al., 2000a; Valnot et al., 2000b; Weraarpachai et al., 2009; Weraarpachai et al., 2012; Zhu et al., 1998). Although CcO deficient patients display heterogeneous clinical presentations, it has been noted that mutations in the assembly factors involved in the same pathway exhibit similar clinical phenotypes. For example, patients with pathogenic mutations in the copper metallochaperones SCO1 and SCO2, which are involved in copper delivery to the $Cu_A$ site of CcO subunit COX2, typically develop neonatal encephalopathy and hypertrophic cardiomyopathy (Jaksch et al., 2000; Papadopoulou et al., 1999; Stiburek et al., 2009; Valnot et al., 2000a). Similarly, patient mutations in *COA6* also result in neonatal hypertrophic cardiomyopathy (Baertling et al., 2015; Calvo et al., 2012); however, the precise role of COA6 in CcO assembly has remained unknown.

We first reported that COA6 is essential for CcO assembly in yeast, zebrafish and human cells possibly by delivering copper to COX2 subunit (Ghosh et al., 2014). While

up to nine factors have been implicated in copper delivery to CcO subunits COX1 and COX2, the precise role of many of them remains obscure (Soto et al., 2012). The components of the copper delivery pathway that have been reconstituted *in vitro* suggest that COX17 receives copper from a mitochondrial matrix pool (Cobine et al., 2004) and donates it to copper metallochaperones COX11 and SCO1/SCO2 (Horng et al., 2004), which ultimately transfer copper to the $Cu_B$ site in COX1 and $Cu_A$ site in COX2, respectively (Hiser et al., 2000; Leary et al., 2004). Multiple other proteins, including COA6, have been implicated in this copper delivery pathway, but it is not clear where they act in the pathway.

Our initial findings linking COA6 to COX2 biogenesis and mitochondrial copper metabolism have been corroborated by two recent studies that show reduced stability of nascent COX2 in COA6 deficient cells and that COA6 binds to copper *in vitro* (Pacheu-Grau et al., 2015; Stroud et al., 2015). While these studies have also identified physical interactions between COA6 and copper metallochaperones SCO1 and SCO2, the functional significance of the interaction is not known. Here, we have used genetic epistasis analysis in yeast to demonstrate that *COA6* is essential for Cox2 expression in the absence of SCO2 and COX12, a structural subunit of CcO. This synthetic interaction between Coa6, Sco2 and Cox12 proteins suggests their overlapping functions in Cox2 biogenesis. Consistent with this observation, we find that overexpression of Cox12 and Sco proteins partially rescues the respiratory deficient growth phenotype of *coa6Δ* cells. We further substantiate these genetic data by demonstrating a physical interaction between Coa6, Cox12, Cox2 and Sco proteins. Taken together, our study not only places Coa6 in

the copper delivery pathway to Cox2, but also implicates *COX12*, a yeast orthologue of the human mitochondrial disease gene *COX6B*, in copper metabolism and Cox2 biogenesis.

**Results**

Yeast and human COA6 are orthologues

Previously, we showed that COA6 is an evolutionarily conserved protein that is required for the expression of CcO subunits including COX2 in yeast, zebrafish and human cells (Ghosh et al., 2014). Sequence alignment of yeast and human COA6 showed that these two proteins are highly conserved except in the N-terminal region (Ghosh et al., 2014), possibly because of differences in N-terminal mitochondrial targeting sequences in these two species. The sequence conservation and their common role in CcO expression suggested that yeast and human COA6 are orthologues. To experimentally test the functional similarity of these two proteins, we performed a complementation experiment by heterologous expression of human COA6 in yeast *coa6Δ* cells. We episomally expressed yeast *COA6 (yCOA6)*, human *COA6 (hCOA6)* or yeast–human hybrid *COA6 (hyCOA6)* in *coa6Δ* cells and tested for their ability to rescue the respiratory growth deficiency of *coa6Δ* cells. The *hyCOA6* was constructed by fusing the gene segments corresponding to the N-terminus of yeast Coa6 (amino acid residues 1–24) and the C-terminus of human COA6 (amino acids residues 57–125) containing the evolutionarily conserved $Cx_9Cx_nCx_{10}C$ motif (Fig. 4.1A). As expected, *yCOA6* completely rescued the respiratory growth defect of *coa6Δ* cells, but *hCOA6* was not able to rescue this growth

defect (Fig. 4.1B). However, hyCOA6 was able to completely restore respiratory growth (Fig. 4.1B) suggesting that yeast and human COA6 are orthologues.

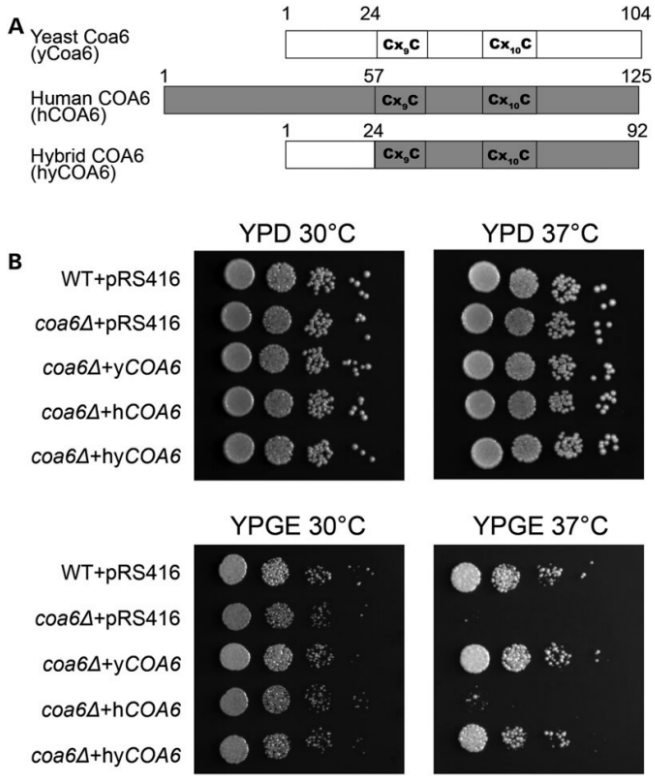


**Figure 4.1 Heterologous expression of yeast–human hybrid COA6 rescues respiratory growth defect of yeast *coa6Δ* cells.**
(A) Schematic representation of yeast Coa6, human COA6 and hybrid COA6 proteins. The sequence from yeast Coa6 is shown in white, and the sequence from human COA6 is shown in gray. (B) Ten-fold serial dilutions of WT and *coa6Δ* cells transformed with either empty vector (pRS416) or with pRS416 expressing yeast *COA6 (yCOA6)*, human *COA6* (*hCOA6*) or hybrid COA6 (*hyCOA6*) were spotted on fermentable (YPD) and non-fermentable (YPGE) growth media. Plates were incubated at 30°C and 37°C and images were taken after 2–4 days of growth. These data are representative of three independent experiments.

Coa6 is regulated by mitochondrial biogenesis factors

Having established the orthologous relationship between the human and yeast Coa6 protein, we decided to use yeast as a model system to study the function and regulation of Coa6. To study the regulation of the endogenous yeast Coa6 protein, we generated polyclonal antibodies against native Coa6 protein. We confirmed antibody specificity by detecting a Coa6 specific band of ~12 kDa in cellular extracts from wild type (WT) and Coa6 overexpressing cells (Fig. 4.2A). We hypothesized that Coa6, as a mitochondrial protein, would be regulated by mitochondrial biogenesis factors including carbon source, growth phase and the presence of mitochondrial DNA. Growth of yeast cells in respiro-fermentable (YPGal) or non-fermentable (YPGE) media is known to stimulate mitochondrial biogenesis, and accordingly, Coa6 levels were higher in cells grown in YPGal and YPGE medium compared with fermentable medium (YPD) (Fig. 4.2B). In glucose containing YPD medium, Coa6 expression increased late in the growth phase, likely because of derepression of glucose-mediated inhibition of mitochondrial biogenesis (Fig. 4.2B). Interestingly, we found that an increase in Coa6 levels precedes an increase in Cox2 levels (Fig. 4.2B), implying that the presence of Coa6 is essential for Cox2 expression. Consistent with a previous report, which showed a suppression of mitochondrial biogenesis in mitochondrial DNA deficient ρ0 yeast cells (Epstein et al., 2001), we observed a dramatic decrease in Coa6 levels in ρ0 cells (Fig. 4.2C), further confirming that Coa6 levels are regulated by mitochondrial biogenesis.

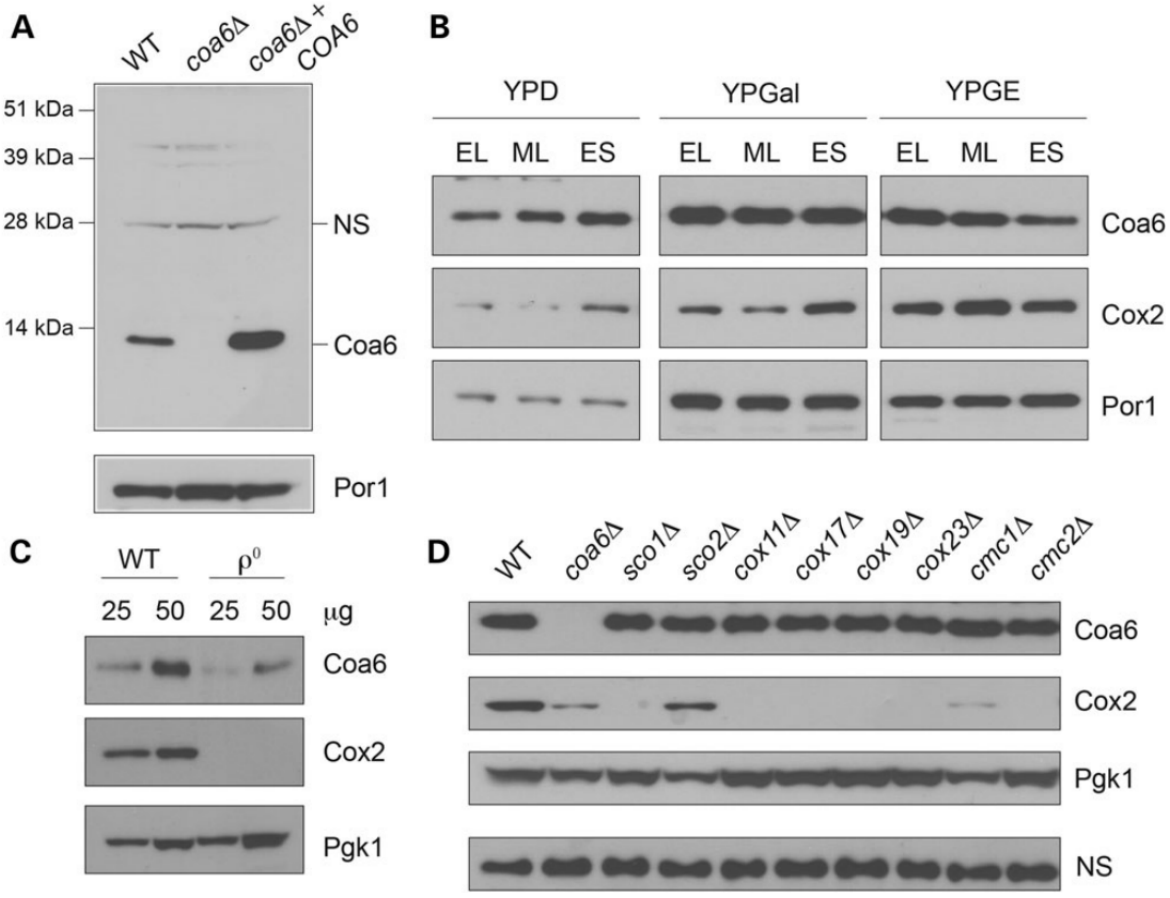


**Figure 4.2 Coa6 expression is regulated by mitochondrial biogenesis factors and is independent of CcO assembly factors.**
(A) Total cellular protein was extracted from BY4741 WT, *coa6Δ* and *coa6Δ* transformed with pRS426-COA6 and subjected to SDS PAGE/western blot. Yeast Coa6 protein was detected using purified polyclonal Coa6 antibody; NS designates a non-specific protein band detected by polyclonal Coa6 antibody. Porin (Por1) was used as a loading control. (B) Western blot analysis of Coa6 and Cox2 protein levels in total cellular extracts from BY4741 WT yeast cells grown in YPD, YPGal or YPGE to early logarithmic, mid-logarithmic (ML) and early stationary (ES) growth phase. Por1 was used as a loading control. (C) Western blot analysis of Coa6 and Cox2 levels in BY4741 WT and ρ0 cells grown in YPGal medium to ML growth phase. Pgk1 was used as a loading control. As indicated, 25 or 50 μg of protein was loaded in each lane. (D) Western blot analysis of Coa6, Cox2 and Pgk1 protein levels in the indicated knockout strains grown to ML growth phase in YPGal medium. Since Pgk1 levels increased in cells completely lacking Cox2, a nonspecific (NS) band was used as a loading control. The data in panels B-D are representative of three independent experiments.

It has been shown that steady-state levels of some of the CcO assembly factors are reciprocally regulated. For example, levels of Cmc1, a copper-binding mitochondrial intermembrane space (IMS) protein, increase in response to deletion of Cmc2, another CcO assembly factor (Horn et al., 2010). To tie Coa6 to CcO assembly factors involved in copper metabolism, we explored the possibility that Coa6 levels are regulated by other CcO assembly factors. Therefore, we measured Coa6 levels in various yeast strains lacking known copper metallochaperones including Cox11, Cox17, Sco1 and Sco2 and twin $Cx_9C$ motif-containing proteins implicated in CcO assembly, including Cox19, Cox23, Cmc1 and Cmc2. We found that the levels of Coa6 did not change in the knockout strains tested (Fig. 4.2D). Interestingly, we noticed that the levels of Pgk1, a glycolytic enzyme used as a loading control, increased in all CcO assembly factor mutants that are completely devoid of Cox2 (Fig. 4.2D). Therefore, we used a non-specific band to confirm equal loading (Fig. 4.2D). The increase in Pgk1 could be a homeostatic mechanism to maintain cellular ATP production in Cox2 deficient cells that are unable to produce mitochondrial ATP. In a reciprocal experiment, we measured the levels of copper metallochaperones and CcO subunits, Cox17, Sco1, Sco2, Cmc1, Cox12 and Cox2 in *coa6Δ* cells and, except for a decrease in the Cox2 and Cox12 levels, we did not find any significant change in the levels of the other proteins measured (Fig. 4.3). This result suggests that Coa6 abundance is independent of the presence of these CcO assembly factors and vice-versa.

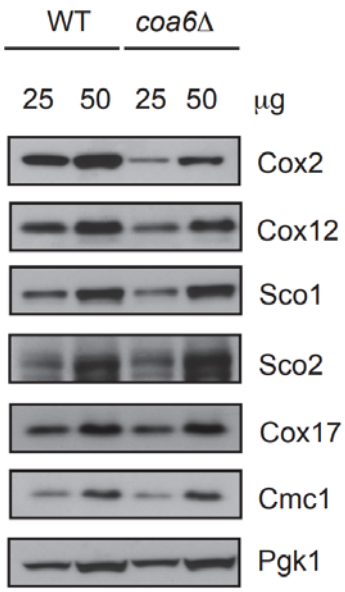


**Figure 4.3 Levels of CcO assembly factors do not change in *coa6Δ* cells.**
Western blot analysis of the indicated CcO subunits and assembly factors in total cellular protein extract from WT and *coa6Δ* cells grown to mid-logarithmic growth phase in YPGal medium. The blot was probed with the indicated antibodies. Pgk1 was used as a loading control.

Coa6 levels change in response to extracellular copper abundance

A recent study has shown that levels of iron-containing proteins in the MRC decrease in response to increasing amounts of the iron chelator deferoxamine in mouse muscle cells (Rensvold et al., 2013). Since Coa6 has been implicated in the copper delivery pathway to CcO (Ghosh et al., 2014) and has recently been shown to bind copper (Pacheu-Grau et al., 2015; Stroud et al., 2015), we hypothesized that Coa6 levels would alter in response to copper chelation and supplementation. In order to identify the optimal concentration of copper-specific chelator bathocuproinedisulfonic acid (BCS) and copper, WT yeast were grown in respiro-fermentable YPGal medium supplemented with increasing amounts of BCS or copper chloride ($CuCl_2$). We found that 25 μM or more of

BCS reduced yeast growth in YPGal medium by limiting bioavailable copper required for respiratory growth, whereas up to 100 μM copper supplementation did not alter yeast growth (Fig. 4.4A and B). We observed that Coa6 levels decreased with increasing concentrations of BCS, whereas copper supplementation modestly increased Coa6 levels (Fig. 4.4C). Similarly, Cox2 levels decreased drastically under copper limiting conditions, while copper supplementation slightly increased Cox2 (Fig. 4.4C). The decrease in Coa6 with BCS supplementation is more pronounced in mitochondrial samples isolated from chromosomal hemagglutinin (HA) tagged-Coa6 cells (Fig. 4.4D). These results suggest that, like the copper-containing protein Cox2, Coa6 expression is dependent on bioavailable copper, further implicating it in mitochondrial copper metabolism.

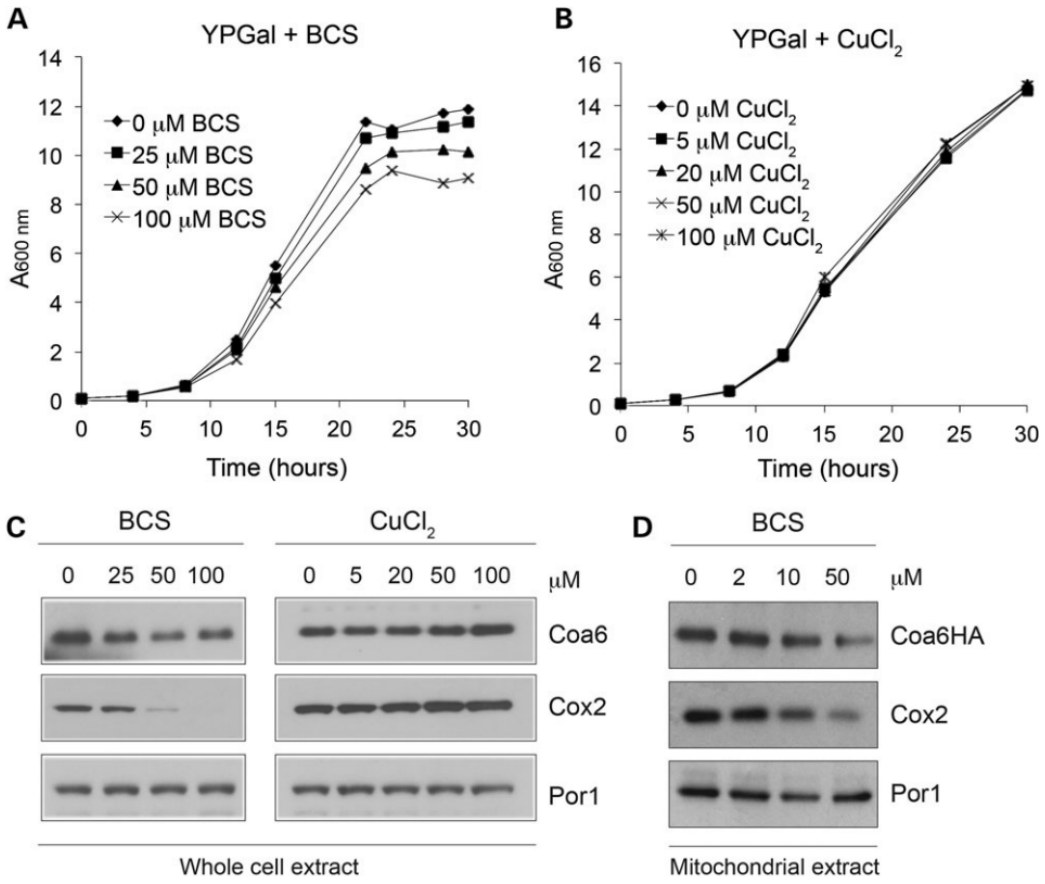


**Figure 4.4 Coa6 levels are regulated by copper availability.**
WT yeast cells were grown in YPGal medium with increasing concentrations of (A) the copper chelator, BCS or (B) $CuCl_2$. Growth was analyzed by measuring absorbance at 600 nm. (C) Western blot analysis of Coa6 and Cox2 levels in whole cell protein lysate prepared from WT yeast cells grown to ML growth phase in YPGal medium with increasing amounts of BCS or $CuCl_2$. (D) Western blot analysis of Coa6HA and Cox2 levels in mitochondria isolated from chromosomally HA-tagged COA6 cells grown in YPD to ES growth phase with increasing amounts of BCS. Por1 was used as a loading control. The blots are representative of at least two independent experiments.

Coa6 acts in parallel with Cox12 and Sco2 to maintain Cox2 levels

Our previous results showed that copper supplementation rescues the *coa6Δ* respiratory-deficient phenotype (Ghosh et al., 2014) and our current study shows that Coa6 levels are regulated by copper availability. Together, these studies strongly suggest that

Coa6 plays a role in copper delivery to CcO. In order to place Coa6 in the CcO copper delivery pathway, a genetic epistasis analysis was performed where *coa6Δ* cells were crossed with the deletion strains of the known copper metallochaperones and $Cx_9C$ proteins implicated in CcO assembly. The resulting double knockouts were extensively phenotyped in different growth conditions (Table 4.1). Analysis of the growth phenotypes of both the parental single knockouts and the double knockouts identified strong synthetic lethal interactions of *COA6* with *SCO2* and *COX12* (Fig. 4.5A and B). To probe for the mechanism that leads to synthetic lethality of double knockouts in respiratory media, we measured levels of the copper containing CcO subunit Cox2. Cox2 levels are decreased in *coa6Δ, sco2Δ* and *cox12Δ* to different degrees, but completely absent in both *coa6Δsco2Δ* and *coa6Δcox12Δ* cells (Fig. 4.5C and D). Exogenous supplementation of copper fails to rescue the growth defect and Cox2 deficiency of either double knockout (Fig. 4.5A–D). These data suggest that Coa6, Sco2 and Cox12 play overlapping roles in the copper delivery to Cox2.

**Table 4.1 Genetic interaction study of Coa6 with known CcO assembly factors involved in copper metabolism.**

| Strain | YPD | YPGal | YPGE | SCD | SCGal | SCG |
|---|---|---|---|---|---|---|
| BY4741 WT | ++++ | ++++ | ++++ | ++++ | ++++ | ++++ |
| BY4742 *coa6Δ* | ++++ | ++++ | ++++ | ++++ | ++++ | ++++ |
| BY4741 *cox11Δ* | ++++ | ++++ | - | ++++ | ++ | - |
| STY2 *coa6Δcox11Δ* | ++++ | ++++ | - | ++++ | ++ | - |
| BY4741 *cox12Δ* | ++++ | ++++ | - | ++++ | +++ | - |
| STY3 *coa6Δcox12Δ* | ++++ | ++++ | - | ++++ | ++ | - |
| BY4741 *cox17Δ* | ++++ | ++++ | - | ++++ | - | - |
| STY1 *coa6Δcox17Δ* | ++++ | ++++ | - | ++++ | - | - |
| BY4741 *cox19Δ* | ++++ | +++ | - | ++++ | ++ | - |
| STY4 *coa6Δcox19Δ* | ++++ | +++ | - | ++++ | ++ | - |
| BY4741 *cox23Δ* | ++++ | +++ | - | ++++ | ++ | - |
| STY5 *coa6Δcox23Δ* | ++++ | +++ | - | ++++ | ++ | - |
| BY4741 *cmc1Δ* | ++++ | ++++ | ++++ | ++++ | ++++ | ++ |
| STY6 *coa6Δcmc1Δ* | ++++ | ++++ | ++++ | ++++ | ++++ | ++++ |
| BY4741 *sco1Δ* | ++++ | +++ | - | ++++ | ++ | - |
| STY9 *coa6Δsco1Δ* | ++++ | +++ | - | ++++ | ++ | - |
| BY4741 *sco2Δ* | ++++ | ++++ | ++++ | ++++ | ++++ | ++++ |
| STY10 *coa6Δsco2Δ* | ++++ | ++++ | - | ++++ | ++++ | ++ |
| BY4741 *pic2Δ* | ++++ | ++++ | ++++ | ++++ | ++++ | ++++ |
| STY11 *coa6Δpic2Δ* | ++++ | ++++ | +++ | ++++ | ++++ | +++ |

Serial dilutions of wild type (WT), single knockouts, and double knockouts were spotted on rich (YP) or synthetic complete (SC) media with different carbon sources as indicated and incubated at 30$^{O}$C for 2-5 days. The plates were scored according to the number of dilutions that grew. Maximal growth of all four dilutions is indicated using "++++," while no growth is indicated by "-".

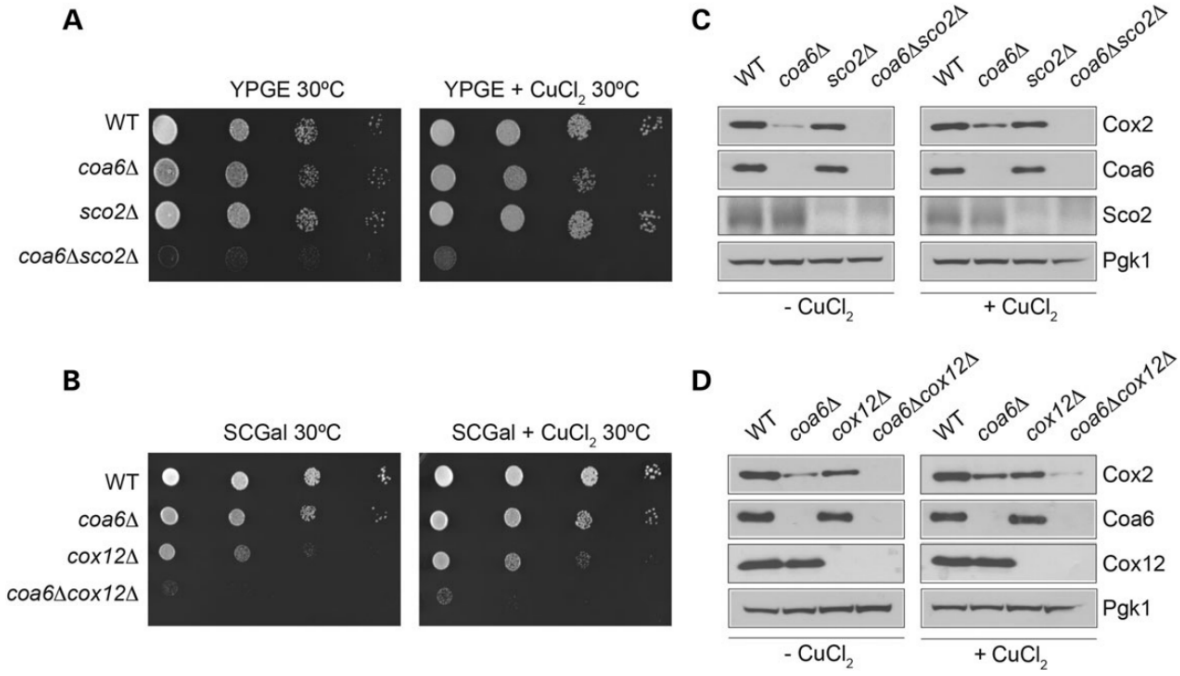


**Figure 4.5 Coa6, Sco2 and Cox12 have an overlapping but non-redundant role in Cox2 expression.**

**(**A) Ten-fold serially diluted WT, *coa6Δ, sco2Δ and coa6Δsco2Δ* cells were spotted on YPGE plates with and without 5 µM $CuCl_2$. (B) Ten-fold serially diluted WT, *coa6Δ*, *cox12Δ* and *coa6Δcox12Δ* cells were spotted on synthetic complete (SC) galactose medium with and without 5 µM $CuCl_2$. Plates were incubated at 30°C and images were taken after 3 days of growth. (C and D) WT, single knockouts of Coa6, Sco2, Cox12 and double knockouts *coa6Δsco2Δ* and *coa6Δcox12Δ* were grown to ML phase in YPGal liquid medium with and without 5 µM $CuCl_2$. Cox2 levels in total cellular protein extracts of WT and mutant cells were analyzed by western blot. Pgk1 was used as a loading control. Coa6, Sco2 and Cox12 have an overlapping but non-redundant role in Cox2 expression. (A) Ten-fold serially diluted WT, *coa6Δ, sco2Δ* and *coa6Δsco2Δ* cells were spotted on YPGE plates with and without 5 µM $CuCl_2$. (B) Ten-fold serially diluted WT*, coa6Δ, cox12Δ* and *coa6Δcox12Δ* cells were spotted on synthetic complete (SC) galactose medium with and without 5 µM $CuCl_2$. Plates were incubated at 30°C and images were taken after 3 days of growth. (C and D) WT, single knockouts of Coa6, Sco2, Cox12 and double knockouts *coa6Δsco2Δ* and c*oa6Δcox12Δ* were grown to ML phase in YPGal liquid medium with and without 5 µM $CuCl_2$. Cox2 levels in total cellular protein extracts of WT and mutant cells were analyzed by western blot. Pgk1 was used as a loading control.

Coa6 physically interacts with Cox2, Cox12 and Sco proteins

Genetic interactors tend to participate in a common pathway and are more likely to physically interact (Tong et al., 2004). To test whether Coa6 physically interacts with Cox2 and copper metallochaperones, we performed co-immunoprecipitation experiments using anti-HA and anti-Cox2 antibodies. Reciprocal co-immunoprecipitation experiments showed that Coa6 specifically interacts with Cox2 protein (Fig. 4.6A) and not with Cox1 or other proteins of the MRC (data not shown). In order to rule out the possibility that the interaction was merely due to Coa6 overexpression, we constructed chromosomal HA-tagged Coa6 cells, where Coa6HA is expressed from its endogenous promoter. In this case, we found a similar interaction between Coa6HA and Cox2 (Fig. 4.6B). Furthermore, to confirm that the interaction we observed was not because of an interaction between Cox2 and the HA tag itself, we performed an immunoprecipitation experiment using polyclonal anti-Coa6 antibodies on WT and *coa6Δ* mitochondria. We again found Coa6–Cox2 interaction and additionally, upon probing with other antibodies, we identified physical interactions between Coa6 and Sco1, Sco2 and Cox12, but not between Coa6 and $Cu_B$ center-containing Cox1 or copper metallochaperone Cox17 (Fig. 4.6C). These results suggest that Coa6 exists as a part of a multimeric protein complex in mitochondria. To detect Coa6-containing complex(es), we performed a blue native polyacrylamide gel electrophoresis (BN PAGE)/western analysis on mitochondrial extracts and found that Coa6 is part of three high molecular weight complexes of ~60, 140 and 200 kDa (Fig. 4.6D). We thus conclude that Coa6 and its interacting partners form complexes that may participate in Cox2 metallation.

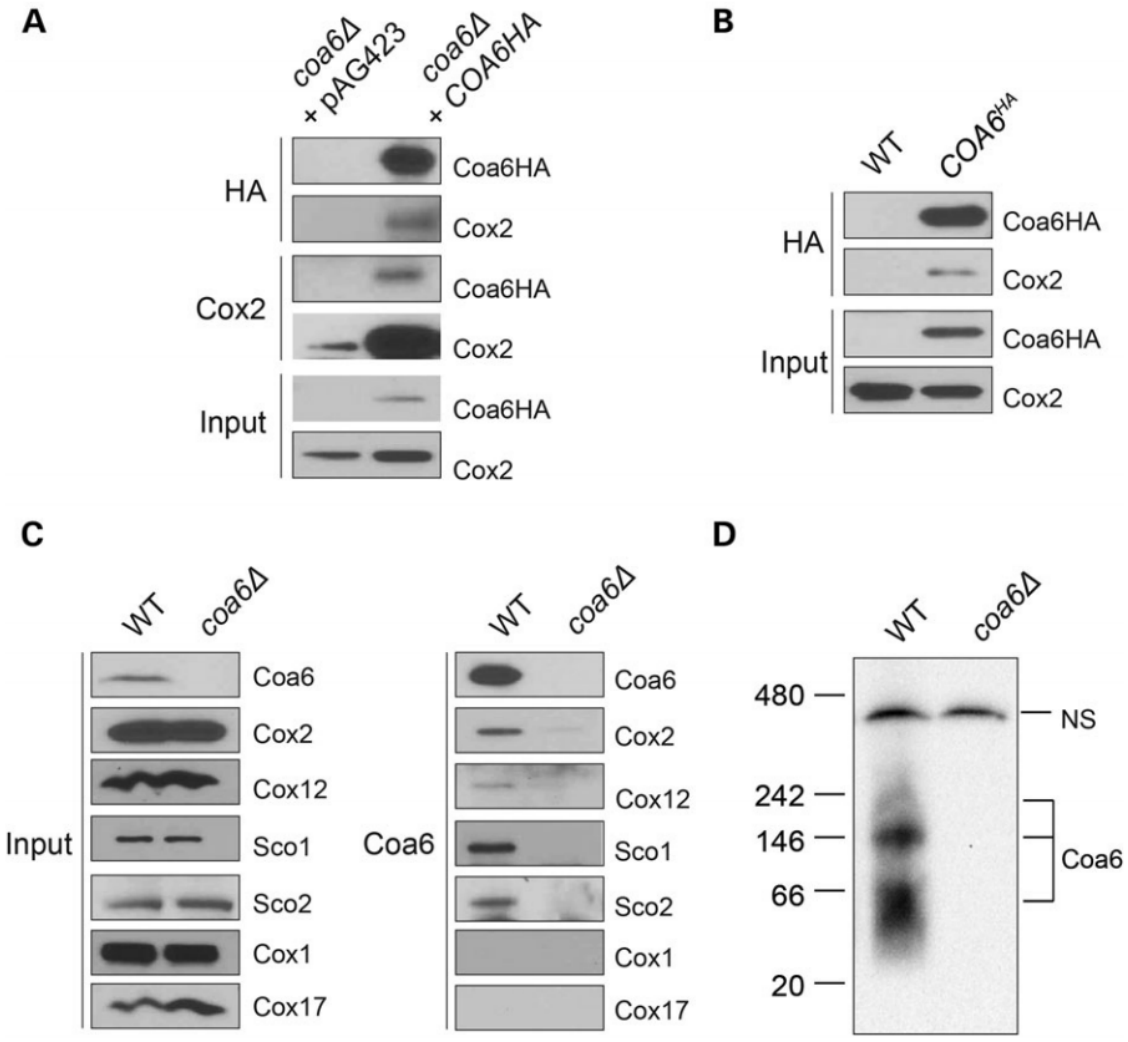


**Figure 4.6 Coa6 physically interacts with Cox2, Cox12 and Sco proteins.**
(A)Western blot detection of Coa6-HA and Cox2 proteins in mitochondrial extracts from *coa6Δ* cells transformed with either empty vector (pAG423) or pAG423-COA6HA before (input) or after immunoprecipitation with anti-HA and anti-Cox2 antibodies. (B)Western blot detection of Coa6-HA and Cox2 proteins in mitochondrial extracts from WT and chromosomally HA-tagged COA6 cells before (input) or after immunoprecipitation with anti-HA antibody. (C)Western blot detection of native Coa6, Cox1, Cox2, Cox12, Sco1 and Sco2 proteins in mitochondrial extracts from WT and *coa6Δ* cells before (input) or after immunoprecipitation with anti-Coa6 antibody. (D) BN PAGE/western blot detection of Coa6-containing complexes from 1% digitonin solubilized mitochondria isolated from WT and *coa6Δ* cells grown in YPGE with 5 μM $CuCl_2$. NS designates a non-specific protein band.

Coa6, Cox12 and Sco proteins have overlapping functions

Our genetic interaction study suggested that Coa6 acts in parallel with Cox12 and Sco2 in Cox2 biogenesis; these proteins are thus likely to have overlapping functions. To test this hypothesis, we overexpressed *COX12, SCO2* and *SCO1,* in *coa6Δ* cells and scored for rescue of respiratory growth on YPGE plates at 37°C. As a control, we expressed other proteins involved in Cox2 biogenesis including *COX17, COX19, COX20* and *COX23* in *coa6Δ* cells. We also expressed the yeast mimic (Sco2 E161K) of the most common human SCO2 patient mutation (E140K) (Papadopoulou et al., 1999) in *coa6Δ* cells to test for its ability to suppress *coa6Δ* growth defect (Fig. 4.7A). As seen in Figure 4.7B, the *coa6Δ* respiratory growth defect was partially suppressed by overexpression of SCO1, SCO2, COX12 and COX20 but not by COX17, COX19 and COX23. Interestingly, the Sco2 E161K mutant also partially rescued *coa6Δ* growth phenotype suggesting that E161 is not essential for yeast Sco2 function (Fig. 4.7B). To further interrogate yeast Sco2 function, we expressed yeast mimics (E161K and S246F) of two human SCO2 patient mutations (E140K and S225F) (Papadopoulou et al., 1999) in *coa6Δsco2Δ c*ells. We found that while E161 is not essential, S246 is critical for *coa6Δsco2Δ* growth and yeast Sco2 function (Fig. 4.7C). While the rescue of the respiratory growth defect of *coa6Δ* cells by overexpression of Sco proteins and Cox20 is not surprising since these proteins are known to cooperate in the late stages of Cox2 biogenesis (Bourens et al., 2014), the ability of COX12 to suppress the *coa6Δ* growth defect is surprising and links Cox12 to the copper delivery pathway to Cox2.

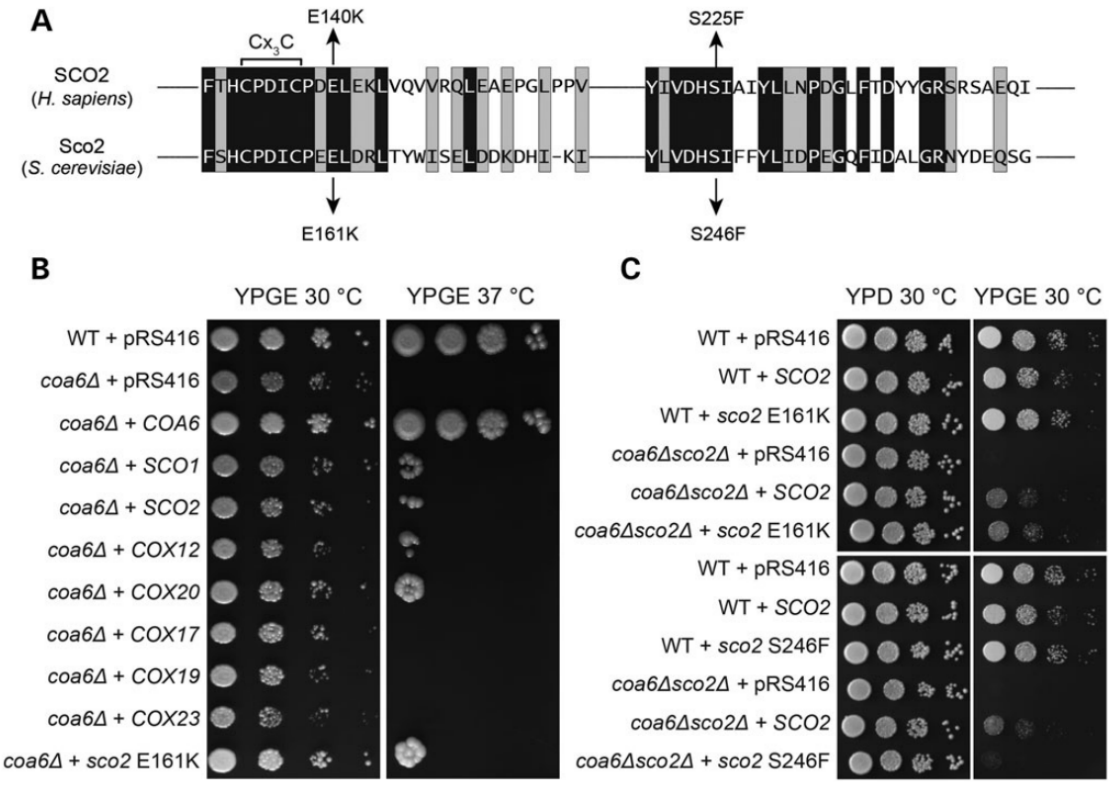


**Figure 4.7 Overexpression of Cox12, Cox20 and Sco proteins partially rescues *coa6Δ* respiratory defect.**

(A) Sequence alignment of conserved regions of human SCO2 and its yeast homolog. Arrows indicate amino acid residues (glutamic acid E140 and serine S225) shown to be mutated in human mitochondrial disease patients. Two mutations in yeast Sco2, E161K and S246F, that mimic the patient mutations are also indicated with arrows. (B) Ten-fold serially diluted WT cells transformed with pRS416 empty vector and *coa6Δ* cells transformed with pRS416 empty vector or pRS416 vector expressing either COA6, SCO1, SCO2, COX12, COX20, COX17, COX19, COX23 and sco2 E161K were spotted on YPGE plates at 30°C and 37°C. Images were taken after 3 days for cells grown at 30°C and 6 days for cells grown at 37°C. (C) Ten-fold serially diluted WT and *coa6Δsco2Δ* cells transformed with pRS416 empty vector or pRS416 vector expressing either SCO2, or sco2 with patient mutation E161K or S225F were spotted on YPD or YPGE plates and incubated at 30°C. Images were taken after 2 days for cells grown on YPD and 4 days for cells grown on YPGE.

Sequence alignment and structural analysis of both yeast and mammalian Coa6 and Cox12 proteins shows presence of a conserved $Cx_9Cx_nCx_{10}C$ motif (Fig. 4.8A) with a similar predicted tertiary structure (Fig. 4.8B), strongly supporting their overlapping function. To further dissect the interaction between Coa6 and Cox12, we performed a reciprocal experiment, whereby we tried to rescue the respiratory growth deficient phenotype of *cox12Δ* with COA6 overexpression. Interestingly, we found that instead of rescuing, COA6 overexpression enhanced the *cox12Δ* growth defect (Fig. 4.8C). Taken together, our results suggest overlapping but non-redundant roles of Coa6, Sco1 Sco2, and Cox12 in Cox2 maturation.

Pathogenic mutations within the conserved $Cx_9Cx_nCx_{10}C$ motif of Coa6 disrupt its interaction with Cox2

Previously, we showed that patient mutations in the $Cx_9Cx_nCx_{10}C$ motif of Coa6 are pathogenic and that the conserved cysteine residues of the motif are essential for Coa6 function (Ghosh et al., 2014). Patient mutations reduced the stability of Coa6, partly explaining the mechanism of pathogenesis (Ghosh et al., 2014). However, it was not clear if reduced levels of Coa6 were sufficient to cause pathogenesis. In addition to Coa6 stability, it is possible that patient mutations may disrupt Coa6 function by preventing its interactions with its binding partners. Therefore, we tested the effect of patient mutations (p.W26C and p.C68A) as well as a mutation in a conserved cysteine residue (p.C25A) on Coa6 interactions (Fig. 4.9A). Co-immunoprecipitation with anti-HA antibodies confirmed that the patient mutations severely disrupted Coa6–Cox2 interaction while only mildly affecting the Coa6–Sco1 interaction (Fig. 4.9B).

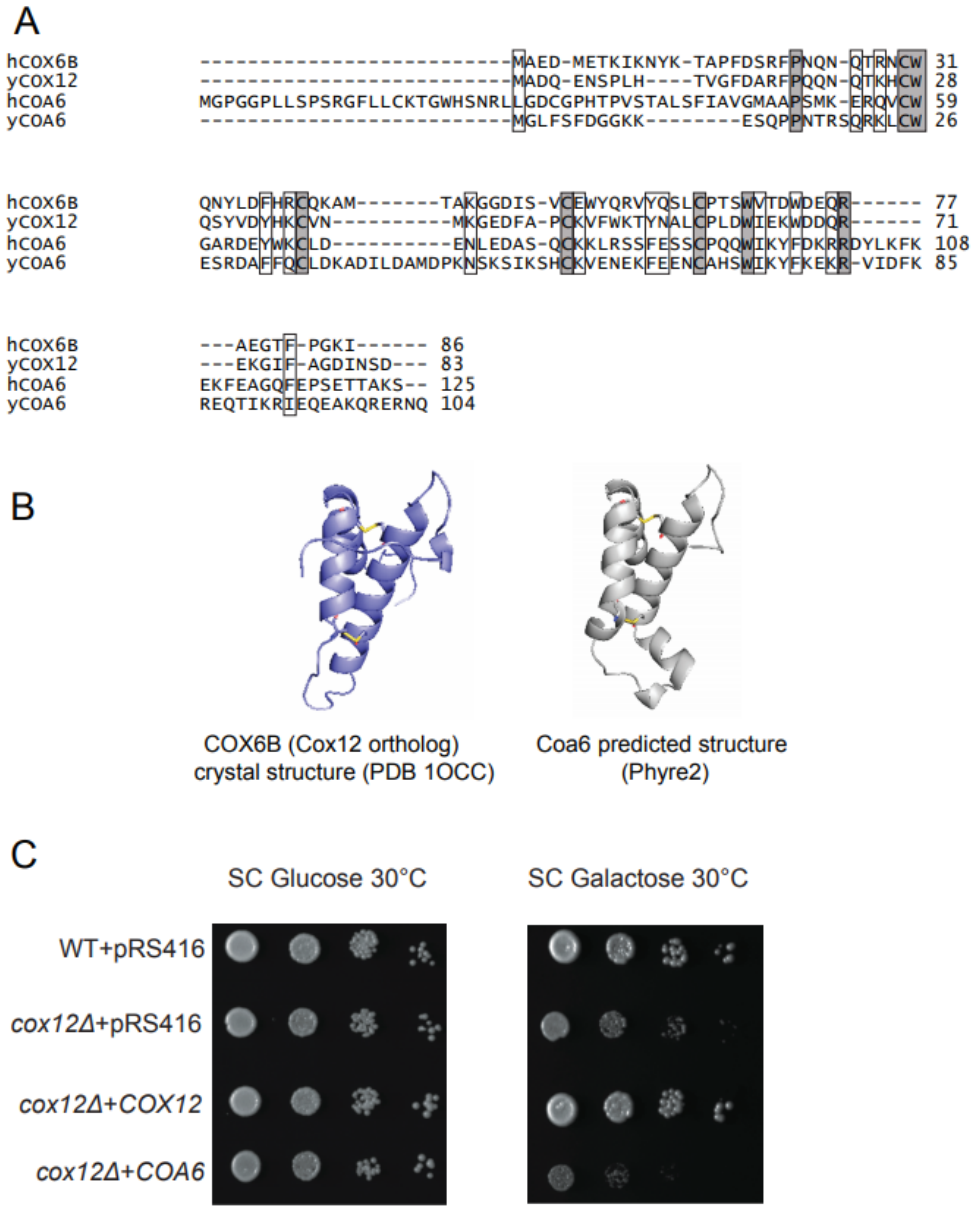


**Figure 4.8 Coa6 and Cox12 exhibit sequence and structural similarity but Coa6 overexpression retards *cox12Δ* growth.**
(A) Sequence alignment of human COX6B, yeast Cox12, human COA6, and yeast Coa6 proteins performed using ClustalW. (B) The yeast Coa6 structure predicted on the basis of the bovine COX6B structure (Protein Data Bank ID 1OCC) using Phyre2 software and was visualized using PyMol. (C) WT and *cox12Δ* cells were transformed with empty vector, pRS416- COX12, or pRS416-COA6 and spotted on SC Galactose plates. Cells were grown at 30°C and images were taken after 3 days.

These results demonstrate that the Coa6 residues mutated in the mitochondrial disease patient are essential for its interaction with Cox2, providing the biochemical basis for the disease pathogenicity.

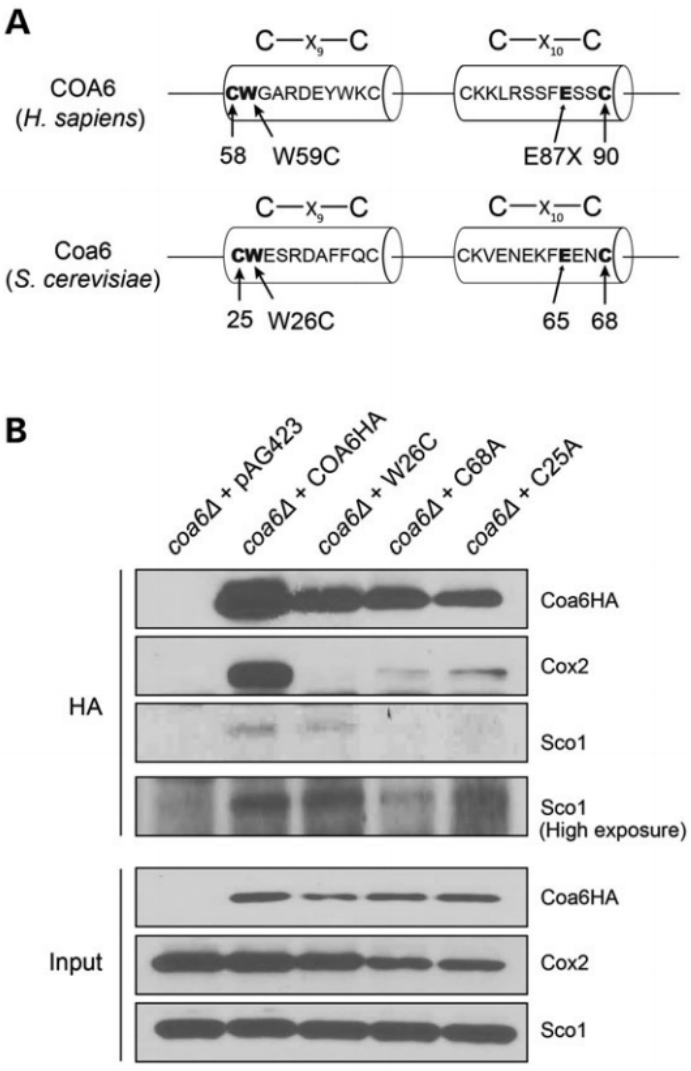


**Figure 4.9 Patient mutations disrupt Coa6 interaction with Cox2.**
(A) Schematic representation of human and yeast Coa6 proteins highlighting the conserved $Cx_9Cx_nCx_{10}C$ motif with conserved residues that are mutated in human mitochondrial disease patient. (B) Western blot detection of Coa6-HA, Cox2 and Sco1 proteins from mitochondrial extracts of *coa6Δ* cells transformed with either empty vector pAG423 or pAG423 expressing COA6HA, or COA6 mutants before (input) or after immunoprecipitation with anti-HA antibodies.

## Discussion

Recent advances in genomic technologies have identified pathogenic mutations in a plethora of uncharacterized genes; however, understanding the function of these disease genes has remained a major bottleneck in elucidating disease pathogenesis. Recently, we uncovered an evolutionarily conserved role of a previously uncharacterized mitochondrial disease gene, *COA6,* in CcO assembly and mitochondrial copper metabolism (Ghosh et al., 2014); however, its precise role in these processes remained unknown. In this study, we place Coa6 in the mitochondrial copper delivery pathway to CcO subunit Cox2. We also show that Coa6 has an overlapping function with a mitochondrial copper metallochaperone, Sco2 and a CcO subunit, Cox12, in Cox2 biogenesis. Like Coa6, mutations in the human orthologues of Sco2 and Cox12 have been shown to result in hypertrophic cardiomyopathy (Abdulhag et al., 2015; Baertling et al., 2015; Calvo et al., 2012; Jaksch et al., 2000; Papadopoulou et al., 1999). Thus, our study not only links three different mitochondrial disease genes known to cause hypertrophic cardiomyopathy to the mitochondrial copper delivery pathway, but also provides mechanistic insights into Cox2 biogenesis and uncovers genetic redundancies in the copper delivery pathway.

We present several lines of evidence demonstrating that Coa6 is a novel member of the mitochondrial copper delivery pathway to Cox2. First, simultaneous deletion of Coa6 and Sco2, a well-known mitochondrial copper metallochaperone, leads to a synthetic growth defect and complete absence of Cox2 in yeast cells (Fig. 4.5A and C). Second, overexpression of copper metallochaperones Sco1 and Sco2 partially rescues the *coa6Δ* respiratory deficient phenotype (Fig. 4.7). Third, Coa6 physically interacts with Sco1,

Sco2 and Cox2, providing biochemical evidence suggesting these proteins operate in the same pathway (Fig. 4.6C). These results obtained using the yeast model system are consistent with two recent studies in human cell lines showing physical interactions of COA6 with SCO2 and COX2 (Pacheu-Grau et al., 2015), and COA6 with SCO1 and COX2 (Stroud et al., 2015). Together, these findings establish an evolutionarily conserved role of Coa6 in copper delivery to Cox2. Furthermore, overexpression experiments with known Cox2 biogenesis factors helped place Coa6 in the copper delivery pathway to Cox2. Inability of Cox17, Cox19 and Cox23, well-known IMS proteins involved in copper delivery to mitochondria, to rescue the *coa6Δ* growth defect suggests that these proteins act upstream of Coa6. Conversely, rescue of the *coa6Δ* phenotype by Sco1, Sco2, Cox12 and Cox20 suggests that these proteins either act downstream of Coa6 or in a parallel pathway of copper delivery and Cox2 maturation.

Previously, we showed that copper supplementation was able to rescue *coa6Δ* cells, but how copper supplementation is able to bypass the complete absence of Coa6 remained an open question (Ghosh et al., 2014). In light of our current findings that Coa6, Sco2 and Cox12 have an overlapping function, it is conceivable that either Sco2 or Cox12 can substitute for Coa6 when excess copper is available. We suggest Sco2 as the more likely candidate to perform this function, because we are not able to detect any Cox2 in *coa6Δsco2Δ* cells even after copper supplementation (Fig. 4.5C). We do detect a faint band corresponding to Cox2 in copper supplemented *coa6Δcox12Δ* cells (Fig. 4.5D), presumably because Sco2 is able to function in these cells to form Cox2, albeit at a much lower level. This model can also explain the mild respiratory deficient phenotypes of

individual deletions of *COA6* and *SCO2* cells, since the absence of one is partially compensated by the other and vice-versa. The function of Sco2 in yeast cells has remained enigmatic for many years because of the absence of an overt respiratory deficient phenotype of *sco2Δ* cells (Glerum et al., 1996), but our results now firmly tie Sco2 function to Cox2 biogenesis and provide a system to uncover the role of Sco2 *in vivo* (Fig. 4.7C).

The interaction between Coa6 and Cox12 is more intriguing, considering that Cox12, a structural subunit of CcO, has never been linked to the copper delivery pathway (LaMarche et al., 1992). Interestingly, COX6B, the mammalian homolog of Cox12, and Coa6 have highly homologous sequences, including a conserved $Cx_9Cx_nCx_{10}C$ motif, and are predicted to have similar structures (Fig. 4.8A and B), which combined with their synthetic lethal interaction (Fig. 4.2B) strongly supports their overlapping function in Cox2 maturation. Consistent with this possibility, we observed that overexpression of Cox12 is able to partially rescue respiratory growth deficiency of *coa6Δ* cells. Additional evidence in support of overlapping functions of Coa6 and Cox12 comes from a human genetics study showing that a mutation in *COX12/COX6B* results in hypertrophic cardiomyopathy (Abdulhag et al., 2015), a signature clinical presentation in patients with mutations in *COA6* and *SCO2* (Baertling et al., 2015; Calvo et al., 2012; Jaksch et al., 2000; Papadopoulou et al., 1999). Interestingly, Coa6 overexpression in *cox12Δ* fails to rescue the growth defect (Fig. 4.8C), which suggests that Cox12 has an additional function that is not compensated by Coa6.

A recent paper showed that Coa6 is part of a single oligomeric complex in human cells (Pacheu-Grau et al., 2015). Similarly, we identified Coa6 in multimeric complexes in yeast mitochondria (Fig. 4.6D). We predict that these complexes are likely to be Cox2 assembly intermediates composed of assembly factors required for copper delivery to Cox2. Our prediction is supported by co-immunoprecipitation experiments showing physical interactions of Coa6 with Cox2, Cox12, Sco1 and Sco2 proteins (Fig. 4.6A–C). The differences in the size and number of Coa6-containing complexes in yeast and humans could be due to differences in the Cox2 assembly processes in these two organisms. In yeast, modular assembly of mitochondrial encoded Cox1 and Cox3 subunits have been delineated (McStay et al., 2013; Su et al., 2014), however Cox2 assembly intermediates have not yet been characterized. Our findings together with the reagents developed in this study provide the necessary tools to delineate the Cox2 assembly process in detail.

Towards understanding the molecular basis of pathogenesis, it was recently shown that the human COA6 (p.W59C) mutant is mislocalized to the mitochondrial matrix and thus would not retain its function (Pacheu-Grau et al., 2015). In contrast, a subsequent study suggested that the COA6 (p.W59C) mutant retains some functionality and that pathogenesis results from an increased aggregation state of the mutant protein rather than mislocalization (Stroud et al., 2015). Here, we find that yeast Coa6 with the patient mutation (p.W26C) no longer physically interacts with Cox2 (Fig. 4.9B). However, since we are able to still detect interaction of the mutant Coa6 with Sco1, an integral membrane protein that has most of its soluble part facing the IMS, it is unlikely that the mutant Coa6 is mislocalized to mitochondrial matrix. Therefore, we argue that the cause of

pathogenesis in the patient with these Coa6 mutations is loss of interaction between mutant Coa6 and Cox2.

Based on our genetic and biochemical interaction studies, we propose a model placing the Coa6 and Cox12 in the copper delivery to the $Cu_A$ site for Cox2 maturation (Fig. 4.10). Since human COA6 has been shown to bind copper with high affinity, it is possible that Coa6 acts as a metallochaperone. However, an *in vitro* demonstration of $Cu_A$ site formation by Coa6 and its interacting partners will be required to dissect its precise molecular function in copper delivery.

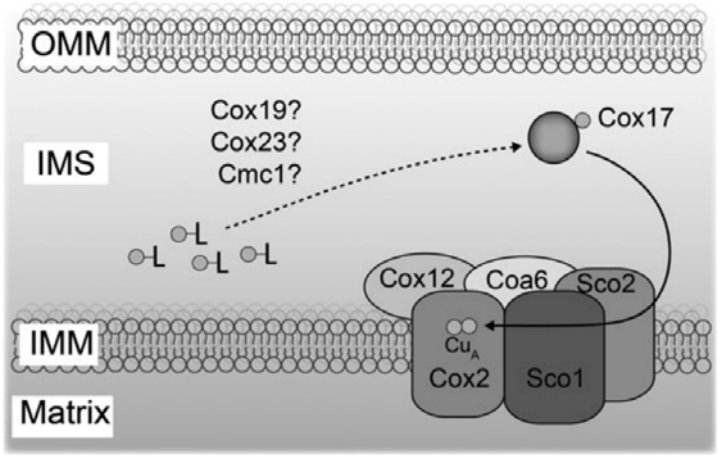


**Figure 4.10 A proposed role of Coa6 in the mitochondrial copper delivery pathway to Cox2.**
Coa6 associates with Cox2, Cox12 and Sco proteins to form a copper delivery complex for CuA center biogenesis. Previously, it has been shown that Cox17 transfers copper to Sco proteins, but the mechanism by which Cox17 receives copper from a ligand bound (-L) copper pool is not known. Although Cmc1, Cox19 and Cox23 are implicated in the copper delivery pathway, we did not detect Coa6 interaction with any of these proteins. OMM, outer mitochondrial membrane; IMM, inner mitochondrial membrane; IMS, intermembrane space.

## Materials and Methods

Yeast strains and culture conditions

All strains used in this study are listed in Table 4.2 and were confirmed by polymerase chain reaction as well as by replica plating on dropout plates. The WT yeast BY4741 cells expressing the *COA6* gene with a 3′ chromosomal HA tag was constructed as previously described (Janke et al., 2004) using primers listed in Table 4.3. Yeast cells were grown in YP (1% yeast extract, 2% bactopeptone) medium with 2% dextrose (YPD), 2% galactose (YPGal) or 3% glycerol + 1% ethanol (YPGE) as a carbon source. Synthetic media was prepared with 0.17% yeast nitrogen base, 0.5% ammonium sulfate, 0.2% dropout amino acid mix and contained either 2% dextrose, 2% galactose or 3% glycerol as a carbon source. Solid media additionally contained 2% agar. Growth medium was supplemented with BCS or CuCl2 wherever indicated. Growth was measured spectrophotometrically at 600 nm in liquid medium or by spotting on solid plates. Transformed yeast cells were grown in selection media to prevent loss of the plasmid. Double knockout yeast strains (Table 4.2) were constructed by sporulation of the diploids followed by tetrad dissection on YPD medium. The identities of all double mutant strains were confirmed by their genotypes. BY4741 ρ0 cells were obtained by culturing WT cells in the presence of ethidium bromide (25 μg/ml) for 2 days. BY4741 *cox17Δ* cells were constructed by one-step gene disruption using a hygromycin cassette (Janke et al., 2004).

**Table 4.2 Yeast strains used in this study.**

| Strain | Genotype | Source |
|---|---|---|
| BY4741 WT | MAT a, *his3Δ1, leu2Δ0, met15Δ0, ura3Δ0* | Greenberg lab |
| BY4742 WT | MAT α, *his3Δ1, leu2Δ0, lys2Δ0, ura3Δ0* | Greenberg lab |
| BY4742 *coa6Δ* | MAT α, *his3Δ1, leu2Δ0, lys2Δ0, ura3Δ0, coa6Δ::NatMX4* | This study |
| BY4741 $COA6^{HA}$ | MAT a, *his3Δ1, leu2Δ0, met15Δ0, ura3Δ0* | This study |
| BY4741 $\rho^0$ | MAT a, *his3Δ1, leu2Δ0, met15Δ0, ura3Δ0* | This study |
| BY4741 *coa6Δ* | MAT a, *his3Δ1, leu2Δ0, met15Δ0, ura3Δ0, coa6Δ:: KanMX4* | Open Biosystems |
| BY4741 *sco1Δ* | MAT a, *his3Δ1, leu2Δ0, met15Δ0, ura3Δ0, sco1Δ::KanMX4* | Open Biosystems |
| BY4741 *sco2Δ* | MAT a, *his3Δ1, leu2Δ0, met15Δ0, ura3Δ0, sco2Δ::KanMX4* | Open Biosystems |
| BY4741 *cox11Δ* | MAT a, *his3Δ1, leu2Δ0, met15Δ0, ura3Δ0, cox11Δ::KanMX4* | Open Biosystems |
| BY4741 *cox12Δ* | MAT a, *his3Δ1, leu2Δ0, met15Δ0, ura3Δ0, cox12Δ::KanMX4* | Open Biosystems |
| BY4741 *cox17Δ* | MAT a, *his3Δ1, leu2Δ0, met15Δ0, ura3Δ0, cox17Δ::HphMX4* | This study |
| BY4741 *cox19Δ* | MAT a, *his3Δ1, leu2Δ0, met15Δ0, ura3Δ0, cox19Δ::KanMX4* | Open Biosystems |
| BY4741 *cox23Δ* | MAT a, *his3Δ1, leu2Δ0, met15Δ0, ura3Δ0, cox23Δ::KanMX4* | Open Biosystems |
| BY4741 *cmc1Δ* | MAT a, *his3Δ1, leu2Δ0, met15Δ0, ura3Δ0, cmc1Δ::KanMX4* | Open Biosystems |
| BY4741 *cmc2Δ* | MAT a, *his3Δ1, leu2Δ0, met15Δ0, ura3Δ0, cmc2Δ::KanMX4* | Barrientos Lab |
| BY4741 *pic2Δ* | MAT a, *his3Δ1, leu2Δ0, met15Δ0, ura3Δ0, pic2Δ ::KanMX4* | This study |
| STY9 *sco1Δcoa6Δ* | MAT a, *his3Δ1, leu2Δ0, ura3Δ0, met15Δ0, sco1Δ::KanMX4, coa6Δ::clonNAT* | This study |
| STY10 *sco2Δcoa6Δ* | MAT a, *his3Δ1, leu2Δ0, ura3Δ0, lys2Δ0, sco2Δ::KanMX4, coa6Δ::NatMX4* | This study |
| STY2 *cox11Δcoa6Δ* | MAT a, *his3Δ1, leu2Δ0, ura3Δ0, cox11Δ::KanMX4,* coa6Δ::*NatMX4* | This study |
| STY3 *cox12Δcoa6Δ* | MAT a, *his3Δ1, leu2Δ0, met15Δ0, ura3Δ0, lys2Δ0, cox12Δ::KanMX4, coa6Δ::NatMX4* | This study |
| STY1 *cox17Δcoa6Δ* | MAT a, *his3Δ1, leu2Δ0, ura3Δ0, lys2Δ0, met15Δ0, cox17Δ::HphMX4, coa6Δ::NatMX4* | This study |
| STY4 *cox19Δcoa6Δ* | MAT a, *his3Δ1, leu2Δ0, ura3Δ0, lys2Δ0, cox19Δ::KanMX4, coa6Δ::NatMX4* | This study |
| STY5 *cox23Δcoa6Δ* | MAT a, *his3Δ1, leu2Δ0, ura3Δ0, cox23Δ::KanMX4, coa6Δ::NatMX4* | This study |
| STY6 *cmc1Δcoa6Δ* | MAT a, *his3Δ1, leu2Δ0, ura3Δ0, lys2Δ0, cmc1Δ::KanMX4, coa6Δ::NatMX4* | This study |
| STY11 *pic2Δcoa6Δ* | MAT a, *his3Δ1, leu2Δ0, ura3Δ0, met15Δ0, pic2Δ::KanMX4, coa6Δ::NatMX4* | This study |

Plasmids

Yeast *COA6* gene was cloned into three different plasmids: (1) a single copy plasmid (pRS416) under control of the native promoter; (2) a multi-copy plasmid (pRS426) under control of the native promoter and (3) a Gateway cloning plasmid (pAG423- GPD-ccdB-HA) as described previously (Ghosh et al., 2014). The h*COA6* (PubMed Gene ID: 388753) and the hy*COA6* gene constructs were codon optimized for yeast, synthesized using GeneArt® Gene Synthesis (Life Technologies) and cloned into pRS416 plasmid under the control of the yeast Coa6 promoter. Yeast *SCO1, SCO2, COX12, COX17, COX19, COX20* and *COX23* were cloned into pRS416 vector under

native yeast promoter. Point mutations in *SCO2* were introduced by site-directed-mutagenesis using Quick Change Lightning kit from the Agilent Technologies. All the primers used in this study are listed in Table 4.3. All constructs were confirmed by DNA sequencing.

**Table 4.3 Primers used in this study.**

| Name | Sequence (5' → 3´) |
|---|---|
| **Cloning in pRS416** | |
| *Sac*I y*COA6*+500bp upstream Forward | ccctgg**GAGCTC**gcaaagacgcgcagccaaaaagccgaacagttta |
| *BamH*I y*COA6* Reverse | gggact**GGATCC**tcactgatttcgttccctctgtttagcttcctgctcgat |
| *Xho*I 500bp upstream Reverse | ccctaa**CTCGAG**cgctatattactactattccttc |
| *Xho*I h*COA6* Forward | cccggc**CTCGAG**atgggtccaggtggtccattattgtc |
| *Xho*I Hy*COA6* Forward | cccggc**CTCGAG**atgggtttgttctctttcgacgg |
| *BamH*I h/Hy*COA6* Reverse | cccatt**GGATCC**tcaggacttagcagtagtttcag |
| **Cloning in pAG423GPD** | |
| AttB1 y*COA*6 Forward | GGGGACAAGTTTGTACAAAAAAGCAGGCTTCatgggcttattttcatttgatggtggc |
| AttB2 y*COA6* Reverse | GGGGACCACTTTGTACAAGAAAGCTGGGTCctgatttcgttccctctgtttagc |
| **Cloning in pYM14 chromosomal HA tag** | |
| S3 y*COA6* Forward | aagagaatcgagcaggaagctaaacagagggaacgaaatcag**CGTACGCTGCAGGTCGAC** |
| S2 y*COA6* Reverse | atatatatgttaatatgagccaataactcactaaaaactca**ATCGATGAATTCGAGCTCG** |
| **Site Directed mutagenesis primers** | |
| y*COA6* W26C Forward | agaaagttgtgctgcgagtccagggacgc |
| y*COA6* W26C Reverse | gcgtccctggactcgcagcacaactttct |
| y*COA6* C68A Forward | gtggaaaatgaaaaatttgaggagaatgccgcccatagctgga |
| y*COA6* C68A Reverse | tccagctatgggcggcattctcctcaaatttttcattttccac |
| y*COA6* C25A Forward | gttcacagagaaagttggcctgggagtccagggacg |
| y*COA6* C25A Reverse | cgtccctggactcccaggccaactttctctgtgaac |
| y*SCO2* E161K Forward | taatctgtcaagcttttctggacaaatgtcggggc |
| y*SCO2* E161K Reverse | gccccgacatttgtccagaaaagcttgacagatta |
| y*SCO2* S246F Forward | gggtcgatcaaatagaaaaatatgaaatggtccactaagtaatcctgg |
| y*SCO2* S246F Reverse | ccaggattacttagtggaccatttcatatttttctatttgatcgaccc |

Coa6 purification and antibody generation

Yeast *COA6* was first cloned into a pET28a-His6-GFP-TEV plasmid using *EcoRI* and *XhoI* restriction sites. This construct was then transformed into Rosetta DE3 *Escherichia coli* cells to express recombinant Coa6 protein. Protein purification was performed using a HisTrap™ HP column (GE Healthcare Life Sciences) and a gel filtration Superdex 200 column (GE Healthcare Life Sciences). Purified Coa6 (1.5 mg) was used to generate rabbit polyclonal antisera (Rockland Immunochemicals, Inc.). In order to obtain purified Coa6 antibody, rabbit antisera was incubated with Coa6 protein coupled to Affi-Gel 10 beads (Biorad) for 2–4 h at room temperature in a 5 ml Qiagen column. The column was then washed with 50–100 ml phosphate buffered saline (PBS) and antibodies were eluted using 0.2 M glycine, 500 mM NaCl, (pH 2.0) buffer into a tube containing 1.5M Tris (pH 8.8) to neutralize the pH. Aliquots of purified antibody were stored at −20°C.

Whole cell yeast protein extraction and isolation of mitochondrial fractions

Yeast cells (60–80 mg wet weight) were suspended in 350 µl SUMEB buffer (1.0% sodium dodecyl sulfate (SDS), 8 M urea, 10 mM MOPS, pH 6.8, 10mM EDTA) containing 1 mM PMSF and protease inhibitor cocktail (Roche Diagnostics). Cells were transferred to a fresh tube containing 350 mg of acid-washed glass beads (Sigma-Aldrich) and were vortexed three times for 1 min each, with 30 s incubation on ice between every vortex step. Lysed cells were kept on ice for 10 min to reduce bubbles and then heated at 70°C for 10 min. Cell debris and glass beads were spun down at 14 000 g for 10 min at 4°C. The supernatant was transferred to a separate tube and protein was quantified by the

Pierce BCA protein assay kit (Thermo Scientific). Mitochondria were isolated from yeast cells as described previously (Meisinger et al., 2006) and mitochondrial protein concentration was quantified using a BCA assay.

SDS-polyacrylamide gel electrophoresis, BN PAGE and western blotting

SDS-polyacrylamide gel electrophoresis (SDS PAGE) and BN PAGE were performed to separate denatured and native protein complexes. For SDS PAGE, whole cell yeast protein lysate (50 μg) or mitochondria (20 μg) were separated and blotted onto a polyvinylidene difluoride membrane. For BN PAGE sample preparation, yeast mitochondria (40 μg) were solubilized in 1% digitonin and soluble lysate was resolved on a 3–12% gradient native PAGE Bis-Tris gel (Life Technologies). Membranes were blocked for 1 h in 5% nonfat milk dissolved in Tris-buffered saline with 0.1% Tween 20 (TBST-milk), followed by overnight incubation with primary antibody in TBST-milk at 4°C. Primary antibodies were used at the following dilutions: coa6, 1:1,000; Cox1, 1:1000 (Abcam 110270), Cox2, 1:10 000 (Abcam 110271); HA, 1:10 000 (Sigma H9658); Sco1, 1:500; Sco2, 1:600 and Cox17, 1:250 (from Dr Alexander Tzagoloff ); Cox12, 1:1000 (from Dr Chris Meisinger); Cmc1, 1:500 (from Dr Antoni Barrientos); Porin, 1:50 000 (Abcam 110326); Pgk1, 1:50 000 (Life Technologies 459250).

Immunoprecipitation

Immunoprecipitation with anti-HA was performed using mitochondrial extracts of *coa6Δ* cells transformed with empty vector (pAG423), pAG423 expressing *COA6HA* or *COA6* mutants (W26C, C25A, C68A). Mitochondrial protein (3 mg) were solubilized with RIPA buffer (Thermo Scientific) with protease inhibitor cocktail (Roche Diagnostics) for

1 h at 4°C and then centrifuged at 14 000 g for 10 min. After removal of insoluble materials, mitochondrial lysates (input) were incubated overnight with anti- HA antibody at 4°C. Protein A-agarose beads were then mixed for 2 h at 4°C to bind antibodies. After washing the beads four times with buffer containing 50mM Tris, pH 7.4, 0.25% deoxycholate, 1% NP-40, 150 mM NaCl, 1 mM EDTA and once with PBS, beads were suspended in NuPAGE LDS sample buffer and boiled for 5 min prior to performing SDS PAGE. For immunoprecipitation with anti-Coa6 antibodies, mitochondria were isolated from WT and *coa6Δ* cells grown in YPGE with 5 μM CuCl2 and then solubilized with buffer containing 20 mM 4-(2-hyrdoxyethyl)-1-piperazineethanesulfonic acid, pH 7.4, 100 mM NaCl, 1mM CaCl2, 1.5% digitonin and 10% glycerol with protease inhibitor cocktail (Roche Diagnostics) for 30 min in a rotator at 4°C. Insoluble mitochondrial fraction was pelleted at 20 000 g and the remaining soluble supernatant was used for immunoprecipitation. Immunoprecipitation was performed using Dynabeads® Protein G Immunoprecipitation Kit (Life Technologies) as per manufacturer's protocol. Briefly, anti-Coa6 was coupled to Dynabeads® Protein G and incubated with mitochondrial extract in a rotator for 2 h at room temperature. After three washes, proteins were eluted and boiled with NuPAGE LDS sample buffer prior to SDS PAGE and western blotting.

# CHAPTER V

# SUMMARY AND CONCLUSIONS

## Summary

My work is focused on understanding how copper is delivered to cytochrome *c* oxidase, the main site of mitochondrial respiration. Delivery of copper to the catalytic core subunits of CcO is an intricate process that requires many assembly factors, which are present in the mitochondrial IMS. The precise molecular functions of these assembly factors remain unclear, but it is known that mutations in these proteins result in debilitating mitochondrial disorders. Using an integrative approach based on clues from evolutionary history, yeast genetics, and human disease biology, our lab had identified a new member of this copper delivery pathway, COA6 (Ghosh et al., 2014). In a follow-up study, in which I participated, we showed that Coa6 genetically and physically interacts with other members of the copper delivery pathway including Sco1 and Sco2 for the maturation of the $Cu_A$ site in Cox2 subunit of CcO (Ghosh et al., 2016).

Despite our progress in placing COA6 in the copper delivery pathway to CcO, the precise molecular function of COA6 remained elusive. To understand the molecular function of COA6, I purified the recombinant human COA6 protein and solved the solution structure of COA6 using NMR, which showed that COA6 is a helical protein with four helices and it adapts a CHCH fold where helices 1 and 2 are stabilized by two disulfide bonds between them. By mapping COA6 patient mutations, W59C and W66R, on the COA6 structure, I found that they are on the first helix of COA6 where the tryptophan side chain of both the residues faces the solvent, pointing away from the

structure, which suggests that these residues likely participate in the interaction with its target proteins- SCO or COX2. Through protein-protein interaction studies using gel filtration analysis, NMR and docking we have shown that COA6 strongly interacts with SCO1 through its C-terminal region, likely to keep SCO1 and COX2 in close proximity. The presence of CHCH fold pointed to a redox-related function of COA6, which we confirmed by demonstrating that COA6 function can be bypassed in reducing conditions. In a direct biochemical evidence for its redox activity, we showed that COA6 can reduce cysteine disulfides of COX2 and SCO proteins in an *in vitro* reconstitution assay. Furthermore, we showed that the reduction of SCO1 and COX2 by COA6 is thermodynamically favorable, because the redox potential of COA6 was determined to be lower than both SCO1 and COX2. Based on these results, we propose that the main biochemical function of COA6 is to reduce cysteine disulfides in SCO1 and COX2 proteins. This thiol-disulfide reductase activity is essential in the oxidizing environment of the mitochondrial IMS to keep the copper-binding thiols of metallochaperones or the copper coordinating cysteines of COX2 in reduced state, such that they can bind copper. Interestingly, bacterial periplasmic space where copper insertion into the bacterial CcO takes place, also contains a thiol-disulfide reductase, which is essential for the metallation of CcO. Thus, my work uncovers evolutionarily conserved requirements of thiol-disulfide reductase activity in the copper delivery to CcO.

The loss-of-function mutations in COA6, SCO1, and SCO2, which cause lethal mitochondrial disorders due to a block in copper delivery to CcO, motivated my search for the pharmacological agents that can effectively deliver copper to the mitochondrial

CcO. Towards this goal, I utilized copper auxotrophy of *coa6Δ* cells and screened for compounds that can efficiently transport copper across biological membranes and restore CcO function. This approach identified an investigational anti-cancer drug, elesclomol (ES). Follow-up biochemical experiments with ES showed that it rescues respiratory defects of *coa6Δ* yeast cells by increasing mitochondrial copper content and restoring CcO activity. I further showed that ES can also rescues respiratory defects in other yeast mutants of copper metabolism, suggesting its broader applicability. Using different copper deficient mammalian cells, including those derived from a *SCO2* patient, we demonstrated that the efficacy of ES in restoring CcO activity is retained in higher eukaryotes. Moreover, low nanomolar concentrations of ES reinstated the copper-containing subunits of CcO in a zebrafish model of copper deficiency. These findings reveal that ES can restore intracellular copper homeostasis by mimicking the function of missing transporters and chaperones of copper, and may have potential in treating human disorders of copper metabolism (Soma et al., 2018).

**Future Directions**

One of the most significant outcomes of my doctoral studies is the identification of ES as a potential therapeutic agent in the treatment of human disorders of copper metabolism. Our findings on ES has given a new hope for treating copper deficiency disorders like Menkes, a fatal copper deficiency disorder for which there is no cure (Tumer and Moller, 2010). Patients with Menkes disorder often present with neurological symptoms, failure to thrive, kinky hair, and CcO deficiency (Tumer and Moller, 2010). Having shown the efficacy of ES in restoring CcO function in zebrafish model of copper deficiency, the next

obvious step would be test the efficacy of ES in a mouse model of Menkes disease. Based on my findings, I predict that ES will be able to rescue CcO deficiency in Menkes mouse and perhaps other cuproenzymes as well. A successful demonstration of the efficacy of ES in restoring systemic and organ copper levels and the accompanying neurological phenotypes in a mouse model Menkes will pave the way for future clinical trials on Menkes patients.

To fully realize the therapeutic potential of elesclomol, it is essential to understand the mechanism of its selective copper delivery to the mitochondria. Currently, the mechanism by which ES-bound copper is selectively released in the mitochondria is unknown. Therefore, identifying specific biomolecules or the conditions that promote copper release from ES will be the next critical steps. Simple *in vitro* spectrophotometric assays could be used to test conditions that release copper from ES (Hasinoff et al., 2014). The copper binding properties of ES can be harnessed to synthesize ES analogs that can target it to cellular compartments other than mitochondria, especially the Golgi compartment, where a number of cuproenzymes of secretory pathway are metallated.

Another major outcome of this study is the elucidation of the molecular function of COA6 in the copper delivery pathway to the $Cu_A$ site of CcO. We have shown that the main biochemical function of COA6 is to reduce cysteine disulfides in the COX2 protein, thereby enabling it to receive copper from SCO1. To strengthen this model, future studies aimed at determining the X-ray crystallographic structures of the SCO1-COA6 and COX2-COA6 complexes will be instrumental in providing high-resolution information of the interaction surface between these key players of $Cu_A$ site maturation.

# REFERENCES


Abajian, C., and Rosenzweig, A.C. (2006). Crystal structure of yeast Sco1. J. Biol. Inorg. Chem. *11*, 459-466.

Abajian, C., Yatsunyk, L.A., Ramirez, B.E., and Rosenzweig, A.C. (2004). Yeast cox17 solution structure and Copper(I) binding. J. Biol. Chem. *279*, 53584-53592.

Abdulhag, U.N., Soiferman, D., Schueler-Furman, O., Miller, C., Shaag, A., Elpeleg, O., Edvardson, S., and Saada, A. (2015). Mitochondrial complex IV deficiency, caused by mutated COX6B1, is associated with encephalomyopathy, hydrocephalus and cardiomyopathy. Eur. J. Hum. Genet. *23*, 159-164.

Abicht, H.K., Scharer, M.A., Quade, N., Ledermann, R., Mohorko, E., Capitani, G., Hennecke, H., and Glockshuber, R. (2014). How periplasmic thioredoxin TlpA reduces bacterial copper chaperone ScoI and cytochrome oxidase subunit II (CoxB) prior to metallation. J. Biol. Chem. *289*, 32431-32444.

Abriata, L.A., Banci, L., Bertini, I., Ciofi-Baffoni, S., Gkazonis, P., Spyroulias, G.A., Vila, A.J., and Wang, S. (2008). Mechanism of Cu(A) assembly. Nat. Chem. Biol. *4*, 599-601.

Antonicka, H., Mattman, A., Carlson, C.G., Glerum, D.M., Hoffbuhr, K.C., Leary, S.C., Kennaway, N.G., and Shoubridge, E.A. (2003). Mutations in COX15 produce a defect in the mitochondrial heme biosynthetic pathway, causing early-onset fatal hypertrophic cardiomyopathy. Am. J. Hum. Genet. *72*, 101-114.

Baertling, F., M, A M van den Brand M., Hertecant, J.L., Al-Shamsi, A., P van den Heuvel L., Distelmaier, F., Mayatepek, E., Smeitink, J.A., Nijtmans, L.G., and Rodenburg, R.J. (2015). Mutations in COA6 cause cytochrome c oxidase deficiency and neonatal hypertrophic cardiomyopathy. Hum. Mutat. *36*, 34-38.

Baker, Z.N., Cobine, P.A., and Leary, S.C. (2017). The mitochondrion: a central architect of copper homeostasis. Metallomics *9*, 1501-1512.

Banci, L., Bertini, I., Calderone, V., Ciofi-Baffoni, S., Mangani, S., Martinelli, M., Palumaa, P., and Wang, S. (2006). A hint for the function of human Sco1 from different structures. Proc. Natl. Acad. Sci. U. S. A. *103*, 8595-8600.

Banci, L., Bertini, I., Cefaro, C., Ciofi-Baffoni, S., Gallo, A., Martinelli, M., Sideris, D.P., Katrakili, N., and Tokatlidis, K. (2009a). MIA40 is an oxidoreductase that catalyzes oxidative protein folding in mitochondria. Nat. Struct. Mol. Biol. *16*, 198-206.

Banci, L., Bertini, I., Ciofi-Baffoni, S., Gerothanassis, I.P., Leontari, I., Martinelli, M., and Wang, S. (2007a). A structural characterization of human SCO2. Structure *15*, 1132-1140.

Banci, L., Bertini, I., Ciofi-Baffoni, S., Hadjiloi, T., Martinelli, M., and Palumaa, P. (2008a). Mitochondrial copper(I) transfer from Cox17 to Sco1 is coupled to electron transfer. Proc. Natl. Acad. Sci. U. S. A. *105*, 6803-6808.

Banci, L., Bertini, I., Ciofi-Baffoni, S., Janicka, A., Martinelli, M., Kozlowski, H., and Palumaa, P. (2008b). A structural-dynamical characterization of human Cox17. J. Biol. Chem. *283*, 7912-7920.

Banci, L., Bertini, I., Ciofi-Baffoni, S., Leontari, I., Martinelli, M., Palumaa, P., Sillard, R., and Wang, S. (2007b). Human Sco1 functional studies and pathological implications of the P174L mutant. Proc. Natl. Acad. Sci. U. S. A. *104*, 15-20.

Banci, L., Bertini, I., Ciofi-Baffoni, S., and Tokatlidis, K. (2009b). The coiled coil-helix-coiled coil-helix proteins may be redox proteins. FEBS Lett. *583*, 1699-1702.

Bhadhprasit, W., Kodama, H., Fujisawa, C., Hiroki, T., and Ogawa, E. (2012). Effect of copper and disulfiram combination therapy on the macular mouse, a model of Menkes disease. J. Trace Elem. Med. Biol. *26*, 105-108.

Bhattacharya, A., Tejero, R., and Montelione, G.T. (2007). Evaluating protein structures determined by structural genomics consortia. Proteins *66*, 778-795.

Bingham, M.J., Ong, T.J., Summer, K.H., Middleton, R.B., and McArdle, H.J. (1998). Physiologic function of the Wilson disease gene product, ATP7B. Am. J. Clin. Nutr. 67, 982s-987s.

Bode, M., Woellhaf, M.W., Bohnert, M., van der Laan, M., Sommer, F., Jung, M., Zimmermann, R., Schroda, M., and Herrmann, J.M. (2015). Redox-regulated dynamic interplay between Cox19 and the copper-binding protein Cox11 in the intermembrane space of mitochondria facilitates biogenesis of cytochrome c oxidase. Mol. Biol. Cell *26*, 2385-2401.

Boulet, A., Vest, K.E., Maynard, M.K., Gammon, M.G., Russell, A.C., Mathews, A.T., Cole, S.E., Zhu, X., Phillips, C.B., Kwong, J.Q.*, et al.* (2018). The mammalian phosphate carrier SLC25A3 is a mitochondrial copper transporter required for cytochrome c oxidase biogenesis. J. Biol. Chem. *293*, 1887-1896.

Bourens, M., Boulet, A., Leary, S.C., and Barrientos, A. (2014). Human COX20 cooperates with SCO1 and SCO2 to mature COX2 and promote the assembly of cytochrome c oxidase. Hum. Mol. Genet. *23*, 2901-2913.

Calvo, S.E., Compton, A.G., Hershman, S.G., Lim, S.C., Lieber, D.S., Tucker, E.J., Laskowski, A., Garone, C., Liu, S., Jaffe, D.B.*, et al.* (2012). Molecular diagnosis of infantile mitochondrial disease with targeted next-generation sequencing. Sci. Transl. Med. *4*, 118ra110.

Calvo, S.E., and Mootha, V.K. (2010). The mitochondrial proteome and human disease. Annu. Rev. Genomics Hum. Genet. 11, 25-44.

Carr, H.S., George, G.N., and Winge, D.R. (2002). Yeast Cox11, a protein essential for cytochrome c oxidase assembly, is a Cu(I)-binding protein. J. Biol. Chem. *277*, 31237-31242.

Chambers, A., Krewski, D., Birkett, N., Plunkett, L., Hertzberg, R., Danzeisen, R., Aggett, P.J., Starr, T.B., Baker, S., Dourson, M.*, et al.* (2010). An exposure-response curve for copper excess and deficiency. J. Toxicol. Environ. Health B Crit. Rev. *13*, 546-578.

Cobine, P.A., Ojeda, L.D., Rigby, K.M., and Winge, D.R. (2004). Yeast contain a non-proteinaceous pool of copper in the mitochondrial matrix. J. Biol. Chem. *279*, 14447-14455.

Cobine, P.A., Pierrel, F., Bestwick, M.L., and Winge, D.R. (2006). Mitochondrial matrix copper complex used in metallation of cytochrome oxidase and superoxide dismutase. J. Biol. Chem. *281*, 36552-36559.

Culotta, V.C., Klomp, L.W., Strain, J., Casareno, R.L., Krems, B., and Gitlin, J.D. (1997). The copper chaperone for superoxide dismutase. J. Biol. Chem. *272*, 23469-23472.

Dancis, A., Yuan, D.S., Haile, D., Askwith, C., Eide, D., Moehle, C., Kaplan, J., and Klausner, R.D. (1994). Molecular characterization of a copper transport protein in S. cerevisiae: an unexpected role for copper in iron transport. Cell 76, 393-402.

Danks, D.M., Campbell, P.E., Walker-Smith, J., Stevens, B.J., Gillespie, J.M., Blomfield, J., and Turner, B. (1972). Menkes' kinky-hair syndrome. Lancet *1*, 1100-1102.

De Feo, C.J., Aller, S.G., Siluvai, G.S., Blackburn, N.J., and Unger, V.M. (2009). Three-dimensional structure of the human copper transporter hCTR1. Proc. Natl. Acad. Sci. U. S. A. *106*, 4237-4242.

Dziuba, N., Hardy, J., and Lindahl, P.A. (2018). Low-molecular-mass iron in healthy blood plasma is not predominately ferric citrate. Metallomics. *10*, 802-817.

Epstein, C.B., Waddle, J.A., Hale, W.t., Dave, V., Thornton, J., Macatee, T.L., Garner, H.R., and Butow, R.A. (2001). Genome-wide responses to mitochondrial dysfunction. Mol. Biol. Cell *12*, 297-308.

Ferguson-Miller, S., and Babcock, G.T. (1996). Heme/Copper Terminal Oxidases. Chem. Rev. *96*, 2889-2908.

Fornuskova, D., Stiburek, L., Wenchich, L., Vinsova, K., Hansikova, H., and Zeman, J. (2010). Novel insights into the assembly and function of human nuclear-encoded cytochrome c oxidase subunits 4, 5a, 6a, 7a and 7b. Biochem. J. *428*, 363-374.

Foster AW, Dainty SJ, Patterson CJ, Pohl E, Blackburn H, Wilson C, Hess CR, Rutherford JC, Quaranta L, Corran A, Robinson NJ. (2014). A chemical potentiator of copper-accumulation used to investigate the iron-regulons of Saccharomyces cerevisiae. Mol. Microbiol. *93*, 317-330.

Franco, L.V.R., Su, C.H., McStay, G.P., Yu, G.J., and Tzagoloff, A. (2018). Cox2p of yeast cytochrome oxidase assembles as a stand-alone subunit with the Cox1p and Cox3p modules. J. Biol. Chem. *293*, 16899-16911.

Freisinger, P., Horvath, R., Macmillan, C., Peters, J., and Jaksch, M. (2004). Reversion of hypertrophic cardiomyopathy in a patient with deficiency of the mitochondrial copper binding protein Sco2: is there a potential effect of copper? J. Inherit. Metab. Dis. *27*, 67-79.

Ghezzi, D., Saada, A., D'Adamo, P., Fernandez-Vizarra, E., Gasparini, P., Tiranti, V., Elpeleg, O., and Zeviani, M. (2008). FASTKD2 nonsense mutation in an infantile mitochondrial encephalomyopathy associated with cytochrome c oxidase deficiency. Am. J. Hum. Genet. *83*, 415-423.

Ghezzi, D., and Zeviani, M. (2012). Assembly factors of human mitochondrial respiratory chain complexes: physiology and pathophysiology. Adv. Exp. Med. Biol. *748*, 65-106.

Ghosh, A., Pratt, A.T., Soma, S., Theriault, S.G., Griffin, A.T., Trivedi, P.P., and Gohil, V.M. (2016). Mitochondrial disease genes COA6, COX6B and SCO2 have overlapping roles in COX2 biogenesis. Hum. Mol. Genet. *25*, 660-671.

Ghosh, A., Trivedi, P.P., Timbalia, S.A., Griffin, A.T., Rahn, J.J., Chan, S.S., and Gohil, V.M. (2014). Copper supplementation restores cytochrome c oxidase assembly defect in a mitochondrial disease model of COA6 deficiency. Hum. Mol. Genet. *23*, 3596-3606.

Glerum, D.M., Shtanko, A., and Tzagoloff, A. (1996). SCO1 and SCO2 act as high copy suppressors of a mitochondrial copper recruitment defect in Saccharomyces cerevisiae. J. Biol. Chem. *271*, 20531-20535.

Gohil, V.M., Nilsson, R., Belcher-Timme, C.A., Luo, B., Root, D.E., and Mootha, V.K. (2010). Mitochondrial and nuclear genomic responses to loss of LRPPRC expression. J. Biol. Chem. *285*, 13742-13747.

Gow, P.J., Smallwood, R.A., Angus, P.W., Smith, A.L., Wall, A.J., and Sewell, R.B. (2000). Diagnosis of Wilson's disease: an experience over three decades. Gut *46*, 415-419.

Guntert, P., and Buchner, L. (2015). Combined automated NOE assignment and structure calculation with CYANA. J. Biomol. NMR *62*, 453-471.

Guntert, P., Mumenthaler, C., and Wuthrich, K. (1997). Torsion angle dynamics for NMR structure calculation with the new program DYANA. J. Mol. Biol. *273*, 283-298.

Halliwell, B., and Gutteridge, J.M. (1984). Oxygen toxicity, oxygen radicals, transition metals and disease. Biochem. J. *219*, 1-14.

Hasinoff, B.B., Yadav, A.A., Patel, D., and Wu, X. (2014). The cytotoxicity of the anticancer drug elesclomol is due to oxidative stress indirectly mediated through its complex with Cu(II). J. Inorg. Biochem. *137*, 22-30.

Hedley, D., Shamas-Din, A., Chow, S., Sanfelice, D., Schuh, A.C., Brandwein, J.M., Seftel, M.D., Gupta, V., Yee, K.W., and Schimmer, A.D. (2016). A phase I study of elesclomol sodium in patients with acute myeloid leukemia. Leuk. Lymphoma *57*, 2437-2440.

Helsel, M.E., and Franz, K.J. (2015). Pharmacological activity of metal binding agents that alter copper bioavailability. Dalton Trans. *44*, 8760-8770.

Herrmann, J.M., Kauff, F., and Neuhaus, H.E. (2009). Thiol oxidation in bacteria, mitochondria and chloroplasts: common principles but three unrelated machineries? Biochim. Biophys. Acta *1793*, 71-77.

Hiser, L., Di Valentin, M., Hamer, A.G., and Hosler, J.P. (2000). Cox11p is required for stable formation of the Cu(B) and magnesium centers of cytochrome c oxidase. J. Biol. Chem. *275*, 619-623.

Horn, D., Zhou, W., Trevisson, E., Al-Ali, H., Harris, T.K., Salviati, L., and Barrientos, A. (2010). The conserved mitochondrial twin Cx9C protein Cmc2 Is a Cmc1 homologue essential for cytochrome c oxidase biogenesis. J. Biol. Chem. *285*, 15088-15099.

Horng, Y.C., Cobine, P.A., Maxfield, A.B., Carr, H.S., and Winge, D.R. (2004). Specific copper transfer from the Cox17 metallochaperone to both Sco1 and Cox11 in the assembly of yeast cytochrome C oxidase. J. Biol. Chem. *279*, 35334-35340.

Huigsloot, M., Nijtmans, L.G., Szklarczyk, R., Baars, M.J., van den Brand, M.A., Hendriksfranssen, M.G., van den Heuvel, L.P., Smeitink, J.A., Huynen, M.A., and Rodenburg, R.J. (2011). A mutation in C2orf64 causes impaired cytochrome c oxidase assembly and mitochondrial cardiomyopathy. Am. J. Hum. Genet. *88*, 488-493.

Jaksch, M., Ogilvie, I., Yao, J., Kortenhaus, G., Bresser, H.G., Gerbitz, K.D., and Shoubridge, E.A. (2000). Mutations in SCO2 are associated with a distinct form of hypertrophic cardiomyopathy and cytochrome c oxidase deficiency. Hum. Mol. Genet. *9*, 795-801.

Jaksch, M., Paret, C., Stucka, R., Horn, N., Muller-Hocker, J., Horvath, R., Trepesch, N., Stecker, G., Freisinger, P., Thirion, C.*, et al.* (2001). Cytochrome c oxidase deficiency due to mutations in SCO2, encoding a mitochondrial copper-binding protein, is rescued by copper in human myoblasts. Hum. Mol. Genet. *10*, 3025-3035.

Janke, C., Magiera, M.M., Rathfelder, N., Taxis, C., Reber, S., Maekawa, H., Moreno-Borchart, A., Doenges, G., Schwob, E., Schiebel, E.*, et al.* (2004). A versatile toolbox for PCR-based tagging of yeast genes: new fluorescent proteins, more markers and promoter substitution cassettes. Yeast *21*, 947-962.

Jomova, K., and Valko, M. (2011). Advances in metal-induced oxidative stress and human disease. Toxicology *283*, 65-87.

Kim, B.E., Nevitt, T., and Thiele, D.J. (2008). Mechanisms for copper acquisition, distribution and regulation. Nat. Chem. Biol. *4*, 176-185.

Klomp, L.W., Lin, S.J., Yuan, D.S., Klausner, R.D., Culotta, V.C., and Gitlin, J.D. (1997). Identification and functional expression of HAH1, a novel human gene involved in copper homeostasis. J. Biol. Chem. *272*, 9221-9226.

Kodama, H., Murata, Y., and Kobayashi, M. (1999). Clinical manifestations and treatment of Menkes disease and its variants. Pediatr. Int. *41*, 423-429.

Kodama, H., Okabe, I., Yanagisawa, M., and Kodama, Y. (1989). Copper deficiency in the mitochondria of cultured skin fibroblasts from patients with Menkes syndrome. J. Inherit. Metab. Dis. *12*, 386-389.

Koritzinsky, M., Levitin, F., van den Beucken, T., Rumantir, R.A., Harding, N.J., Chu, K.C., Boutros, P.C., Braakman, I., and Wouters, B.G. (2013). Two phases of disulfide bond formation have differing requirements for oxygen. J. Cell Biol. *203*, 615-627.

Krummeck, G., and Rodel, G. (1990). Yeast SCO1 protein is required for a post-translational step in the accumulation of mitochondrial cytochrome c oxidase subunits I and II. Curr. Genet. *18*, 13-15.

LaMarche, A.E., Abate, M.I., Chan, S.H., and Trumpower, B.L. (1992). Isolation and characterization of COX12, the nuclear gene for a previously unrecognized subunit of Saccharomyces cerevisiae cytochrome c oxidase. J. Biol. Chem. *267*, 22473-22480.

Leary, S.C., Antonicka, H., Sasarman, F., Weraarpachai, W., Cobine, P.A., Pan, M., Brown, G.K., Brown, R., Majewski, J., Ha, K.C.*, et al.* (2013a). Novel mutations in SCO1 as a cause of fatal infantile encephalopathy and lactic acidosis. Hum. Mutat. *34*, 1366-1370.

Leary, S.C., Cobine, P.A., Nishimura, T., Verdijk, R.M., de Krijger, R., de Coo, R., Tarnopolsky, M.A., Winge, D.R., and Shoubridge, E.A. (2013b). COX19 mediates the transduction of a mitochondrial redox signal from SCO1 that regulates ATP7A-mediated cellular copper efflux. Mol. Biol. Cell *24*, 683-691.

Leary, S.C., Kaufman, B.A., Pellecchia, G., Guercin, G.H., Mattman, A., Jaksch, M., and Shoubridge, E.A. (2004). Human SCO1 and SCO2 have independent, cooperative functions in copper delivery to cytochrome c oxidase. Hum. Mol. Genet. *13*, 1839-1848.

Leary, S.C., and Sasarman, F. (2009). Oxidative phosphorylation: synthesis of mitochondrially encoded proteins and assembly of individual structural subunits into functional holoenzyme complexes. Methods Mol. Biol. *554*, 143-162.

Leary, S.C., Sasarman, F., Nishimura, T., and Shoubridge, E.A. (2009). Human SCO2 is required for the synthesis of CO II and as a thiol-disulphide oxidoreductase for SCO1. Hum. Mol. Genet. *18*, 2230-2240.

Lee, J., Petris, M.J., and Thiele, D.J. (2002). Characterization of mouse embryonic cells deficient in the ctr1 high affinity copper transporter. Identification of a Ctr1-independent copper transport system. J. Biol. Chem. *277*, 40253-40259.

Lee, J., Prohaska, J.R., and Thiele, D.J. (2001). Essential role for mammalian copper transporter Ctr1 in copper homeostasis and embryonic development. Proc. Natl. Acad. Sci. U. S. A. *98*, 6842-6847.

Lightowlers, R.N., Taylor, R.W., and Turnbull, D.M. (2015). Mutations causing mitochondrial disease: What is new and what challenges remain? Science *349*, 1494-1499.

Lim, S.C., Smith, K.R., Stroud, D.A., Compton, A.G., Tucker, E.J., Dasvarma, A., Gandolfo, L.C., Marum, J.E., McKenzie, M., Peters, H.L.*, et al.* (2014). A founder mutation in PET100 causes isolated complex IV deficiency in Lebanese individuals with Leigh syndrome. Am. J. Hum. Genet. *94*, 209-222.

Macomber, L., and Imlay, J.A. (2009). The iron-sulfur clusters of dehydratases are primary intracellular targets of copper toxicity. Proc. Natl. Acad. Sci. U. S. A. *106*, 8344-8349.

Maehara, M., Ogasawara, N., Mizutani, N., Watanabe, K., and Suzuki, S. (1983). Cytochrome *c* oxidase deficiency in Menkes kinky hair disease. Brain Dev. *5*, 533-540.

Massa, V., Fernandez-Vizarra, E., Alshahwan, S., Bakhsh, E., Goffrini, P., Ferrero, I., Mereghetti, P., D'Adamo, P., Gasparini, P., and Zeviani, M. (2008). Severe infantile encephalomyopathy caused by a mutation in COX6B1, a nucleus-encoded subunit of cytochrome c oxidase. Am. J. Hum. Genet. *82*, 1281-1289.

McStay, G.P., Su, C.H., and Tzagoloff, A. (2013). Modular assembly of yeast cytochrome oxidase. Mol. Biol. Cell *24*, 440-452.

Meisinger, C., Pfanner, N., and Truscott, K.N. (2006). Isolation of yeast mitochondria. Methods Mol. Biol. *313*, 33-39.

Mohorko, E., Abicht, H.K., Buhler, D., Glockshuber, R., Hennecke, H., and Fischer, H.M. (2012). Thioredoxin-like protein TlpA from Bradyrhizobium japonicum is a reductant for the copper metallochaperone ScoI. FEBS Lett. *586*, 4094-4099.

Monty, J.F., Llanos, R.M., Mercer, J.F., and Kramer, D.R. (2005). Copper exposure induces trafficking of the menkes protein in intestinal epithelium of ATP7A transgenic mice. J. Nutr. *135*, 2762-2766.

Mootha, V.K., Lepage, P., Miller, K., Bunkenborg, J., Reich, M., Hjerrild, M., Delmonte, T., Villeneuve, A., Sladek, R., Xu, F., *et al.* (2003). Identification of a gene causing human cytochrome c oxidase deficiency by integrative genomics. Proc. Natl. Acad. Sci. U. S. A. *100*, 605-610.

Morgada, M.N., Abriata, L.A., Cefaro, C., Gajda, K., Banci, L., and Vila, A.J. (2015). Loop recognition and copper-mediated disulfide reduction underpin metal site assembly of CuA in human cytochrome oxidase. Proc. Natl. Acad. Sci. U. S. A. *112*, 11771-11776.

Nagai, M., Vo, N.H., Shin Ogawa, L., Chimmanamada, D., Inoue, T., Chu, J., Beaudette-Zlatanova, B.C., Lu, R., Blackman, R.K., Barsoum, J., *et al.* (2012). The oncology drug elesclomol selectively transports copper to the mitochondria to induce oxidative stress in cancer cells. Free Radic. Biol. Med. *52*, 2142-2150.

Nittis, T., George, G.N., and Winge, D.R. (2001). Yeast Sco1, a protein essential for cytochrome c oxidase function is a Cu(I)-binding protein. J. Biol. Chem. *276*, 42520-42526.

Nose, Y., Kim, B.E., and Thiele, D.J. (2006). Ctr1 drives intestinal copper absorption and is essential for growth, iron metabolism, and neonatal cardiac function. Cell Metab. 4, 235-244.

O'Day, S.J., Eggermont, A.M., Chiarion-Sileni, V., Kefford, R., Grob, J.J., Mortier, L., Robert, C., Schachter, J., Testori, A., Mackiewicz, J., *et al.* (2013). Final results of phase III SYMMETRY study: randomized, double-blind trial of elesclomol plus paclitaxel versus paclitaxel alone as treatment for chemotherapy-naive patients with advanced melanoma. J. Clin. Oncol. *31*, 1211-1218.

Ostergaard, E., Weraarpachai, W., Ravn, K., Born, A.P., Jonson, L., Duno, M., Wibrand, F., Shoubridge, E.A., and Vissing, J. (2015). Mutations in COA3 cause isolated complex IV deficiency associated with neuropathy, exercise intolerance, obesity, and short stature. J. Med. Genet. *52*, 203-207.

Pacheu-Grau, D., Bareth, B., Dudek, J., Juris, L., Vogtle, F.N., Wissel, M., Leary, S.C., Dennerlein, S., Rehling, P., and Deckers, M. (2015). Cooperation between COA6 and SCO2 in COX2 maturation during cytochrome c oxidase assembly links two mitochondrial cardiomyopathies. Cell Metab. *21*, 823-833.

Papadopoulou, L.C., Sue, C.M., Davidson, M.M., Tanji, K., Nishino, I., Sadlock, J.E., Krishna, S., Walker, W., Selby, J., Glerum, D.M., *et al.* (1999). Fatal infantile

cardioencephalomyopathy with COX deficiency and mutations in SCO2, a COX assembly gene. Nat. Genet. *23*, 333-337.

Petrukhin, K., Lutsenko, S., Chernov, I., Ross, B.M., Kaplan, J.H., and Gilliam, T.C. (1994). Characterization of the Wilson disease gene encoding a P-type copper transporting ATPase: genomic organization, alternative splicing, and structure/function predictions. Hum. Mol. Genet. *3*, 1647-1656.

Rae, T.D., Schmidt, P.J., Pufahl, R.A., Culotta, V.C., and O'Halloran, T.V. (1999). Undetectable intracellular free copper: the requirement of a copper chaperone for superoxide dismutase. Science *284*, 805-808.

Rensvold, J.W., Ong, S.E., Jeevananthan, A., Carr, S.A., Mootha, V.K., and Pagliarini, D.J. (2013). Complementary RNA and protein profiling identifies iron as a key regulator of mitochondrial biogenesis. Cell Rep *3*, 237-245.

Roberts, B.R., Lim, N.K., McAllum, E.J., Donnelly, P.S., Hare, D.J., Doble, P.A., Turner, B.J., Price, K.A., Lim, S.C., Paterson, B.M.*, et al.* (2014). Oral treatment with Cu(II)(atsm) increases mutant SOD1 in vivo but protects motor neurons and improves the phenotype of a transgenic mouse model of amyotrophic lateral sclerosis. J. Neurosci. *34*, 8021-8031.

Schulze, M., and Rodel, G. (1988). SCO1, a yeast nuclear gene essential for accumulation of mitochondrial cytochrome c oxidase subunit II. Mol. Gen. Genet. *211*, 492-498.

Schwieters, C.D., Kuszewski, J.J., Tjandra, N., and Clore, G.M. (2003). The Xplor-NIH NMR molecular structure determination package. J. Magn. Reson. *160*, 65-73.

Shen, Y., Delaglio, F., Cornilescu, G., and Bax, A. (2009). TALOS+: a hybrid method for predicting protein backbone torsion angles from NMR chemical shifts. J. Biomol. NMR *44*, 213-223.

Shoubridge, E.A. (2001). Cytochrome c oxidase deficiency. Am. J. Med. Genet. *106*, 46-52.

Shteyer, E., Saada, A., Shaag, A., Al-Hijawi, F.A., Kidess, R., Revel-Vilk, S., and Elpeleg, O. (2009). Exocrine pancreatic insufficiency, dyserythropoeitic anemia, and calvarial hyperostosis are caused by a mutation in the COX4I2 gene. Am. J. Hum. Genet. *84*, 412-417.

Smith, A.D., Logeman, B.L., and Thiele, D.J. (2017). Copper Acquisition and Utilization in Fungi. Annu. Rev. Microbiol. *71*, 597-623.

Soma, S., Latimer, A.J., Chun, H., Vicary, A.C., Timbalia, S.A., Boulet, A., Rahn, J.J., Chan, S.S.L., Leary, S.C., Kim, B.E., *et al.* (2018). Elesclomol restores mitochondrial function in genetic models of copper deficiency. Proc. Natl. Acad. Sci. U. S. A. *115*, 8161-8166.

Soto, I.C., Fontanesi, F., Liu, J., and Barrientos, A. (2012). Biogenesis and assembly of eukaryotic cytochrome c oxidase catalytic core. Biochim. Biophys. Acta *1817*, 883-897.

Stiburek, L., Vesela, K., Hansikova, H., Hulkova, H., and Zeman, J. (2009). Loss of function of Sco1 and its interaction with cytochrome c oxidase. Am. J. Physiol. Cell Physiol. *296*, C1218-1226.

Stroud, D.A., Maher, M.J., Lindau, C., Vogtle, F.N., Frazier, A.E., Surgenor, E., Mountford, H., Singh, A.P., Bonas, M., Oeljeklaus, S., *et al.* (2015). COA6 is a mitochondrial complex IV assembly factor critical for biogenesis of mtDNA-encoded COX2. Hum. Mol. Genet. *24*, 5404-5415.

Su, C.H., McStay, G.P., and Tzagoloff, A. (2014). The Cox3p assembly module of yeast cytochrome oxidase. Mol. Biol. Cell *25*, 965-976.

Szklarczyk, R., Wanschers, B.F., Nijtmans, L.G., Rodenburg, R.J., Zschocke, J., Dikow, N., van den Brand, M.A., Hendriks-Franssen, M.G., Gilissen, C., Veltman, J.A., *et al.* (2013). A mutation in the FAM36A gene, the human ortholog of COX20, impairs cytochrome c oxidase assembly and is associated with ataxia and muscle hypotonia. Hum. Mol. Genet. *22*, 656-667.

Timon-Gomez, A., Nyvltova, E., Abriata, L.A., Vila, A.J., Hosler, J., and Barrientos, A. (2018). Mitochondrial cytochrome c oxidase biogenesis: Recent developments. Semin. Cell Dev. Biol. *76*, 163-178.

Tong, A.H., Lesage, G., Bader, G.D., Ding, H., Xu, H., Xin, X., Young, J., Berriz, G.F., Brost, R.L., Chang, M., *et al.* (2004). Global mapping of the yeast genetic interaction network. Science *303*, 808-813.

Tran-Viet, K.N., Powell, C., Barathi, V.A., Klemm, T., Maurer-Stroh, S., Limviphuvadh, V., Soler, V., Ho, C., Yanovitch, T., Schneider, G., *et al.* (2013). Mutations in SCO2 are associated with autosomal-dominant high-grade myopia. Am. J. Hum. Genet. *92*, 820-826.

Tsukihara, T., Aoyama, H., Yamashita, E., Tomizaki, T., Yamaguchi, H., Shinzawa-Itoh, K., Nakashima, R., Yaono, R., and Yoshikawa, S. (1995). Structures of metal sites of oxidized bovine heart cytochrome c oxidase at 2.8 A. Science *269*, 1069-1074.

Tsukihara, T., Aoyama, H., Yamashita, E., Tomizaki, T., Yamaguchi, H., Shinzawa-Itoh, K., Nakashima, R., Yaono, R., and Yoshikawa, S. (1996). The whole structure of the 13-subunit oxidized cytochrome c oxidase at 2.8 A. Science *272*, 1136-1144.

Tumer, Z., and Moller, L.B. (2010). Menkes disease. Eur. J. Hum. Genet. *18*, 511-518.

Vafai, S.B., and Mootha, V.K. (2012). Mitochondrial disorders as windows into an ancient organelle. Nature *491*, 374-383.

Valnot, I., Osmond, S., Gigarel, N., Mehaye, B., Amiel, J., Cormier-Daire, V., Munnich, A., Bonnefont, J.P., Rustin, P., and Rotig, A. (2000a). Mutations of the SCO1 gene in mitochondrial cytochrome c oxidase deficiency with neonatal-onset hepatic failure and encephalopathy. Am. J. Hum. Genet. *67*, 1104-1109.

Valnot, I., von Kleist-Retzow, J.C., Barrientos, A., Gorbatyuk, M., Taanman, J.W., Mehaye, B., Rustin, P., Tzagoloff, A., Munnich, A., and Rotig, A. (2000b). A mutation in the human heme A:farnesyltransferase gene (COX10) causes cytochrome c oxidase deficiency. Hum. Mol. Genet. *9*, 1245-1249.

van Zundert, G.C., and Bonvin, A.M. (2014). Modeling protein-protein complexes using the HADDOCK webserver "modeling protein complexes with HADDOCK". Methods Mol. Biol. *1137*, 163-179.

Verdijk, R.M., de Krijger, R., Schoonderwoerd, K., Tiranti, V., Smeets, H., Govaerts, L.C., and de Coo, R. (2008). Phenotypic consequences of a novel SCO2 gene mutation. Am. J. Med. Genet. A. *146a*, 2822-2827.

Vest, K.E., Leary, S.C., Winge, D.R., and Cobine, P.A. (2013). Copper import into the mitochondrial matrix in Saccharomyces cerevisiae is mediated by Pic2, a mitochondrial carrier family protein. J. Biol. Chem. *288*, 23884-23892.

Vest, K.E., Wang, J., Gammon, M.G., Maynard, M.K., White, O.L., Cobine, J.A., Mahone, W.K., and Cobine, P.A. (2016). Overlap of copper and iron uptake systems in mitochondria in Saccharomyces cerevisiae. Open Biol *6*, 150223.

Vogtle, F.N., Burkhart, J.M., Gonczarowska-Jorge, H., Kucukkose, C., Taskin, A.A., Kopczynski, D., Ahrends, R., Mossmann, D., Sickmann, A., Zahedi, R.P*., et al.* (2017). Landscape of submitochondrial protein distribution. Nat. Commun. *8*, 290.

Vogtle, F.N., Burkhart, J.M., Rao, S., Gerbeth, C., Hinrichs, J., Martinou, J.C., Chacinska, A., Sickmann, A., Zahedi, R.P., and Meisinger, C. (2012). Intermembrane space proteome of yeast mitochondria. Mol. Cell. Proteomics *11*, 1840-1852.

Vulpe, C., Levinson, B., Whitney, S., Packman, S., and Gitschier, J. (1993). Isolation of a candidate gene for Menkes disease and evidence that it encodes a copper-transporting ATPase. Nat. Genet. *3*, 7-13.

Weraarpachai, W., Antonicka, H., Sasarman, F., Seeger, J., Schrank, B., Kolesar, J.E., Lochmuller, H., Chevrette, M., Kaufman, B.A., Horvath, R.*, et al.* (2009). Mutation in TACO1, encoding a translational activator of COX I, results in cytochrome c oxidase deficiency and late-onset Leigh syndrome. Nat. Genet. *41*, 833-837.

Weraarpachai, W., Sasarman, F., Nishimura, T., Antonicka, H., Aure, K., Rotig, A., Lombes, A., and Shoubridge, E.A. (2012). Mutations in C12orf62, a factor that couples COX I synthesis with cytochrome c oxidase assembly, cause fatal neonatal lactic acidosis. Am. J. Hum. Genet. *90*, 142-151.

Wishart, D.S., and Sykes, B.D. (1994). The 13C chemical-shift index: a simple method for the identification of protein secondary structure using 13C chemical-shift data. J. Biomol. NMR *4*, 171-180.

Wittig, I., Karas, M., and Schagger, H. (2007). High resolution clear native electrophoresis for in-gel functional assays and fluorescence studies of membrane protein complexes. Mol. Cell. Proteomics *6*, 1215-1225.

Yadav, A.A., Patel, D., Wu, X., and Hasinoff, B.B. (2013). Molecular mechanisms of the biological activity of the anticancer drug elesclomol and its complexes with Cu(II), Ni(II) and Pt(II). J. Inorg. Biochem. *126*, 1-6.

Yoshikawa, S., Muramoto, K., Shinzawa-Itoh, K., and Mochizuki, M. (2012). Structural studies on bovine heart cytochrome c oxidase. Biochim. Biophys. Acta *1817*, 579-589.

Zhu, Z., Yao, J., Johns, T., Fu, K., De Bie, I., Macmillan, C., Cuthbert, A.P., Newbold, R.F., Wang, J., Chevrette, M.*, et al.* (1998). SURF1, encoding a factor involved in the biogenesis of cytochrome c oxidase, is mutated in Leigh syndrome. Nat. Genet. *20*, 337-343.